

Sea Surface Temperature Anomalies, Planetary Waves, and Air-Sea Feedback in the Middle Latitudes

CLAUDE FRANKIGNOUL¹

Laboratoire de Physique et Chimie Marines, Université Paris VI, Paris

The mechanisms that contribute to the generation and damping of large-scale mid-latitude sea surface temperature (SST) anomalies are discussed. The SST anomalies reflect primarily the response of the upper ocean to the changes in air-sea fluxes that are associated with daily weather fluctuations. Heat flux forcing is dominant in the lower middle latitudes, while wind-driven entrainment may be most effective in the high latitudes; advection by anomalous Ekman current is generally less important, and Ekman pumping is negligible. The SST anomalies decay in part because of entrainment effects associated with mixed-layer deepening and oceanic mixing and in part because of heat exchanges with the atmosphere. The three approaches commonly used to model the evolution of SST anomalies are reviewed: case studies based on monthly or seasonal anomaly maps of the large-scale SST and atmospheric anomalies, numerical simulations with one-dimensional mixed-layer models, and stochastic forcing models. We stress the similarities in the different approaches and discuss their main advantages and limitations. The response of the atmosphere to mid-latitude SST anomalies is considered. First, we discuss the poorly known relationship between SST anomalies and diabatic heating. Using a crude assumption for the air-sea coupling, we consider a two-layer quasi-geostrophic channel model and discuss the stationary wave response to SST anomaly forcing and the resulting air-sea feedback. It is found that the back interaction of the SST anomalies onto the atmosphere causes a weak SST anomaly damping at large scales and a strong one at small scales; the air-sea coupling should also act as an eastward propagator for the SST anomalies. The response of more realistic linear wave models to prescribed diabatic heating is then reviewed, and it is suggested that realistic mid-latitude SST anomalies have a weak influence on the atmospheric circulation, corresponding to changes in the geopotential height of 10–30 m at most. This order of magnitude is consistent with the results of general circulation model experiments and with the limited climate predictability associated with mid-latitude SST anomalies.

CONTENTS

Introduction	357
Sea surface temperature anomaly dynamics	361
Governing equations	361
The atmospheric forcing	363
Damping and feedback mechanisms	365
The eddy noise	368
Sea surface temperature anomaly modeling	369
Case studies of large-scale SST anomaly developments	369
Numerical simulations of the mixed-layer variability	371
Stochastic models and the statistical properties of SST anomalies	371
Atmospheric response to SST anomalies	375
Stationary wave response to diabatic heating anomalies	375
Air-sea feedback in β plane models	378
Linear wave response in a spherical atmosphere	383
GCM experiments with prescribed SST anomalies	385
Discussion	386

1. INTRODUCTION

It has long been known that large-scale air-sea interactions play an important role in the variability of both ocean and atmosphere on monthly and seasonal time scales. In the early 1960's there developed a belief that anomalous ocean temperature could influence the atmospheric circulation in a persistent manner, and there have been a growing number of studies aimed at determining the role of the oceans in the observed short-term climate changes. For climate forecasts, both the sea

surface temperature anomaly impact and its evolution have to be predicted, and work proceeded in the two directions. Concomitantly, there has also been a need to obtain accurate model predictions of oceanic mixed-layer depth and temperature, as well as a strong interest from the fisheries community in forecasting oceanic thermal anomalies, since their biological implications can be important.

The dominant scale of the sea surface temperature (SST) anomalies, which are defined as the departures from the long-term seasonal mean, is large, nearly basin-wide. It can be illustrated by the strong SST anomaly observed in the North Pacific during the winter of 1976–1977 (Figure 1), which has often been used in sensitivity studies with atmospheric general circulation models (GCM's). Quite a similar anomaly was also observed during the winter of 1980–1981 [*Namias and Cayan, 1981*], and the pattern corresponds closely to the dominant mode of SST variability. This is clearly seen in a decomposition of SST anomalies in terms of empirical orthogonal functions (EOF's), which provides a description of the SST variability in terms of orthogonal patterns ordered in a decreasing sequence with regard to their contribution to the total variance. EOF's have been calculated for different oceans by *Davis [1976]*, *Weare et al. [1976]*, *Weare [1977]*, and others, and they are illustrated for the North Pacific in Figure 8 below. The scale is largest for the most energetic patterns, and it decreases with decreasing contribution to the total variances (red spectrum). Observations [e.g., *Saunders, 1972*] suggest that there is another energy peak at wavelengths of the order of 100 km, which is presumably associated with mesoscale eddies. There is also some coupling between the dominant mid-latitude and tropical SST anomalies, particularly for the "El Niño" mode which dominates the Pacific [*Weare et al., 1976*] and the global [*Hsiung and Newell, 1983*] variability. However, mid-latitude and tropical SST anomalies have dif-

¹ Also at Department of Earth, Atmospheric and Planetary Sciences, Massachusetts Institute of Technology, Cambridge.

Copyright 1985 by the American Geophysical Union.

Paper number 5R0580.
8755-1209/85/005R-0580\$15.00

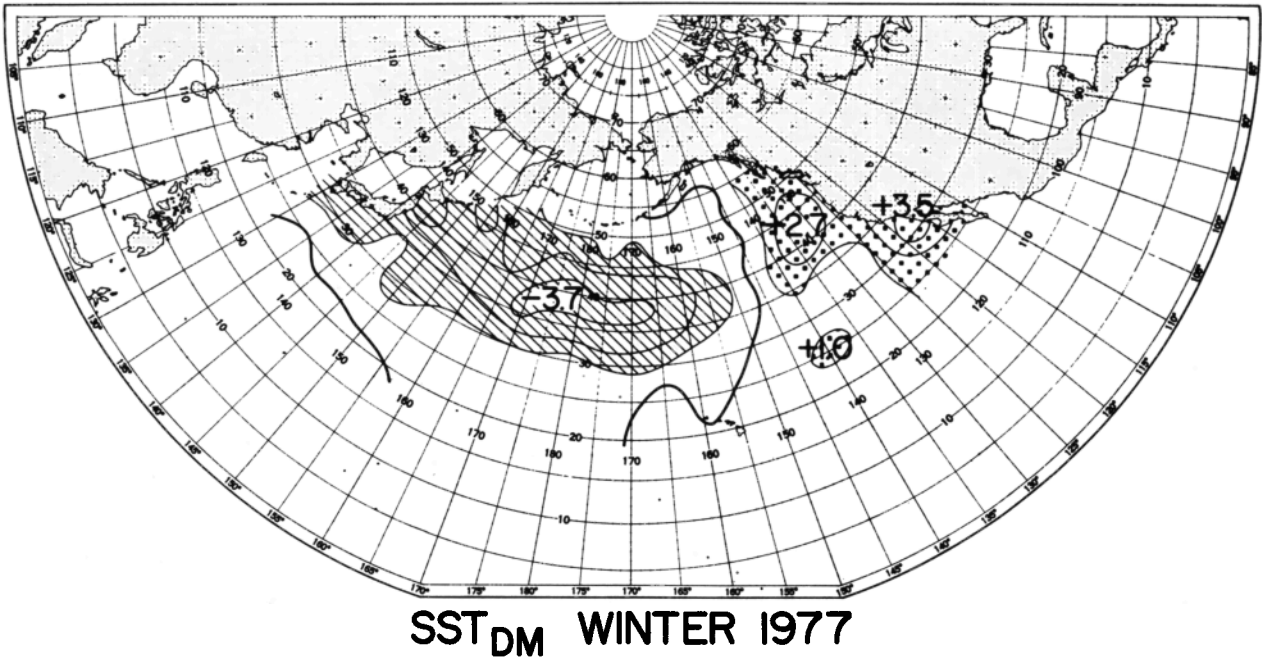


Fig. 1. SST anomaly (degrees Fahrenheit) in the North Pacific for the winter of 1976-1977 [from Namias, 1979].

ferent time scales and behavior. For our purposes we can therefore discuss the mid-latitude SST anomalies separately, keeping in mind that they have a relation to the tropical ones. The surface temperature anomalies extend throughout the

oceanic mixed layer [White and Walker, 1974; Barnett, 1981b], which has a large heat capacity. As a result, the SST anomalies are rather persistent, with a typical *e*-folding time of 3 months. Observations show a scale dependence for the per-

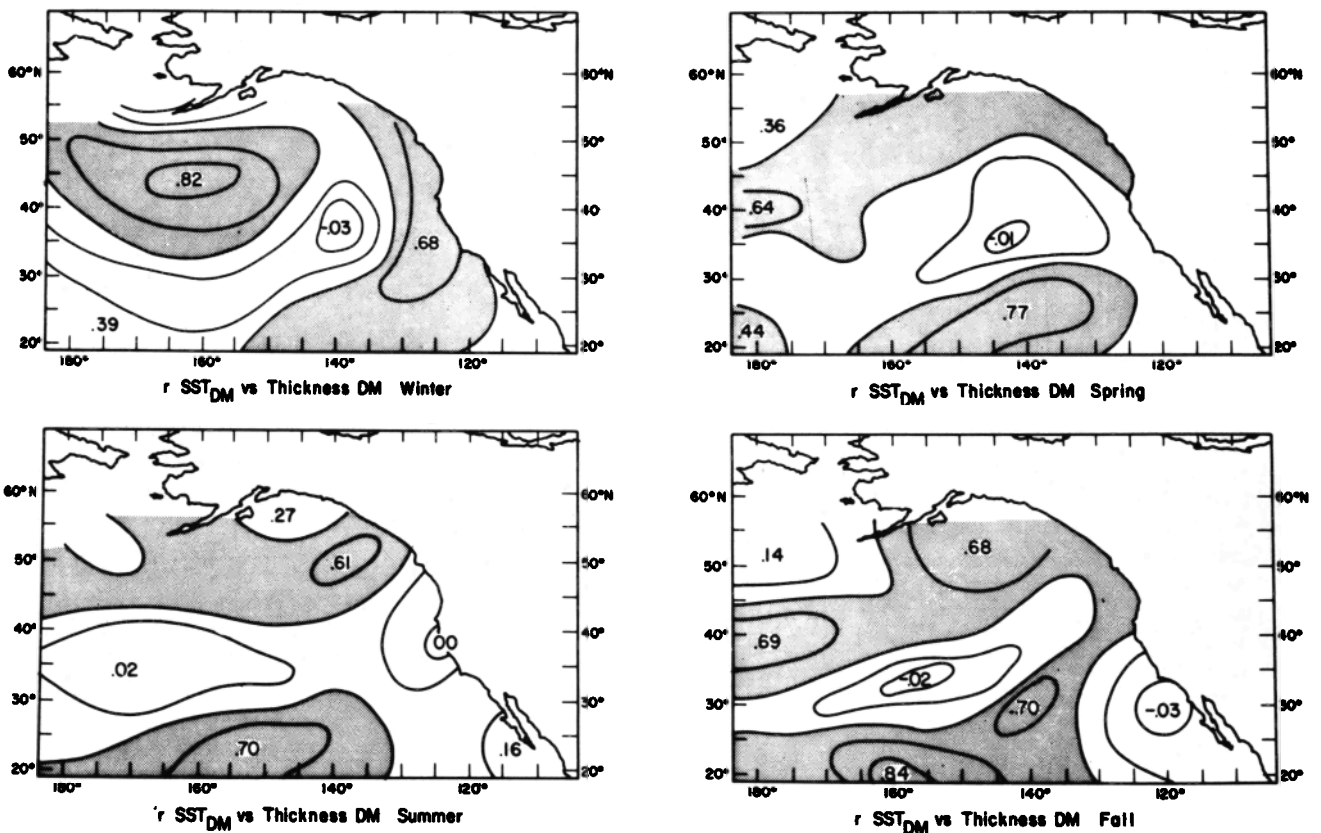


Fig. 2. Isopleths of correlations between SST and 1000-700 mbar thickness anomalies for winters, springs, summers, and falls of 1947-1971. Isopleths are drawn for each 0.2 with centers indicated by numbers. Shaded areas indicate when correlations at one grid point exceed the 5% level of significance [from Namias, 1973].

sistence, seen in Figure 19 below, where the e -folding time for North Pacific anomalies ranges between 5 months at the largest scales and 1 month at the smallest. Areal averages have an even longer duration, and fluctuations with a period of several years are observed for the whole North Pacific [Namias and Cayan, 1981]. In contrast, the dominant atmospheric patterns show generally very little persistence. The SST anomalies have been observed to propagate eastward in the middle latitudes. Namias [1959] and Favorite and McLain [1973] have suggested that the North Pacific SST anomalies are advected along the gyre, while Michaelsen [1982] has found from an EOF analysis in the frequency domain that the main anomaly pattern was expanding both in size and in intensity as it moved eastward across the North Pacific. This suggests that complex ocean-atmosphere interactions are involved in the generation, propagation, and decay of the SST anomalies.

In the 1960's the two most important advocates of large-scale ocean-atmosphere interactions were Namias [e.g., Namias 1959, 1963, 1969], who mostly stressed the middle latitudes, and Bjerknes [e.g., Bjerknes 1966, 1969], who emphasized the tropics and the global scale. The middle latitudes received most attention at first. The early empirical studies emphasized the relationships between SST and atmospheric circulation anomaly patterns. Contemporary correlation received much attention, and it was shown that anomalies in one medium could well specify anomalies in the other (Figure

2). It was also often speculated that SST anomalies arise through positive ocean-atmosphere feedback processes, by which the presence of an SST anomaly would modify the atmospheric circulation in such a manner that the anomaly is strengthened [e.g., Namias, 1963]. Since the atmospheric patterns generally have much less persistence than the SST anomalies, it was believed that SST anomalies could be used for climate forecasts, even though the question of cause and effect was left somewhat unanswered. Subsequently, Davis [1976] estimated the lag correlation between SST and sea level pressure anomalies over the North Pacific and demonstrated that the atmosphere was driving the ocean, rather than vice versa. Similar results were found by Trenberth [1975] and Haworth [1978]. These findings were substantiated by the numerical simulations of Salmon and Hendershott [1976] and the stochastic climate model of Frankignoul and Hasselmann [1977], who showed that SST anomalies could arise in response to the natural variability of the air-sea fluxes. The stochastic model provides a useful framework for understanding the origin of the SST variability. Atmospheric variables have a time scale of a few days and are essentially unpredictable on the longer time scale of SST anomalies. Hence the air-sea fluxes act on the ocean as a white noise forcing, and "random walk" SST anomalies develop.

Although this picture of an essentially passive ocean in the middle latitudes was confirmed to zero order by later studies [e.g., Frankignoul and Reynolds, 1983], it also became clear that SST anomalies in certain seasons and at certain locations were significantly correlated with subsequent atmospheric patterns. In 1976, Namias demonstrated that summer SST anomalies in the Aleutian area are significantly correlated with the atmospheric flow over the North Pacific and with air temperature and precipitation in the United States in the following fall. The difference with Davis's [1976] earlier result was due to the use of seasonally stratified statistics. Davis [1978] found that up to 20% of the variance of autumn and winter sea level pressure anomalies over the North Pacific could be predicted from summer and fall SST anomalies (Figure 3), while there was no skill in the other seasons. Davis also found that sea level pressure was an equally effective predictor, however, so that the role of the ocean was not entirely clear. Later work by Barnett [1981a] suggested that SST anomalies in the equatorial Pacific may have been the origin of both correlations.

Attempts to verify these empirical studies with simple or complex atmospheric models have not been very successful [e.g., Egger, 1977; Salmon and Hendershott, 1976; Spar, 1973; Houghton et al., 1974; Chervin et al., 1976]. In particular, only GCM experiments with highly amplified mid-latitude SST anomalies showed a significant effect of these anomalies on the atmospheric circulation [Kutzbach et al., 1977; Chervin et al., 1980]. Although the failure in detecting the SST effects was partly due to the small number of GCM runs and to the resulting weakness of the signal-to-noise ratio, there has been a growing feeling among many researchers that mid-latitude SST anomalies have few effects, if any, on the atmospheric circulation. On the other hand, GCM studies showed a larger sensitivity to tropical SST anomalies [e.g., Rowntree, 1972; Shukla, 1975; Julian and Chervin, 1978], which has produced a gradual shift of interest toward the low latitudes. This has been fueled by the recent emphasis on teleconnections between tropical and extratropical latitudes [Horel and Wallace, 1981] and by the increasing awareness of the global impact of the El Niño Southern Oscillation phenomenon.

Yet there are still some indications that mid-latitude SST

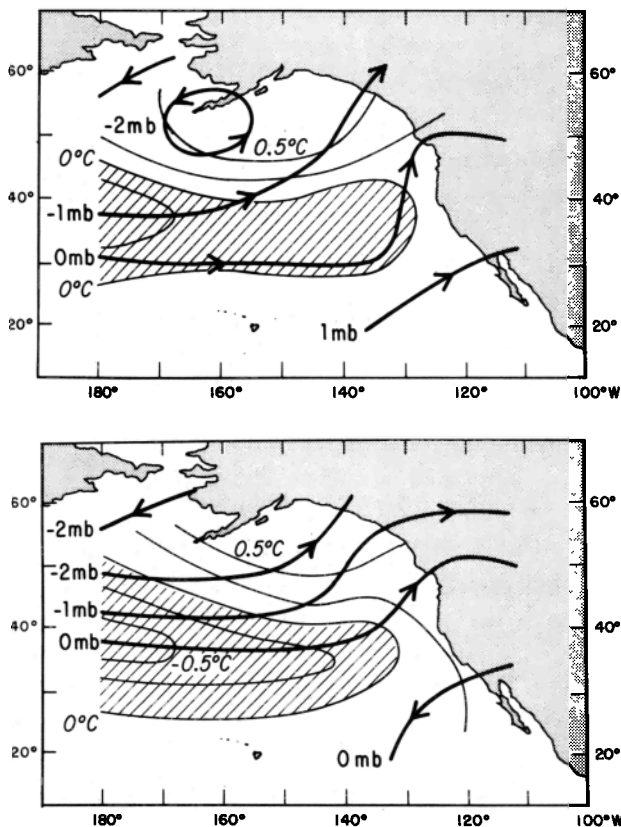
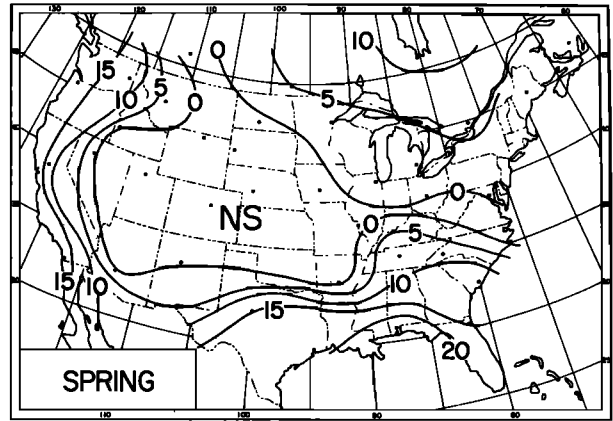
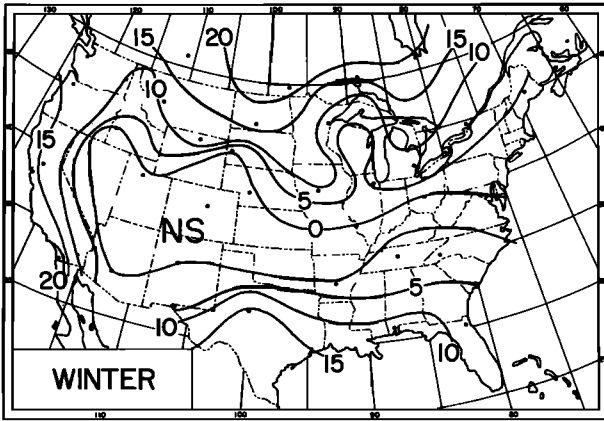
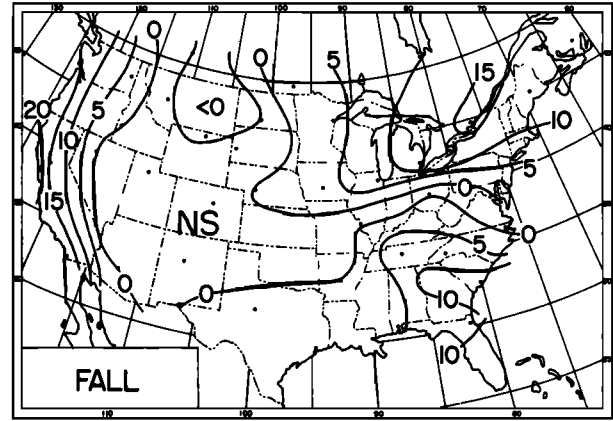
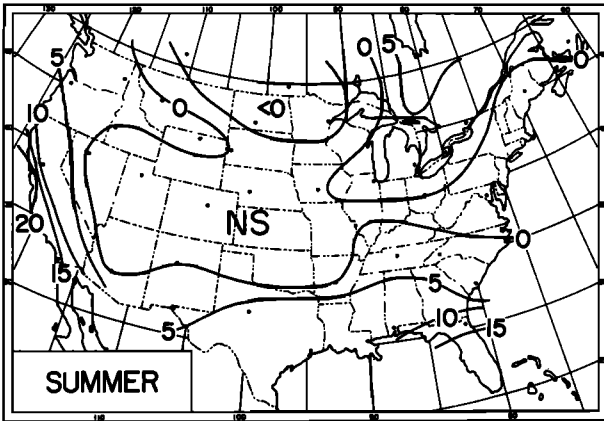


Fig. 3. Principal data and estimand patterns for predicting autumn sea level pressure from July SST (upper panel), and winter sea level pressure from October SST (lower panel). The patterns shown have an amplitude corresponding to one standard deviation of the principal data amplitude, but the sign is arbitrary, with both patterns reversing together. The contour interval is 0.25°C for SST, with negative anomaly shaded, and 1 mbar for sea level pressure, with arrows indicating geostrophic flow direction [from Davis, 1978].

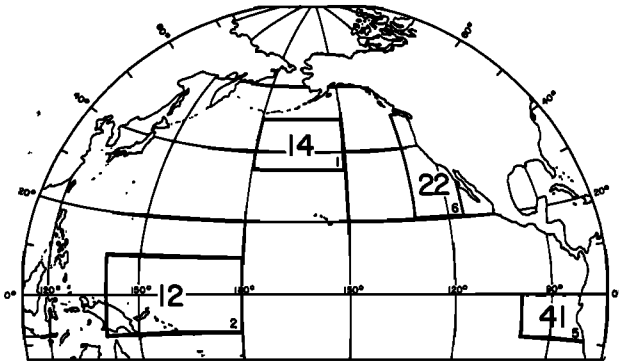


SST SKILL

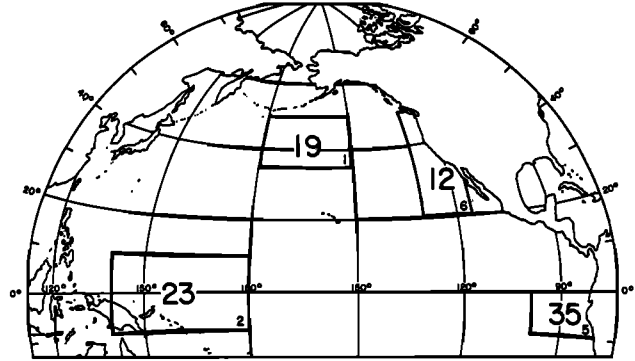


COMPOSITE PRINCIPAL SST PREDICTOR

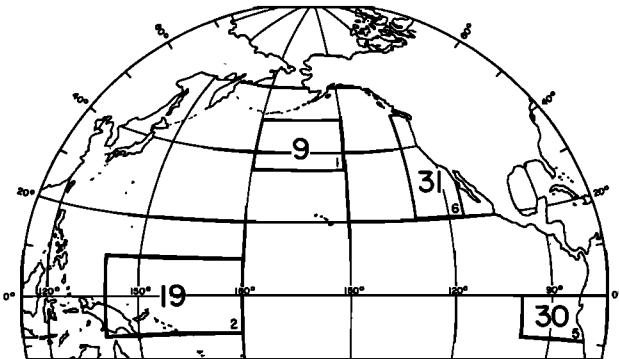
WINTER



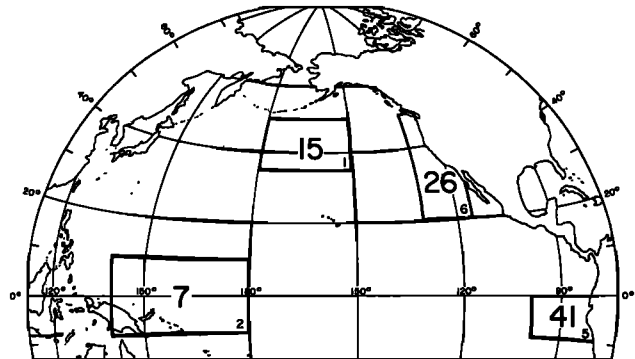
SPRING



SUMMER



FALL



anomalies have some influence on the atmospheric circulation. Indeed, the extensive literature on statistical climate forecasting, as summarized, for example, by *Namias and Cayan* [1981] and *Barnett and Sommerville* [1983], indicates that the SST anomalies are effective predictors of short-term climate changes. Most work has been done for climate prediction over the United States, and results differ somewhat because of differences in techniques and data. Nonetheless, it is generally found that Pacific SST anomalies show significant forecast skill over certain regions, particularly during the cold season. The skills are weak but better than random and better than the skills based on simple persistence or on atmospheric predictors. The skills are also better for seasonal forecasts than for monthly ones [*Harnack*, 1979]. Because of the interrelation between SST anomalies in different regions, the oceanic locations that contribute most to the predictability have not yet been clearly established, in particular the relative role of mid-latitude and tropics. *Barnett* [1981a] has suggested that tropical SST anomalies were more effective as predictors for the North American temperature changes, although significant predictive skill was associated with the mid-latitude anomalies (Figure 4), while *Harnack* [1982] has stressed the importance of the North Pacific SST field. Surface air temperature fluctuations over Eurasia are only weakly related to prior SST anomalies in the Atlantic, where the most important regions are the eastern Atlantic and the equatorial zone [*Barnett et al.*, 1984].

A second sign of SST anomaly impact is found in recent sensitivity studies with atmospheric GCM's. With the increase in computational capabilities and the development of more powerful methods of statistical analysis, GCM experiments are beginning to show that mid-latitude SST anomalies have a significant influence on the atmospheric circulation [e.g., *Hannoschöck and Frankignoul*, 1985]. The effects are weak, and their precise origin is not yet understood. Nonetheless, the magnitude of the SST anomaly-induced changes is of the same order as that predicted by simpler atmospheric linear wave models.

It seems timely therefore to attempt a review of the large-scale air-sea interactions in the middle latitudes. In the present paper we shall discuss both the causes and the effects of the sea surface temperature variability, with the main focus on the dynamical aspects. Lack of time has limited our discussion of the observations and has prevented us from considering the teleconnections with the low latitudes. The paper is organized as follows. In section 2 we establish the governing equations for the large-scale SST anomalies. We then discuss the scales and strength of different atmospheric forcing mechanisms, and we consider the damping and feedback processes that control the SST changes. In section 3 we review the SST anomaly modeling problem, stressing the similarities between three commonly used approaches: case studies, numerical simulation of mixed-layer variability, and statistical modeling. Section 4 deals with some aspects of the atmospheric response to existing SST anomalies. First, we discuss the relation between

SST and diabatic heating anomalies; then we use a simple linear wave model to describe the stationary atmospheric response and the resulting air-sea feedback. Results of more realistic linear wave models are then reviewed briefly (a full account of forced planetary wave theory can be found in the recent literature [e.g., *World Meteorological Organization*, 1980; *Held*, 1983]). Finally, we touch upon some results of GCM experiments with prescribed SST anomalies in the middle latitudes.

2. SEA SURFACE TEMPERATURE ANOMALY DYNAMICS

2.1. Governing Equations

The observations show that the upper layer of the ocean is generally well mixed by turbulent motions, with a nearly uniform distribution of temperature and salinity. The transition between the turbulent mixed layer and the stratified water below occurs in a thin entrainment zone which can have large gradients of density and velocity. The depth of the mixed layer varies on a day-to-day basis but also undergoes strong seasonal variations. In the spring the daily solar warming becomes larger than the nighttime cooling, which results in the progressive buildup of a strong vertical temperature gradient at a shallow depth. The seasonal thermocline remains near the surface throughout summer. In early fall the wind increases, and the surface water starts to lose more heat to the atmosphere than it gains from the sun. This results in the erosion of the seasonal thermocline and the deepening of the mixed layer, which persists until late winter (Figure 5). Below the largest depth reached by the mixed layer, no significant seasonal change in temperature and salinity is observed in the middle latitudes, and the variability is dominated by internal wave and quasi-geostrophic motions.

To understand the SST variability on the relatively short climatic time scales of interest in this paper, it seems sufficient to consider the dynamics of the near surface oceanic layers. As summarized, for example, by *Niiler and Kraus* [1977], the main features can be described with a slab or integral model of the mixed layer, where it is assumed that temperature, salinity, and horizontal velocity are uniform within the mixed layer and that the entrainment zone is thin enough to be modeled as a discontinuity in the different variables. Considerable simplifications then arise by vertically integrating the governing equations through the mixed layer.

The conservation equation for heat is

$$\frac{\partial}{\partial t} \hat{T} + \nabla \cdot (\hat{v} \hat{T}) + \frac{\partial}{\partial z} (\hat{w} \hat{T}) + \nabla \cdot (\hat{v}^t T^t) + \frac{\partial}{\partial z} (\hat{w}^t T^t) = \frac{1}{\rho C_p} \frac{\partial}{\partial z} \hat{q} \quad (1)$$

where the circumflex denotes ensemble mean and superscript t turbulent fluctuations. Here T is the temperature; v and w the horizontal and vertical velocity; q the penetrating flux of shortwave solar radiation; ρ the water density and C_p its specific heat; $\nabla = (\partial/\partial x, \partial/\partial y)$; and (x, y, z) the coordinates, positive eastward, northward, and upward, respectively. If the variations of the free surface are neglected, integration of (1) from the surface (at $z = 0$) to just below the mixed layer (at depth $z = -h$) yields

$$h \frac{\partial}{\partial t} T + h v \cdot \nabla T + (T - T_+) w_e - \kappa h \nabla^2 T + \frac{Q - Q_+}{\rho C_p} = 0 \quad (2)$$

Fig. 4. (Opposite) (Top) Ability of seasonal SST anomalies to hindcast fluctuations in surface air temperature one season in advance during the period 1902–1972. Contours are the percent of variance accounted for by the SST model; NS indicates regions for which no significant model could be constructed. (Bottom) Percentage of overall hindcast skill accounted for by individual SST predictor regions. For example, 41% of the winter forecast skill over North American came from the eastern equatorial Pacific in the preceding year [from *Barnett*, 1981a].

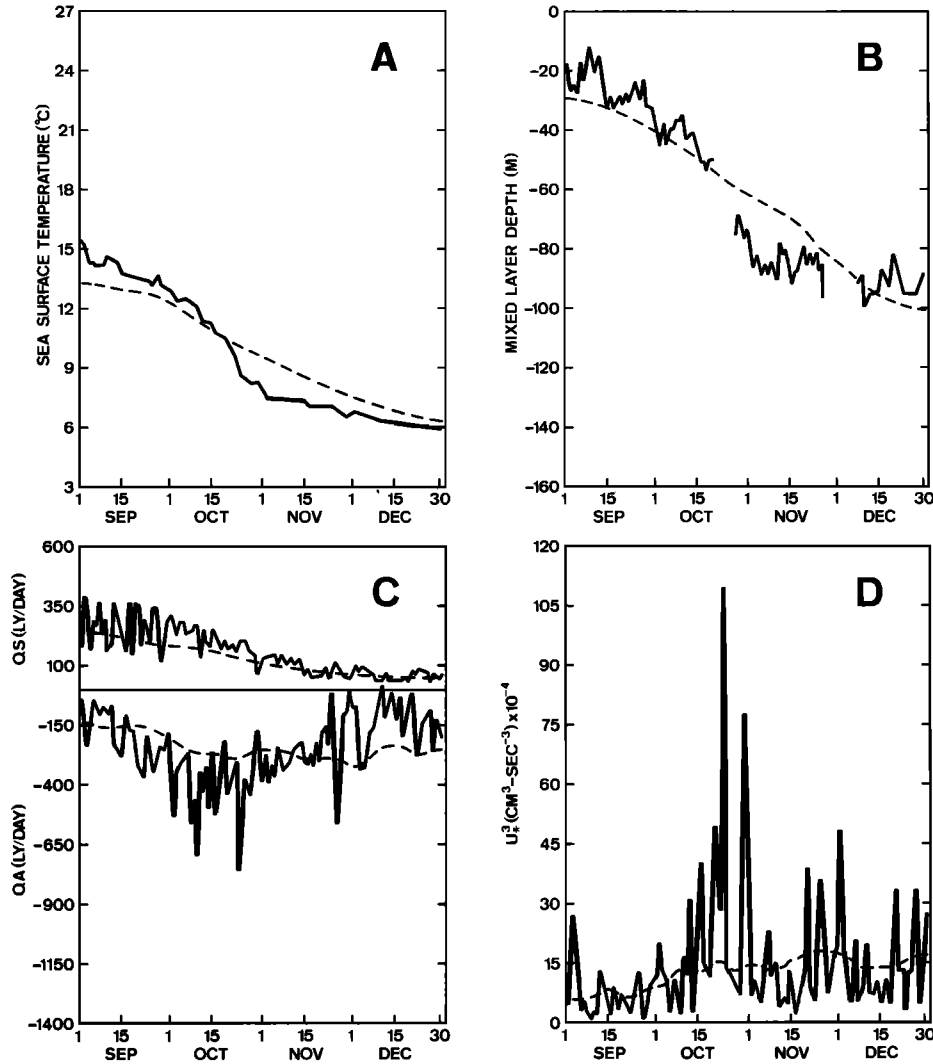


Fig. 5. Daily averaged values of (a) sea surface temperature, (b) mixed-layer depth, (c) insolation (QS) and surface heat flux plus back radiation (QA), and (d) u_*^3 at weather ship P (50°N , 145°W) during the 1963 season. Dashed lines represent the long-term (24 year) values [from *Elsberry and Camp*, 1978].

where T and \mathbf{v} denote temperature and velocity in the mixed layer, and the subscript plus indicates values at the bottom of the entrainment zone. To derive (2), we have used the incompressibility condition $\nabla \cdot \mathbf{v} + \partial w / \partial z = 0$, which reads, after vertical integration,

$$\nabla \cdot (h\mathbf{v}) - w_+ - \mathbf{v}_+ \cdot \nabla h = 0 \quad (3)$$

The entrainment velocity w_e is defined by

$$w_e = \Lambda \left(\frac{\partial h}{\partial t} + \nabla \cdot (h\mathbf{v}) \right) \quad (4)$$

with $\Lambda = 1$ for $\partial h / \partial t + \nabla \cdot (h\mathbf{v}) > 0$ and $\Lambda = 0$ otherwise. This function has been introduced because entrainment (adding stratified water to the mixed layer) causes changes in the mixed-layer temperature, whereas detrainment (leaving behind mixed-layer water because mixing is not strong enough to reach the bottom of the mixed layer when heat is added) does not change the mixed-layer temperature [Kraus and Turner, 1967]. We have also introduced a horizontal diffusion coefficient κ to parameterize horizontal mixing. In (2), Q denotes

the net heat flux across the air-sea interface (positive upward). We shall neglect the heat flux Q_+ at the bottom of the mixed layer, which is a reasonable approximation except when the seasonal thermocline is at shallow depth and solar radiation penetrates below the mixed layer (see *Simpson and Dickey* [1981] for downward irradiance effects). Since we have assumed that the mixed layer is homogeneous, (2) describes the rate of change of the sea surface temperature. Under light winds, there may also be diurnal temperature changes in the first few meters, but this effect need not be considered for the time scales of interest here.

The equation for the conservation of salinity can be treated similarly. However, salinity has generally little influence on the mixed-layer dynamics in the middle latitudes, and it will be neglected here. Salinity effects are discussed by *Miller* [1976].

The horizontal momentum equation can be written as

$$\frac{\partial}{\partial t} \hat{\mathbf{v}} + \hat{\mathbf{v}} \cdot \nabla \hat{\mathbf{v}} + \hat{w} \frac{\partial}{\partial z} \hat{\mathbf{v}} + f\mathbf{n}\Lambda \hat{\mathbf{v}} + \frac{\nabla \hat{p}}{\rho} + \widehat{\mathbf{v}^t \cdot \nabla \mathbf{v}^t} + \widehat{w^t \frac{\partial}{\partial z} \mathbf{v}^t} = 0 \quad (5)$$

where p is the pressure, \mathbf{n} the vertical unit vector, $f = 2\Omega \cos \phi$ the Coriolis parameter, Ω the angular velocity, and ϕ the latitude. Equation (5) can be integrated vertically as before [see *Stevenson, 1983; Schopf and Cane, 1983*]. For our purposes it is sufficient to note that the large-scale currents in the upper layers can be divided into ageostrophic and quasi-geostrophic components. The ageostrophic or Ekman currents are wind driven and vary primarily on the inertial time scale. At low frequencies there is an approximate balance between friction and Coriolis forces, so that if we make the reasonable assumption that the Reynolds stress vanishes below the mixed layer, the Ekman current is zero below the entrainment zone, and the mass transport is given by [*Gill and Niiler, 1973*]

$$hf\mathbf{n}\Delta\mathbf{v}_E = \boldsymbol{\tau}/\rho \quad (6)$$

Here $\boldsymbol{\tau}$ denotes the surface wind stress, and the index E the Ekman current; divergent effects have been neglected, as well as the effect of surface waves.

In mixed-layer models, the depth h of the mixed layer is determined by the turbulent kinetic energy budget. The vertical integration of the kinetic energy equation through the mixed layer is rather elaborate and involves various assumptions and parameterizations as discussed, for example, by *Niiler and Kraus [1977]* or *Garwood [1979]*. A simplified form for the energy budget is

$$\begin{aligned} \frac{1}{2}w_e[\alpha gh(T - T_+) - m_s|\mathbf{v} - \mathbf{v}_+|^2] \\ = m_0u_*^3 + \frac{1}{2}\frac{\alpha ghQ}{\rho C_p} - \varepsilon h \end{aligned} \quad (7)$$

where u_* is the friction velocity related to the surface wind stress by $|\boldsymbol{\tau}| = \rho u_*^2$, g is gravity, α is the coefficient of thermal expansion such that $\partial\rho/\partial T = -\alpha$, and ε is the turbulent dissipation. On the left-hand side the first term is the rate of working needed to lift and mix the denser entrained water, and the second term is the rate of mean flow energy reduction by mixing across the mixed-layer base. On the right-hand side the three terms represent the wind generation of turbulent energy, the rate of potential energy change produced by the surface fluxes, and the turbulent dissipation, respectively. The parameters m_0 and m_s are empirical constants which are often used as tuning parameters. During detrainment the depth of the mixed layer is determined by the relation

$$h = m_s u_*^3 \left[-\frac{1}{2} \frac{\alpha g Q}{\rho C_p} + \varepsilon \right]^{-1} \quad (8)$$

which expresses the balance between energy input by wind stress and by surface heat exchanges and the turbulent dissipation. The mixed layer is basically decoupled from the thermocline. During entrainment a number of physical regimes are possible, which may vary with the particular model [see *Niiler and Kraus, 1977; Price et al., 1978*].

To understand the mechanisms governing the rate of change of SST anomalies, it is sufficient at this stage to consider the heat content equation (2). If each variable is decomposed into a seasonally varying mean (denoted by an overbar) and an anomaly (denoted by a prime), the SST anomaly equation can be written in a form appropriate to time stepping:

$$\frac{dT'}{dt} = \underbrace{-\frac{Q'}{\rho C_p h}}_A - \underbrace{\frac{(\overline{h\nu})' \cdot \nabla(\overline{T} + T')}{h}}_B - \underbrace{\frac{h'}{h} \frac{\partial \overline{T}}{\partial t}}_C$$

$$- \underbrace{\frac{(T' - T_+)(\overline{w}_e + w_e')}{h}}_D - \underbrace{\frac{(\overline{T} - \overline{T}_+)}{h} w_e'}_E + \underbrace{\kappa \nabla^2 T'}_F \quad (9)$$

where the terms of the right-hand side describe the effect of the following processes:

- A anomalies in the net surface heat flux;
- B temperature advection by anomalous current;
- C anomalies in the mixed-layer depth;
- D anomalies in the temperature jump in the entrainment zone;
- E anomalies in the entrainment velocity;
- F horizontal mixing.

Also,

$$\frac{d}{dt} = \frac{\partial}{\partial t} + \bar{\mathbf{v}} \cdot \nabla \quad (10)$$

is the time derivation following the mean motion. Mean products of anomalies like $(\overline{h\nu})' \cdot \nabla T'$ primarily contribute to T' at zero frequency and have been neglected, as well as some of the contribution of the horizontal mixing, since our eddy diffusivity parameterization is very crude anyway. We have also neglected $\partial T'/\partial t$ as compared to $\partial \overline{T}/\partial t$ in term C. Indeed, seasonal changes strongly dominate the SST variability in extratropical regions (in the North Pacific the rms value of $\partial \overline{T}/\partial t$ is found to be typically 5 times larger than that of $\partial T'/\partial t$).

Three types of terms can be distinguished. The first category represents the effect of the atmospheric forcing on the SST anomalies via heat flux (A), wind-driven currents (B), mixed-layer depth changes (C), and entrainment (D and E). The second category represents the effects of the variability in the ocean interior, mainly quasi-geostrophic eddy motions, which distort the upper layer by horizontal advection (B) and vertical motion near the mixed-layer base (C-E). The third category includes all terms that contribute to the damping of SST anomalies; atmospheric feedback (mainly via A), oceanic feedback (D), and horizontal mixing (F); vertical mixing below the mixed layer could have been included as well by keeping Q^+ in (2).

Before discussing the solution of the SST equation, these three types of terms are considered in more detail.

2.2. The Atmospheric Forcing

In the middle latitudes the largest exchanges of heat, momentum, and energy at the air-sea interface are associated with the passage of eastward traveling cyclones and anticyclones at the synoptic and larger scales. The dominant time scale of the atmospheric forcing fields is a few days, and it is much smaller than that of SST anomalies, even though substantial SST changes may occur over short periods (Figure 5). Changes in the mixed-layer depth also occur on relatively short time scales because the mechanical inertia of the mixed layer is small.

Since the weather changes irregularly and is largely unpredictable beyond a few days, the frequency spectra of the atmospheric field are approximately white at low frequencies (except for the seasonal peaks (Figure 6)), where the variance is dominated by the "white noise extension" of the daily weather fluctuations [*Madden, 1976*]. Wave number-frequency analysis reveals that the time scale of the atmospheric fluctuations increases at very large scales, so that the dominant period at the planetary scales is of the order of 20-30 days

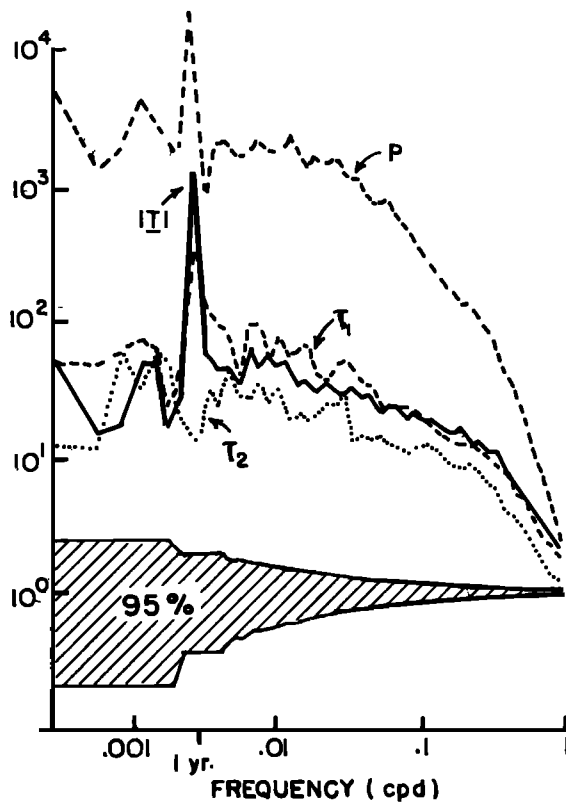


Fig. 6. Spectra of atmospheric pressure (p), east (τ_1) and north (τ_2) wind stress, and wind stress magnitude at weather ship C (52.5°N, 35.5°W) [from Willebrand, 1978].

[Willson, 1975]. Hence the frequency spectra of the fields that are dominated by the largest scales (geopotential height, pressure) start falling off at larger periods, as illustrated by the surface pressure spectrum in Figure 6. Some redness is also found at very low frequencies, in part as a result of tropical and extratropical SST variability. Nonetheless, the surface fluxes are quadratic or higher-order functions of the atmospheric variables, and they are strongly dominated by the short time scale weather changes. Thus they can be considered in a first approximation as short time scale stochastic processes. Note also that at low frequencies the spectra are essentially symmetric in wave number space; i.e., there is no preferred propagation direction [Willebrand, 1978].

Term A in (9) describes the influence of the surface heat flux variability on the SST anomalies. The heat flux is given by the sum of latent heat flux Q_L , sensible heat flux Q_S , shortwave radiation Q_{sw} , and longwave radiation Q_{LW} . The turbulent heat fluxes are generally estimated from the bulk aerodynamic formulae

$$Q_L = \rho^a L C_L u^a (q_s - q^a) \quad (11)$$

$$Q_S = \rho^a C_p^a C_S u^a (T - T^a) \quad (12)$$

where the superscript a indicates atmospheric variables, L the latent heat of evaporation; u^a , T^a , and q^a the wind speed, the air temperature, and the specific humidity at 10 m, respectively; q_s is the saturation specific humidity at the sea surface, and C_L , C_S are bulk exchange coefficients which depend on air stability and wind speed [e.g., Liu *et al.*, 1979]. In climatological studies, the radiation fluxes are calculated from empirical formulae which are not too successful at reproducing direct

observations and are often biased [Simpson and Paulson, 1979; Fung *et al.*, 1984].

The level of variability of each heat flux component is a function of the location and the time of year: Q_L' and Q_S' have maximum variance in fall and winter, whereas Q_{sw}' varies most in spring and summer. However, it is the ratio Q'/\bar{h} that determines the efficiency of the SST anomaly forcing, and it undergoes different seasonal variations. The geographical distribution of the intensity of the heat flux forcing is illustrated for the North Pacific in Figure 7; the main spatial patterns of variability (Figure 8, middle panels) indicate a general decrease in scale with decreasing variance, as is the case for SST anomalies. It is shown below that heat flux forcing is one of the dominant generating mechanisms for the SST anomalies.

Term B in (9) includes the contribution of anomalous Ekman currents to the SST anomaly generation. The currents act mainly by distorting the mean SST gradient, since one has $\nabla \bar{T} \gg \nabla T'$ over most of the ocean. Using (6), one can express this contribution in terms of the surface wind stress and write

$$\frac{-(h\nu_E)' \cdot \nabla(\bar{T} + T')}{\bar{h}} = \frac{-(\tau' \Lambda n) \cdot \nabla(\bar{T} + T')}{\rho f \bar{h}} \quad (13)$$

This formulation is consistent with the slab model of the mixed layer and is based on the assumption of vanishing current below the entrainment zone. Earlier studies of horizontal advection effects on SST anomalies [Namias, 1959, 1965, 1972; Jacob, 1967; Clark, 1972; Adem, 1970, 1975] were based on Ekman's expression for the surface velocity of magnitude $0.0127u^a/(\sin \theta)^{1/2}$ and directed generally 45° to the right of the surface wind (northern hemisphere). This formula is inconsistent with the small current shear and the lack of veering observed in the mixed layer [Davis *et al.*, 1981], and it overestimates the advection. To estimate the wind stress in (13), one uses the bulk formula $\tau = \rho^a C_D u^a u^a$, where the drag coefficient C_D increases slowly with the wind speed [e.g., Garratt, 1977].

The fluctuations in the surface wind stress are largest during fall and winter, but the SST anomaly forcing term (13) has a different seasonal modulation than does the heat flux forcing because it also depends on ∇T , which is generally largest in winter and spring. An estimate of the geographical distribution of the intensity of the anomalous Ekman advection term (slightly underestimated because the wind stress was calculated from low-passed wind data) is also shown for the North Pacific in Figure 7. It is most intense along the subarctic front where the mean temperature gradient is largest, but it has much smaller variance than the heat flux forcing term throughout the North Pacific. This suggests that the latter mechanism is more important for SST anomaly generation (see also Haney [1985]). Figure 8 shows that the characteristic scale of the Ekman advection term also decreases with decreasing variance.

Terms C–E in (9) show the effects of mixed-layer depth variability, which is in part controlled by change in wind stress and heat flux at the surface. The energy budget (7) suggests that the main driving term is the energy input by the wind. Since this term is proportional to u_*^3 , it will have a skewed probability distribution with a majority of values below the mean and most of the contribution coming from a few large events during storms (Figure 5). The skewness of the other forcing terms which are quadratic functions in the atmospheric variables is considerably less [Elsberry and Camp, 1978]. This does not prevent the fluctuations in u_*^3 from being well correlated in time with the fluctuations in the wind

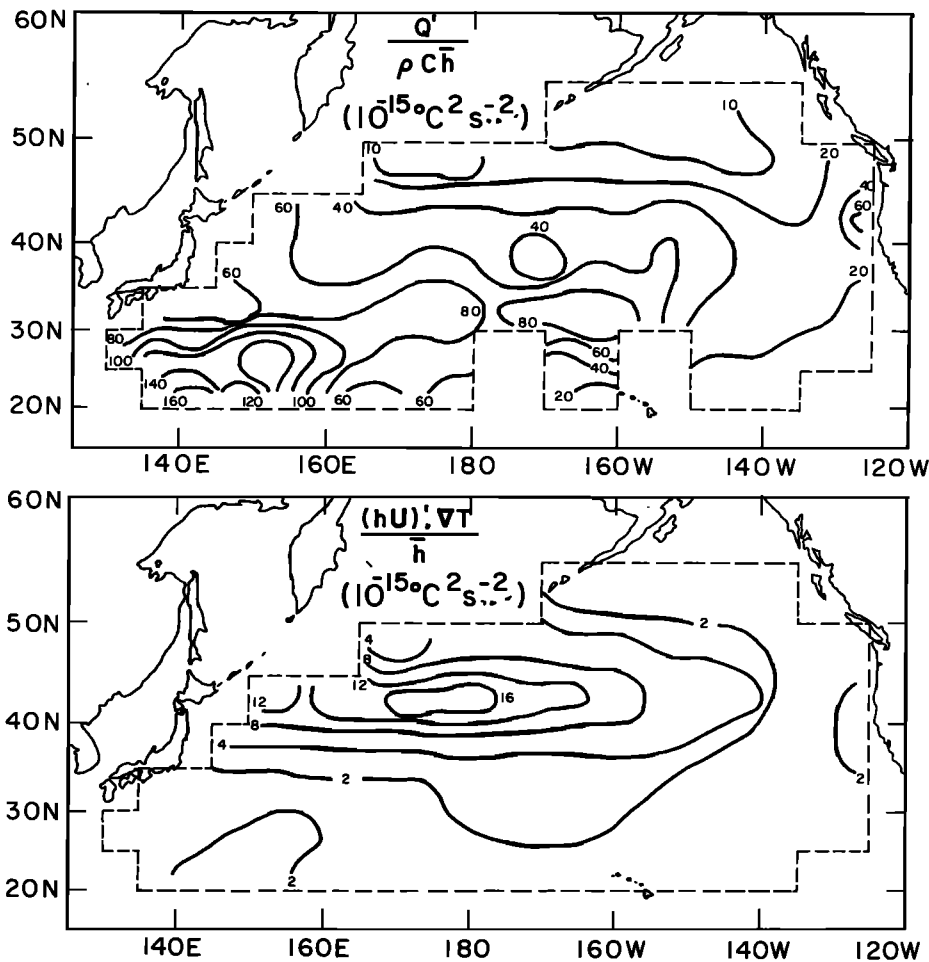


Fig. 7. Variance of monthly anomalies for (top) the heat flux forcing term $Q'/\rho C_p \bar{h}$ and (bottom) the Ekman advection term $-(\tau' \Lambda n) \cdot \nabla T / \bar{h}$ estimated for the period 1949–1972 [from Frankignoul and Reynolds, 1983].

stress and the surface heat flux (Figure 9). As discussed in section 3, terms C and E seem to be most important at high latitudes during spring and fall. During spring they largely control the transition between winter (deep mixed layer) and summer (shallow thermocline) regimes; during fall the entrainment flux is largest, since the mixed layer is shallow and the temperature jump at the base of the mixed layer is maximum [see Elsberry and Garwood, 1978].

Wind-induced anomalies in w_e' and h' also result from the divergence of the horizontal currents in the mixed layer which create vertical motions at its base. At low frequencies the Ekman pumping velocity is given by

$$w_E = \frac{\mathbf{n} \cdot (\nabla \Lambda \tau)}{pf} \quad (14)$$

In contrast to the other atmospheric forcing terms, the wind stress curl has typically little energy at the synoptic scale but much energy at smaller scales. Thus Ekman pumping will generate mainly small-scale SST anomalies, with maximum effects at high latitudes where the wind is strong. Scaling arguments, as well as the numerical simulations of Haney *et al.* [1983], suggest that the Ekman pumping has negligible effects on the large-scale SST anomalies. It should be noted that changes in the thermocline depth may become dominant in upwelling regions, but this is outside the scope of this study,

where we emphasize SST anomaly development in central ocean conditions.

2.3. Damping and Feedback Mechanisms

Although the physics of mixing and feedback processes are different, their dynamical role is basically similar: both processes control the amplitude of the SST anomalies and their persistence. Some of the relevant mechanisms are discussed below.

Horizontal mixing. In (9), horizontal mixing has been represented by an eddy diffusivity term that parameterizes the dispersive effect of “unresolved” motions. Obuko [1971] has summarized data from instantaneous dye release experiments in the oceanic mixed layer, which suggest an increase of the apparent diffusivity with the scale of diffusion; the available length scale extended to 200 km, where κ reaches $200 \text{ m}^2 \text{ s}^{-1}$. There is no evidence that the results can be extrapolated to include the dispersive effects of the strongly nonhomogeneous eddy field. Admittedly, our use of an eddy diffusivity is a poor parameterization of the effect of horizontal mixing. It is nonetheless likely that $\kappa = 500 \text{ m}^2 \text{ s}^{-1}$ gives a reasonable upper bound for central ocean mixing at scales $\geq O(1000 \text{ km})$. This corresponds to a SST anomaly decay time at least one order of magnitude larger than that observed (section 3). Hence horizontal mixing should play a negligible role in the damping

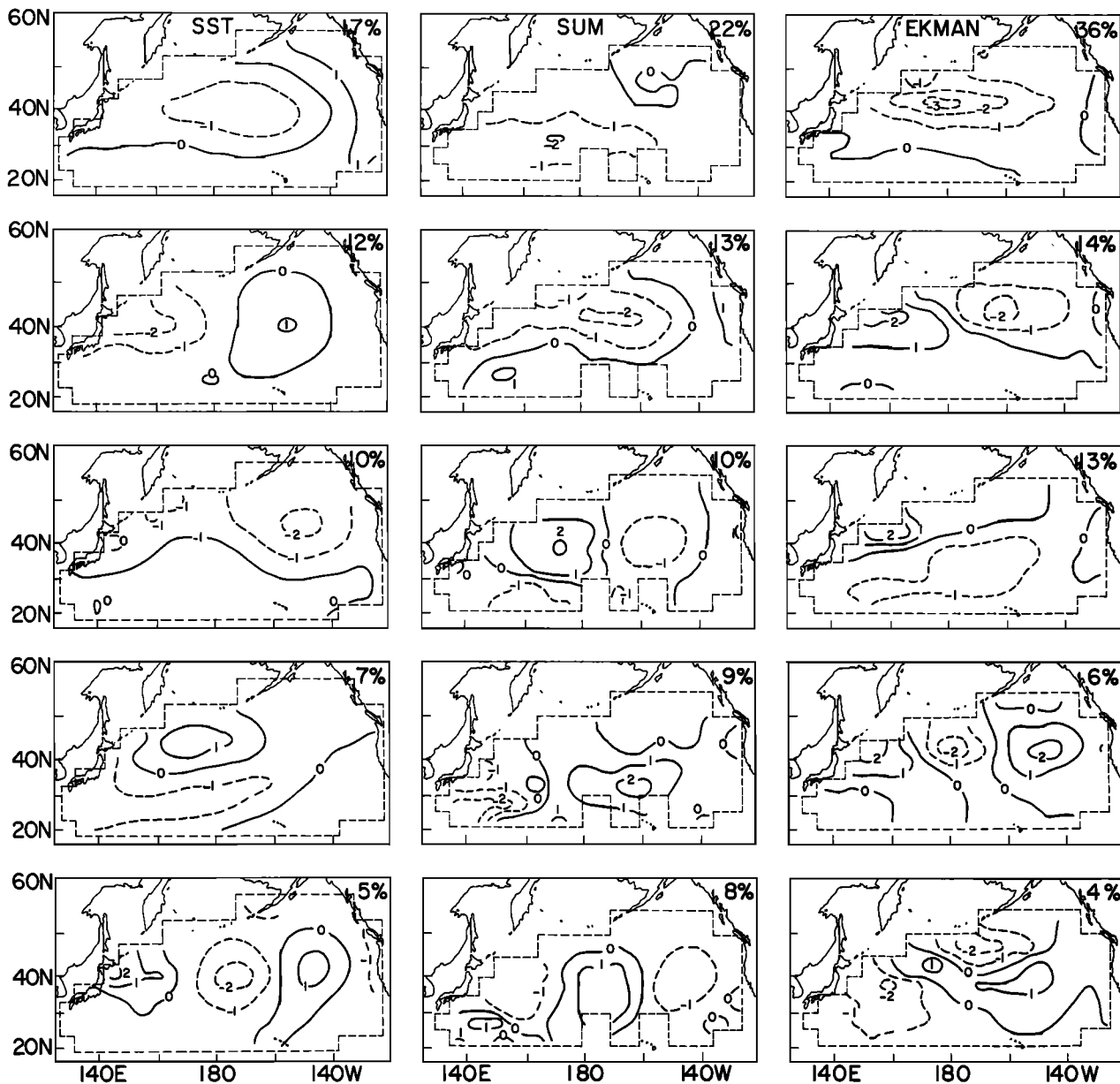


Fig. 8. First five empirical orthogonal functions (EOF's) of anomalies (left) in SST, (middle) in the sum of heat flux plus Ekman transport forcing (reflecting primarily the heat flux forcing), and (right) in Ekman transport from monthly data. The percentage of the variance accounted for by each EOF is in the upper right corner [from Frankignoul and Reynolds, 1983].

of large-scale SST anomalies. This disagrees with Adem's [1970, 1975] claim that horizontal mixing is important for SST anomaly modeling. However, Adem was using too large a value for κ ($3 \times 10^4 \text{ m}^2 \text{ s}^{-1}$) in his numerical simulations. Daly [1978] found indeed with a more realistic model that the inclusion of such a high horizontal diffusivity always led to a deterioration of the SST anomaly hindcasts.

Entrainment effects. Since by definition the entrainment velocity is a positive defined quantity, the mean entrainment term $(T' - T_+)' \bar{w}_e / \bar{h}$ in (9) is normally positive during the mixed-layer deepening season and zero otherwise, causing a seasonal damping of the SST anomalies. Indeed, let us first assume that there is no temperature anomaly in the seasonal thermocline ($T_+' = 0$). Then, the magnitude of an SST anomaly will decay exponentially with time as $e^{-\lambda_e t}$, where

$$\lambda_e = \bar{w}_e / \bar{h} \quad (15)$$

Neglecting in a first approximation the divergence term entering the definition (4) of the entrainment velocity, we can estimate the damping factor (15) from the mean rate of mixed-layer deepening. Figure 5 shows that at weather ship P (50°N , 145°W), λ_e increases from zero in summer to a maximum of about $2 \times 10^{-7} \text{ s}^{-1}$ in early fall (a 2-month decay time) and then decreases slowly and tapers off to zero by late winter. We have used monthly mean mixed-layer depth given by Levitus [1982] to estimate roughly the yearly average of the damping factor λ_e over the North Pacific. Values correspond typically to a 5- or 6-month decay time, with an increase in the south-east North Pacific (Figure 10). The observed SST anomaly damping time is about 2 times shorter than these values (sec-

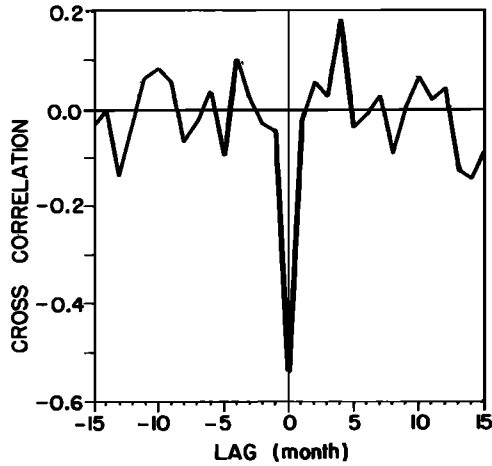


Fig. 9. Cross correlation between monthly anomalies in the net surface heat flux into the ocean, and in u_*^3 at weather ship N for the period 1954-1970. The monthly means were obtained from daily averaged fluxes estimated with bulk formulae.

tion 3); hence the entrainment damping is likely to play a major role in the SST anomaly dynamics. Of course, Figure 10 is only indicative, since divergence effects have been neglected, and we have assumed that there was no temperature anomaly in the seasonal thermocline or, from a statistical point of view, that T' and T_+' are uncorrelated.

A lack of correlation between T' and T_+' is only plausible in a first approximation if vertical mixing is important in the seasonal thermocline and/or if anomalies are rapidly advected away. Otherwise, T_+' will have the same sign as T' during the preceding winter, which would favor the reappearance of the anomaly during the following fall when the mixed layer deepens again [Namias and Born, 1970]. White and Walker [1974] have found some evidence of downward propagation of temperature anomalies into the thermocline at a speed of 50-100 m yr⁻¹, consistent with a vertical diffusivity of the order of 2×10^{-5} m² s⁻¹ in the main pycnocline [White and Bernstein, 1981]. These studies are suggestive of significant vertical mixing effects, which could have been modeled by keeping a heat flux term Q_+' in (9). It is difficult to speculate on the net influence of vertical mixing on the SST anomaly behavior, since it will increase the SST anomaly damping but reduce the strength of the entrainment flux via a positive correlation between T' and T_+' . In any case, SST anomaly data [Namias and Born, 1970; Walsh and Richman, 1981] clearly

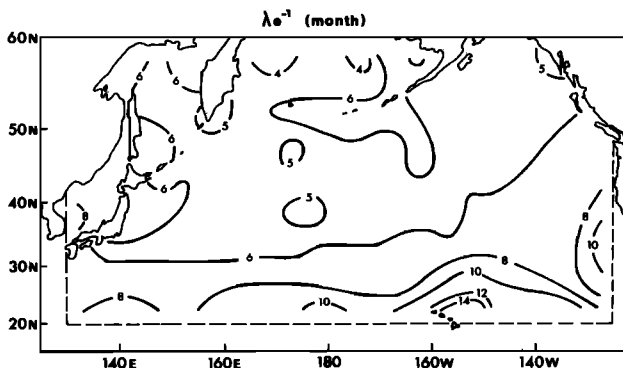


Fig. 10. Yearly averaged value of $\lambda_Q^{-1} = [\bar{w}_e/\bar{h}]^{-1}$ estimated for the North Pacific (in months).

show a seasonal modulation of the damping rate and in particular the expected fast decay in the deepening season (Figure 11).

Atmospheric feedback. Since mid-latitude SST anomalies have some influence on the atmospheric circulation on the hemispheric scale, it is somewhat misleading to discuss how the atmospheric response can locally enhance or destroy the SST anomalies. However, this section may shed some light on the SST anomaly behavior and will prepare for the more thorough investigation of feedback effects in section 4.2.

The main feedback between SST anomalies and atmospheric forcing arises through the surface heat flux term A in (9). This can be evaluated by considering the change in the heat flux forcing term induced by T' , which is given formally by

$$\lambda_Q = \frac{\partial}{\partial T'} \left\langle \frac{Q'}{\rho C_p \bar{h}} \right\rangle \quad (16)$$

where a positive value indicates negative feedback. Because the heat flux has primarily a much shorter time scale than T' , λ_Q should be estimated on the SST anomaly time scale. Anticipating the approach of section 3.3, we have used the angle brackets to denote ensemble mean for given T' , or an average over many realizations of the atmospheric fields. Assuming in a first approximation that the surface wind field is not affected by T' , we find from (12) that the feedback due to the sensible heat flux is given by

$$\lambda_{Q_s} \approx \frac{\rho^a C_p^a C_s u^a}{\rho C_p \bar{h}} \frac{\partial}{\partial T'} (T' - \langle T^a \rangle) \quad (17)$$

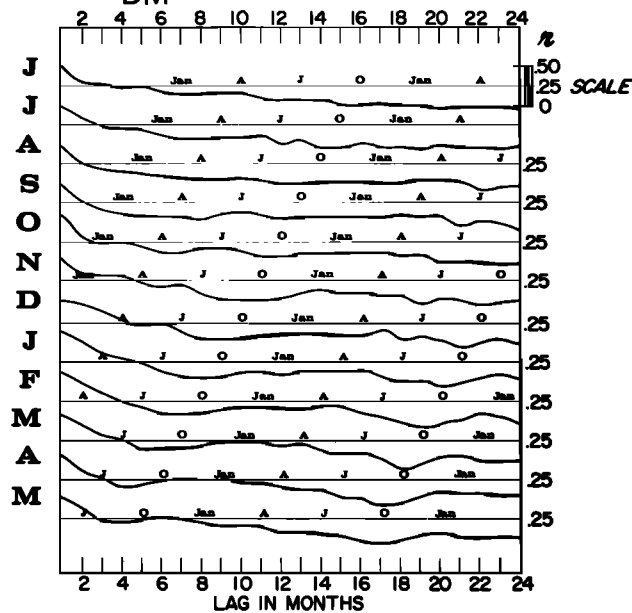
where u^a denotes an appropriate mean wind velocity. To find similarly the feedback due to the evaporation, we have to estimate how the specific humidity in (11) will be affected by the SST anomaly. For simplicity, we assume that the relative humidity R_h remains constant and use the Clausius-Clapeyron equation to relate the saturation vapor pressure to the temperature. To first order in T'/\bar{T} , we find

$$q_s' - q^a \approx \frac{1.2 \times 10^{10}}{\bar{T}^2} e^{-5388/\bar{T}} (T' - R_h T^a) \quad (18)$$

(we have neglected the effect of a mean air-sea temperature difference). Unless $|\langle T^a \rangle|$ is larger than $|T'|$, the feedback via the turbulent heat fluxes is always negative.

The degree of adjustment of the air temperature to a change in SST mainly determines the feedback strength, which depends therefore on the thermodynamics of the atmospheric boundary layer and on the dynamical response of the troposphere to vertical transports of heat. If the air temperature were not affected by the presence of an SST anomaly ($\partial \langle T^a \rangle / \partial T' = 0$), the turbulent heat fluxes would cause a strong negative feedback. For $C_s = C_L = 1.3 \times 10^{-3}$, $\bar{T} = 290^\circ\text{K}$, $R_h = 0.8$, $u^a = 8$ m s⁻¹, $\bar{h} = 60$ m, one finds $\lambda_{Q_s} + \lambda_{Q_L} = 2.1 \times 10^{-7}$ s⁻¹, which corresponds to a ~ 1.8 -month decay time. However, the air temperature adjusts somewhat to the SST, and the negative feedback should be weaker. Because of the difficulties in separating cause and effect in field data, there has been no direct estimate of the air temperature adjustment from observations. An estimate can be obtained from prescribed change experiments made with atmospheric GCM's, since in these experiments (discussed in more detail in section 4.4) the SST anomaly remains fixed. In the experiments of Kutzbach et al. [1977] with the National Center for Atmospheric Research (NCAR) model, the mean change in air temperature was about three quarters of the imposed SST

STANDARDIZED NORTH PACIFIC
SST_{DM} LAG CORRELATION



ANOMALY OF SST_{DM} LAG IN MONTHS

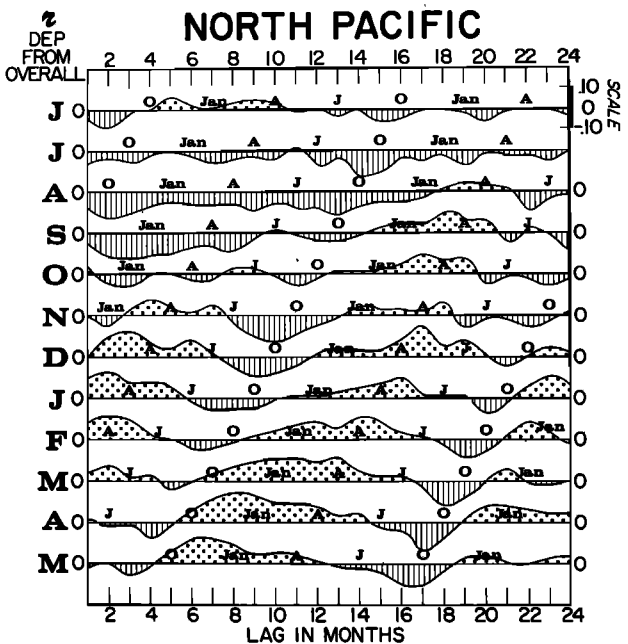


Fig. 11. (Left) Autocorrelation of 5° × 5° monthly SST anomaly in the North Pacific (averaged standardized values) according to initial month, beginning with June. (Right) Deviation of individual months' autocorrelations from the overall autocorrelation, beginning with June [from Namias and Born, 1970].

anomaly, and the mean change in turbulent heat flux was about 20 W m⁻² °C⁻¹, yielding $\lambda_{Q_s} + \lambda_{Q_L} = 8 \times 10^{-8} \text{ s}^{-1}$, or a 4.6-month decay time [Frankignoul, 1979]. However, different GCM's behave differently. Figure 12 suggests a somewhat weaker feedback in the anomaly experiment with the Goddard Laboratory for Atmospheric Sciences (GLAS) model discussed by Shukla and Bangaru [1979]. Here the change in net surface heat flux was about 16 W m⁻² °C⁻¹ (note that the apparent lack of scatter in Figure 12 arises from the data presentation). In an experiment with the Goddard Institute for Space Studies (GISS) model II [Frankignoul, 1985] there was no simple relation between SST and surface heat flux anomalies, so that the concept of a local feedback was not directly applicable.

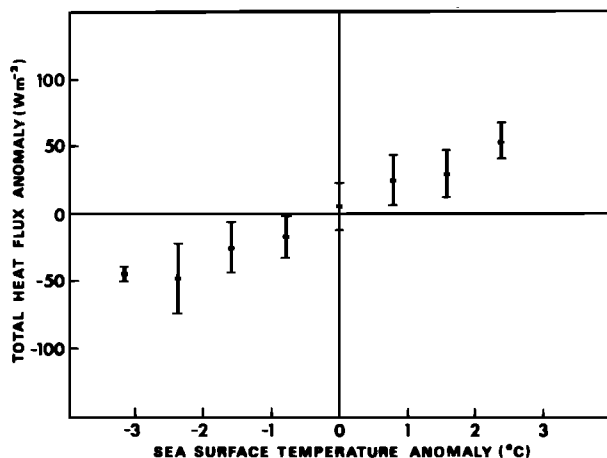


Fig. 12. Changes in the net surface heat flux versus SST anomaly in mid-latitude experiments with the GLAS model. Grid point values have been grouped into 1°C intervals, and only the standard deviations of the heat flux anomalies are indicated (from J. Shukla, personal communication, 1983).

SST anomaly-induced changes in the radiation fluxes or the atmospheric forcing may also cause feedback. Namias [1963, 1969, 1976] has argued that warm SST anomalies increase sensible and latent heat exchanges and hence increase the cloudiness and favor cyclogenesis; cold SST anomalies would have the opposite effects. Since shortwave radiation generally dominates the net radiation balance, this would normally create a negative feedback. However, causes and effects are not unambiguously differentiated in this scenario, and we know of no reliable observation on the relation between cloudiness and SST anomalies in the middle latitudes. Some GCM results have suggested an increase in cyclonic activity and precipitation above warm SST anomalies in mid-latitudes [Chervin et al., 1980] (see also Salmon and Hendershott [1976]). In the GLAS GCM, however, the shortwave radiation does not seem to contribute to feedback, whereas the back radiation contributes a weak negative feedback (J. Shukla, personal communication, 1983).

A different mechanism has been postulated by Bjerknes [1959], who argues that a cyclonic wind anomaly will induce divergent Ekman current on the oceanic surface layer and hence upwelling, "thus exposing the water at the ocean surface to more mixing with the cold water." Conversely, an anticyclonic wind anomaly should create downwelling. Since warm (cold) SST anomaly may increase (decrease) the cyclonicity (see discussion above), the associated change in Ekman pumping could act as a negative feedback. However, we expect this effect to be very small.

2.4. The Eddy Noise

At moderate and large scales the oceanic variability at depth is dominated by quasi-geostrophic "mesoscale" eddies. The eddy field is strongly inhomogeneous, with a high variance near the western boundary currents and less eddy activity in the central and eastern parts of the oceans [Richman

et al., 1977]. The importance of the eddy modulation of the SST depends therefore on the geographical position. Near the Gulf Stream the eddy signal is so strong that the meandering of the stream and the formation and evolution of rings can be routinely monitored from satellite SST observations [e.g., Maul *et al.*, 1978]. In more quiet regions the eddy distortion of the mixed layer is smaller but still contributes significantly to the SST variability [Voorhis *et al.*, 1976; Frankignoul, 1981].

The main eddy signal appears to be the distortion of the surface temperature pattern by the eddy surface current v_g' , which is represented by term B in equation (9). The temperature gradient is generally dominated by the mean meridional temperature gradient $\nabla\bar{T}$; thus the dominant eddy signal is $-v_g' \partial\bar{T}/\partial y$. Since eddy currents become more zonal at low frequencies as a consequence of the β effect [Rhines, 1977], the eddy modulation of the SST should become less effective on time scales larger than a few years. The eddy modulation should be largest in winter and spring, when the meridional temperature gradient is maximum.

Eddies may also change the SST by advecting vertically the mixed-layer base and modifying entrainment. Stevenson [1983] found that the maximum modulation in typical Mid-Ocean Dynamics Experiment (MODE) conditions occurred in the fall, with an amplitude of about 0.35°C. Using $v_g = 0.1 \text{ m s}^{-1}$, $\nabla\bar{T} = 5 \times 10^{-6} \text{ }^\circ\text{C m}^{-1}$, and a characteristic frequency of 2 cycles yr^{-1} , we find for comparison that horizontal advection effects have a typical amplitude of 1.25°C. This signal is much larger and compares well with the amplitude of the observed mesoscale SST changes.

Since the characteristic length scale of eddy currents is much shorter than that of the atmospheric forcing fields discussed above, the eddy signal can be considered in the present context as a low-frequency, short-scale noise. Most climatological studies are based on SST anomaly data averaged over rather large grids, typically $5^\circ \times 5^\circ$. Except in data-poor regions or near strong oceanic fronts, the spatial averaging made to construct such gridded data appears sufficient to largely filter out the eddy noise.

3. SEA SURFACE TEMPERATURE ANOMALY MODELING

We shall distinguish three ways of modeling SST anomalies. The most accurate approach is to solve numerically the system of equations (2), (3), (5), and (7), which determine the mixed-layer evolution for given initial conditions and hourly or daily atmospheric forcing. This has been done quite successfully with one-dimensional models of the mixed layer; advection was either prescribed or neglected. Unfortunately, only a few data sets provide sufficiently detailed and accurate atmospheric and oceanic data for this purpose.

The second approach consists of estimating the terms in (9) with monthly or seasonal anomaly data, which is equivalent to using a low-passed filtered version of the governing equations. Unfortunately, the mixed-layer dynamics is not linear at short time scales, and only limited accuracy can be expected. Also, only part of the forcing terms can be estimated on the ocean basin scale. Monthly maps of the surface wind can be estimated from synoptic data or from ship reports, but their accuracy is questionable. Monthly values of SST and surface heat flux are even less accurate, and there are practically no data on the mixed-layer depth variability.

The third approach is a statistical one in which the governing equations are used to predict the mean statistical properties of SST anomalies rather than to simulate deterministically particular realizations of the air-sea interaction pro-

cesses. The analysis is greatly simplified by the fact that on the time scale of SST anomalies the atmospheric forcing in middle latitudes can be represented, to a first approximation, as a stochastic white noise process.

Following a chronological order, we shall first review briefly the deterministic studies that were made with time-averaged data and then discuss a few results obtained with numerical models of the mixed layer. The bulk of this section is devoted to the statistical studies. It should be stressed that these three approaches correspond only to different ways of looking at the same problem and the same physical mechanisms.

3.1. Case Studies of Large-Scale SST Anomaly Developments

The first attempts at modeling the evolution of SST anomalies were made by Namias [1959, 1965], who tried to reproduce observed cases of monthly or seasonal SST anomaly changes in the North Pacific. In these studies, Namias considered only the advection of the mean temperature gradient by anomalous surface currents that he had estimated from monthly maps of surface geostrophic wind. Jacob [1967] suggested that the inclusion of advection by the mean current and anomalous heating would improve the simulations. Later, Namias [1972] discussed a case where the mean advection along the North Pacific gyre seemed to play a major role while heat exchanges had only small effects. Different results were obtained by Adem [e.g., Adem, 1970, 1975], who found with his strongly diffusive model (section 2.3) that heat forcing alone led to some predictive skill, whereas horizontal advection brought no improvement. Clark [1972] has discussed more systematically a few case studies in the North Pacific, also using monthly or seasonal data. His results suggest that SST anomalies can be rather well specified from the heat flux forcing. In general, including the effect of anomalous horizontal currents did not improve the simulation when $\partial T/\partial t$ was (properly) estimated by centered differences (Figure 13). Note that in all the above studies, the Ekman advection was overestimated, since Ekman's formula for the surface flow was used (section 2.2) and, indeed, the estimated SST anomalies in

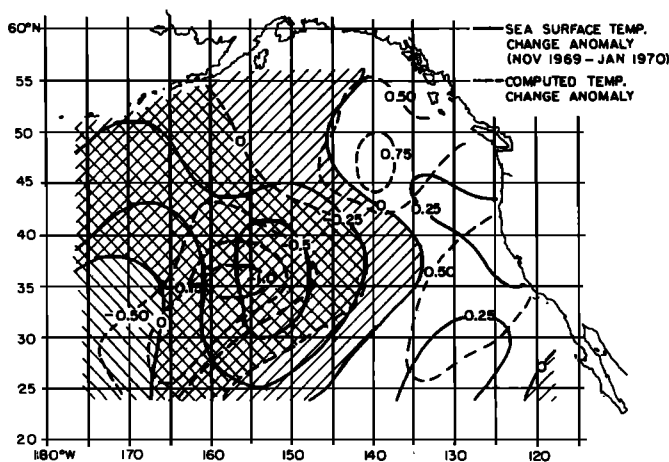


Fig. 13. Isopleths of observed SST anomaly change (degrees Kelvin) for December 1969 (solid lines). The forward slashes show regions of negative temperature anomaly change. Isopleths of SST anomaly change (degrees Kelvin) computed from temperature advection and surface heat transfer (dashed lines). The backward slashes show regions of negative temperature anomaly change [after Clark, 1972].

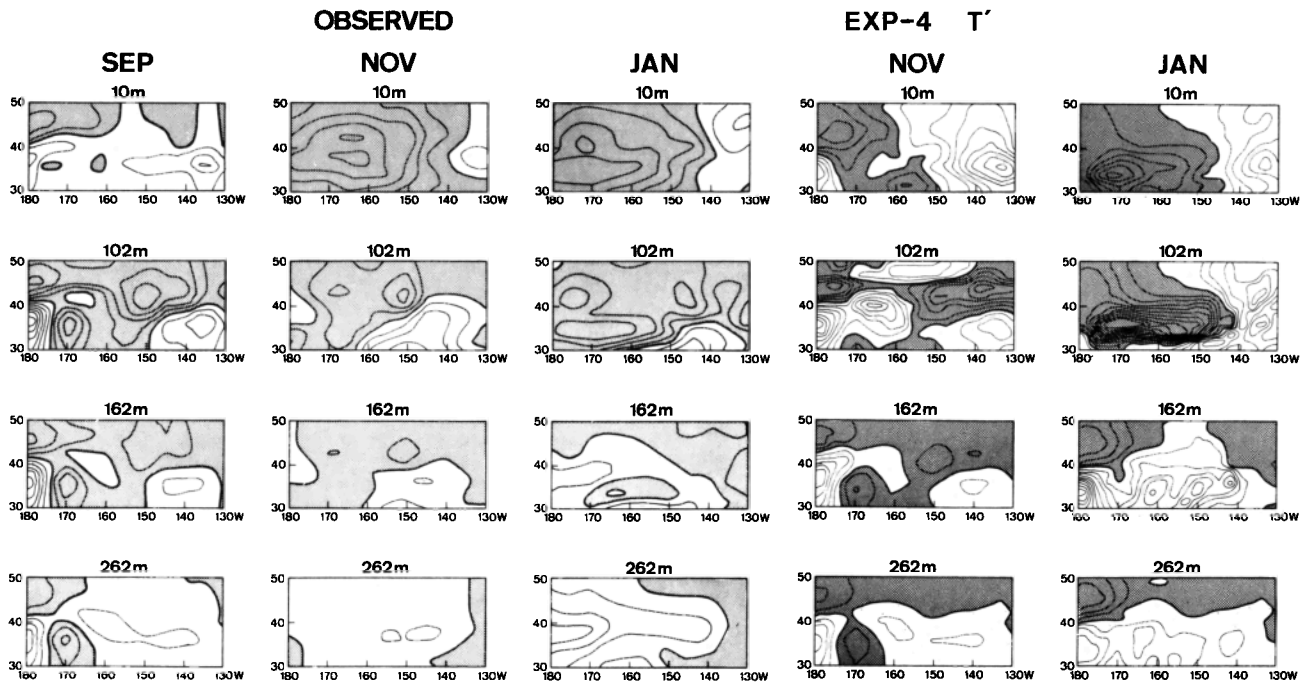


Fig. 14. Monthly mean temperature anomaly observed at different depths in the North Pacific during September 1976 (first column), November 1976 (second column), and January 1977 (third column). Simulated temperature anomaly for November 1976 (fourth column) and January 1977 (fifth column). The contour interval is 0.5°C at 10 m and 0.2°C at the other levels. Negative anomalies are shaded [from Haney, 1980].

the presence of anomalous advection were too large. Clark [1972] also investigated the effect of mixed-layer depth variability by estimating monthly values of $h'Q/h$ at weather ship P. This term turned out to be about 2 times larger than the heat flux forcing term in spring, comparable in summer, and negligible otherwise. The large role of mixed-layer depth variability during the transition between winter and summer regimes (i.e., the appearance of the seasonal thermocline) has been stressed by Elsberry and Garwood [1978]. Three cases of SST anomalies in the North Atlantic have been thoroughly investigated by Daly [1978]. He could not estimate the effect of mixed-layer depth variability, but he considered the other terms in (9). The model predictions compared well with observations for forcing by anomalous heating and advection. The contributions of the two mechanisms were comparable, presumably because the cases are in high-latitude winter conditions where the wind is strong; Ekman pumping did not seem to contribute significantly to the SST anomaly changes.

With the development of multilevel ocean circulation models, more sophisticated case studies of large-scale SST anomalies have been undertaken for the North Pacific. Except for convective adjustment, there is practically no representation of the mixed-layer physics in the work by Haney et al. [1978] and Huang [1979], but a crude parameterization of wind mixing was introduced by Haney [1980]. These models had been spun up to a seasonally varying steady state. Case studies of SST anomalies were carried out by prescribing an additional anomalous forcing field interpolated from observed monthly means, and/or an initial SST anomaly configuration. Haney et al. [1978] and Huang [1979] mainly investigated the effect of anomalous advection, while Haney [1980] also included anomalous heat exchanges and wind mixing. Haney's simulation of the SST anomaly observed in the North Pacific during fall and winter 1976–1977 is reproduced in Figure 14. The anomaly patterns are well simulated at the upper levels

where the water is well mixed, but the amplitude is too large, possibly due to an overestimation of wind mixing and vertical mixing. The latter mechanism and, to a lesser extent, surface cooling were contributing most to the SST anomaly development. Even though such calculations are rather spectacular, they hardly bring more understanding than the earlier diagnostic studies. However, Haney [1985] has recently made a 10-year simulation using winds from a 6-hourly surface analysis, which represents the daily weather fluctuations. Although the hindcast SST anomalies have a much too small amplitude because the heat flux forcing was neglected, they correlate well with the observations, demonstrating that the use of tridimen-

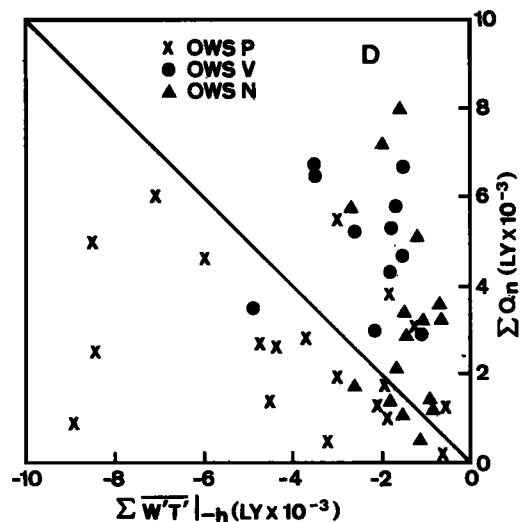


Fig. 15. Cumulative net surface heat flux (from observations) versus cumulative entrainment heat flux at the base of the mixed layer (from model) for 49 case studies of oceanic response to strong wind events [from Camp and Elsberry, 1978].

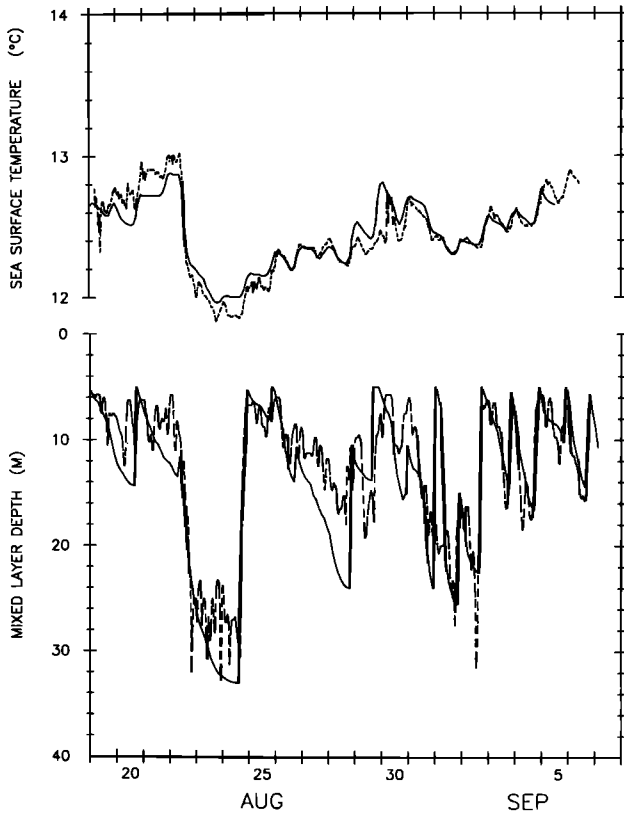


Fig. 16. Best fit model (solid curve) and observed (dashed) temperature and mixed-layer depth during MILE [from Davis *et al.*, 1981].

sional ocean GCM's has become rewarding for SST anomaly studies.

3.2. Numerical Simulations of the Mixed-Layer Variability

There is a large body of work on the numerical simulation of the dynamics of the upper oceanic layers with one-dimensional mixed-layer models. Here we review a few hindcasting studies of the day-to-day changes in the mixed layer which document the main mechanisms of SST variability. A variety of mixed-layer models have been used, ranging from the "integral" models of Pollard *et al.* [1973] and Niiler [1975] to the turbulent closure model of Mellor and Durbin [1975]. These models have been reviewed by, for example, Niiler and Kraus [1977] and Garwood [1979]; hence no emphasis will be given to the model peculiarities or the value of the different tunable parameters that they contain.

Denman and Miyake [1973] first tested a mixed-layer model with observed meteorological data. They considered a 12-day period during spring at weather ship P when shortwave radiation and wind mixing dominate and were able to reproduce very well the observed mixed-layer response. Longer simulations of observed SST variability were made by Thompson [1976, 1977], who simulated 1-year SST observations at weather ship N (30°N, 140°W) with several mixed-layer models. The SST changes were well replicated, but that was largely due to the fact that the calculated SST was used with the observed air temperature to estimate the surface heat fluxes (11) and (12), so the model SST was strongly constrained to agree with the observed one (in view of the strong feedback

discussed in section 2.3 and the good correlation between SST and air temperature). The mixed-layer depth was rather poorly reproduced.

A systematic investigation of the relative importance of heat flux versus wind forcing was carried out by Camp and Elsberry [1978], who simulated 49 cases of oceanic response at weather ships N, P, and V to strong wind events of 10- to 30-day duration during September–December. The best hindcasts were obtained at weather ships N and P (rms errors of 0.35°C for SST and 7 m for the mixed-layer depth) presumably because of the large current and the stronger eddy activity at weather ship V (34°N, 164°E). At weather ship N and to a lesser extent at V the surface heat flux dominated the entrainment flux at the mixed-layer base (terms C–E in (9)), whereas the mechanical forcing dominated at weather ship P (Figure 15); this is related to the geographic location of the three weather ships. When the wind is stronger as in hurricanes, entrainment dominates even more the SST changes, although upwelling and horizontal advection may also become important [Price, 1981].

Horizontal or vertical advection can play a significant role in less extreme conditions, as shown, for example, by Davis *et al.* [1981] in a study of the MILE data at weather ship P. The Mixed-Layer Experiment (MILE) data are the most accurate and complete data set to date on mixed-layer variability, including near-surface currents and direct radiation measurements. During the experiment the air-sea heat exchanges were strongly dominated by the shortwave radiation. However, the heating alone could not explain the observed changes in the heat content which were also influenced by vertical advection, especially during storms. After correcting for advection, Davis *et al.* [1981] were able to simulate very successfully the observed changes in the mixed layer (Figure 16).

Unfortunately, the longer data sets available at weather ships are of lesser quality, without radiation or current measurements. Their use generally results in a heat budget imbalance and a lack of accuracy of mixed-layer model hindcasts, in particular over long periods. This is discussed by C. Frankignoul and M. A. Cane (unpublished manuscript, 1985), who also showed that although the daily heat flux changes are slightly more efficient in generating SST anomalies at weather ship N than the daily changes in the wind energy input, satisfactory simulations could be obtained by keeping the short time scale fluctuations in only one of the two forcing mechanisms and using climatological values for the other. This reflects the good correlation between Q' and u_*^3 (Figure 9) and may explain why good simulations of SST anomaly changes have often been made in case studies with only part of the atmospheric forcing. Note again that if the SST anomaly equations were linear, the mixed-layer models would generate at low frequencies the same anomalies as in the case studies based on averaged data.

3.3. Stochastic Models and the Statistical Properties of SST Anomalies

Because of the irregular and unpredictable character of the weather fluctuations, it is useful to interpret the SST anomalies as a stochastic process. This approach was pioneered by Mitchell [1966], but the usefulness of the stochastic modeling approach was only fully perceived when Hasselmann [1976] developed his theory of stochastic climate models. Using a two-time scale formalism, Hasselmann demonstrated that the excitation of the slowly varying climate system by random short time scale weather changes results in long time scale,

random walk climate fluctuations. This concept was applied to large-scale SST anomalies by *Frankignoul and Hasselmann* [1977], who showed that the statistical properties of the observed SST anomalies in the middle latitudes could be well reproduced by considering the response of the upper ocean to the day-to-day changes in the air-sea fluxes.

To introduce the random walk character of the SST anomalies, we write the SST equation in the form

$$dT'/dt = F \quad (19)$$

where F denotes all terms to the right-hand side of (9) (the eddy noise will be neglected). To separate forcing and feedback in (19), we set $F = \langle F \rangle + F'$, where the angle brackets denote ensemble average. Defining $T' = 0$ to correspond to an equilibrium temperature for which $\langle F \rangle = 0$, we expand F with respect to T' . To lowest order in T' , this yields

$$dT'/dt = F' - \lambda T' \quad (20)$$

where F' will be referred to as the atmospheric forcing function and $\lambda \equiv -(\partial \langle F \rangle / \partial T')_{T'=0}$ as the feedback (positive for negative feedback). From (9) and (13), one has

$$F' \approx -\frac{1}{h} \left(\frac{Q'}{\rho C_p} + \frac{(\tau' \Lambda n) \cdot \nabla T}{\rho f} + h' \frac{\partial \bar{T}}{\partial t} + w_e'(T - T_+) \right) \quad (21)$$

where the approximate sign indicates that the feedback contribution of the terms in (21), mainly given by (16), has been subtracted. Note that the feedback λ in (20) also contains an oceanic contribution.

As mentioned earlier, the atmospheric forcing function F' can be represented as a stochastic process with a characteristic time scale τ_F of a few days, much shorter than the SST anomaly time scale τ_T . Thus F' acts in (20) as a white noise generator for time scales much larger than τ_F , which would result in the absence of feedback effects in a linear increase with time of the SST anomaly variance. However, feedback and dissipation play a role, and a statistically stationary SST anomaly response is obtained. *Hasselmann* [1976] has shown that in the general case the evolution of the climate system is governed by a Fokker-Planck equation for the probability density distribution of climate states in the climate phase space. However, the feedback is essentially linear in the case of SST anomalies, so that their statistical properties can be established directly. We first consider the case where the mean advection term in (20) is small and may be neglected and when there is no appreciable seasonal modulation of the forcing and the feedback. The SST anomaly equation then takes the form

$$\partial T' / \partial t = F' - \lambda T' \quad (22)$$

and one has

$$F_{TT}(\omega) \approx \frac{F_{FF}(0)}{\omega^2 + \lambda^2} \quad (23)$$

for $\omega \ll \tau_F^{-1}$ and

$$R_{TT}(\tau) \approx \frac{\Pi}{\lambda} F_{FF}(0) e^{-\lambda|\tau|} \quad (24)$$

for $\tau \gg \tau_F$, where the notation $F_{xx}(\omega)$ denotes the power spectrum of a variable x , and $R_{xy}(\tau) = \langle x(t+\tau)y(t) \rangle$ the covariance between x and y . Since atmospheric spectra are essentially white at periods larger than 10 or 20 days (section 2.2), $F_{FF}(\omega)$ has been taken as a constant at low frequencies (zero frequency limit). At very low frequencies, $\omega \ll \tau_T$, atmospheric spectra may become red, reflecting the long-term variability of

the climate system. In this case, $F_{FF}(\omega)$ can still be considered as constant in (23); however, it now represents the level of forcing in the frequency range $\tau_F^{-1} \ll \omega \ll \tau_T^{-1}$ (two-time scale approximation). Relations (23) and (24) are characteristic of a first-order Markov process and provide a good representation of the SST properties in central ocean conditions (Figure 17). Note that an advantage of this approach is that the validity of the model (22) can be tested without any quantitative information on λ and on the atmospheric forcing fields, since $F_{FF}(0)$ and λ are parameters that can be estimated from SST anomaly data by a least squares fit method [*Reynolds*, 1978, 1979].

When the advection by mean current is not negligible, the SST anomaly spectrum has a more complex shape which depends on the scale dependence of the forcing and feedback processes. Advection creates significant coupling between neighboring regions; hence a nonlocal SST anomaly model must be used in statistical studies. Still, the advective stochastic forcing model can be tested against field data by considering a vector form of (20) [see *Lemke et al.*, 1980]; this approach has been applied successfully by K. Herterich and K. Hasselmann (unpublished manuscript, 1985) to North Pacific SST anomaly data.

The validity of model (20) can also be tested locally if the advection terms are estimated from mean current data. *Frankignoul and Reynolds* [1983] have shown in this manner that the white noise forcing model is consistent with SST anomaly data over practically the whole North Pacific (Figure 18). The variance of the hypothetical white noise atmospheric forcing compared favorably with the parallel estimate of heat flux and Ekman transport forcing in Figure 7, suggesting that these terms contribute substantially to (21); the averaged feedback factor was $(2.7 \text{ months})^{-1}$, consistent with our estimates in section 2.3 based on both oceanic and atmospheric damping, which seem therefore to be comparable.

There is some indication that the SST anomalies of larger spatial scales have more persistence, as illustrated by the trend in λ for successive EOF's in Figure 19, where the lower EOF's are associated with larger scales (see Figure 8). This is consistent with the lower atmospheric feedback predicted at large scales in section 4.2. Note that *Reynolds* [1978] estimated λ in Figure 19 using a nonadvective model, so that the shorter

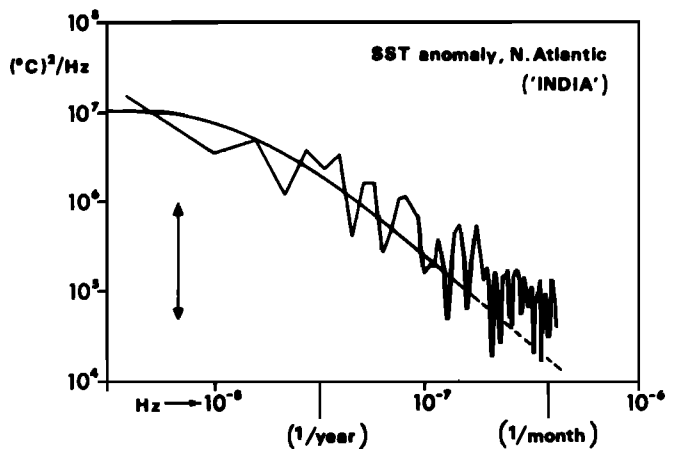


Fig. 17. SST anomaly spectrum at weather ship I (59°N, 19°W) for the period 1949-1964, with 95% confidence interval. The smooth curve was estimated from relation (24) using sensible and latent heat flux forcing only, and $\lambda = (4.5 \text{ month})^{-1}$ [after *Frankignoul and Hasselmann*, 1977].

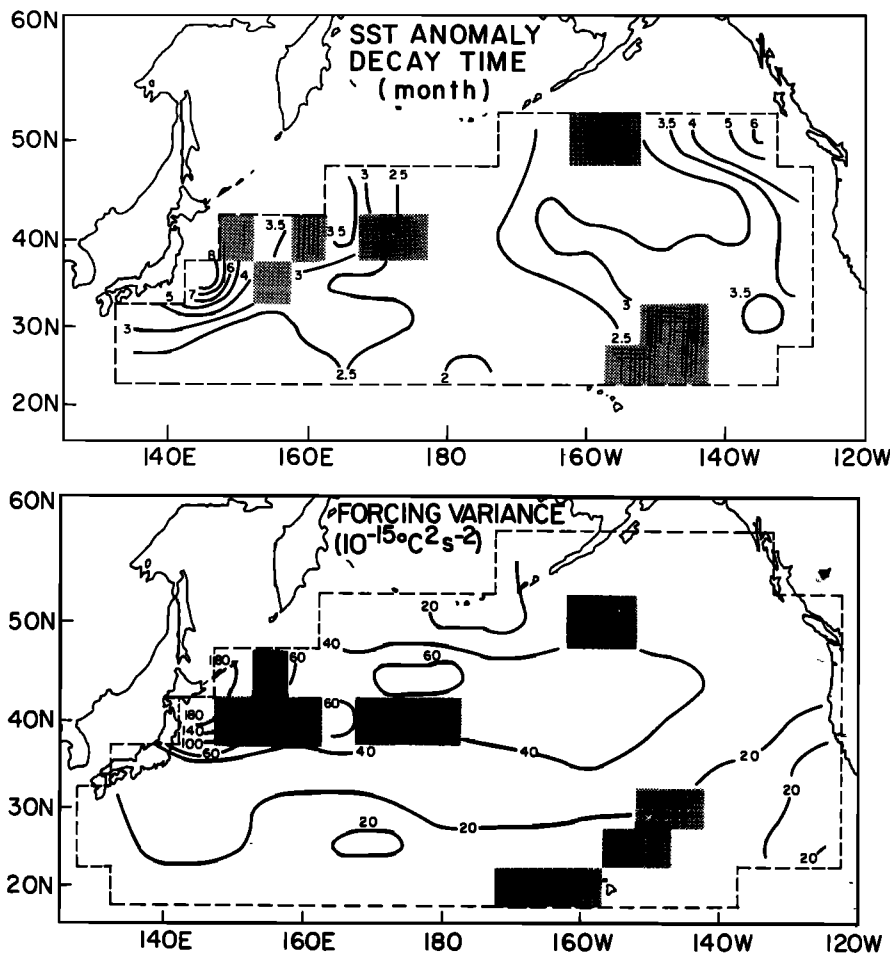


Fig. 18. (Top) Distribution of the anomaly decay time λ^{-1} (in months) estimated with the advective model (21). The SST data for the period 1947–1974 and the mean currents are estimated from ship drift. (Bottom) Distribution of the variance of monthly means (in $10^{-15} \text{ } ^\circ\text{C}^2 \text{ s}^{-2}$), corresponding to the white noise forcing estimated from the local model (23). The variance is practically identical to that obtained with (21) but covers a broader region. Stippled areas indicate where the model is not valid at the 95% level of significance [from Frankignoul and Reynolds, 1983].

lifetime of the smaller EOF patterns may be due in part to advection effects.

Cross correlations and cross spectra provide more determining signatures of cause-and-effect relationships than spectral shapes, and it was indeed by correlation analysis of sea level pressure and SST anomalies (plus a related predictability study) that Davis [1976] showed convincingly that the atmosphere was driving the SST variability rather than vice versa (Figure 20, top). If advection by the mean currents is neglect-

ed, the covariance between atmospheric forcing and SST anomalies can be derived from (22), which yields

$$\frac{\partial}{\partial \tau} R_{TF} = R_{FF} - \lambda R_{TF} \quad (25)$$

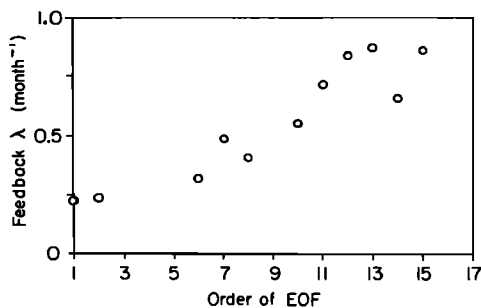


Fig. 19. Fitted value of λ in $(\text{month})^{-1}$ for successive empirical orthogonal functions in the North Pacific that are consistent with (24) at the 95% level of significance [after Reynolds, 1978].

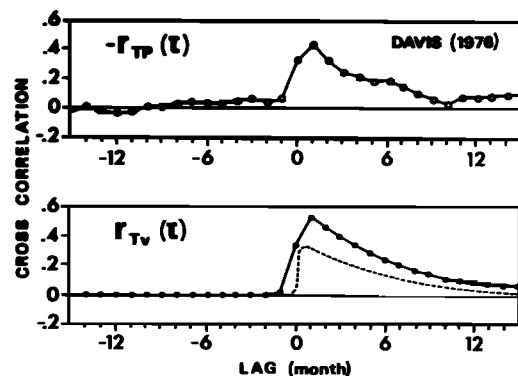


Fig. 20. (Top) Observed correlation between the dominant empirical orthogonal function of SST and sea level pressure anomalies over the North Pacific as estimated by Davis [1976]. (Bottom) Theoretical correlation for $\nu = (8.5 \text{ day})^{-1}$, $\lambda = (6 \text{ month})^{-1}$ without smoothing (dashed line) and as estimated from monthly averaged data (continuous line).

Assuming that F' could itself be represented as a first-order Markov process with a short decay time ν^{-1} , *Frankignoul and Hasselmann* [1977] showed that the cross correlation between T' and F' is, to first order in λ/ν ,

$$\begin{aligned} r_{TF} &\approx (\lambda/\nu)^{1/2} e^{\nu\tau} & \text{for } \tau \leq 0 \\ r_{TF} &\approx (\lambda/\nu)^{1/2} (2e^{-\lambda\tau} - e^{-\nu\tau}) & \text{for } \tau \geq 0 \end{aligned} \quad (26)$$

with $r_{TF}(\tau) = R_{TF}(\tau)/[R_{TT}(0)R_{FF}(0)]^{1/2}$. When the SST leads the atmospheric forcing, the correlation is negligible; when the SST lags, the correlation has a positive maximum at small lag and then decreases slowly on the SST anomaly time scale. The predicted curve was found to be remarkably similar to that calculated by *Davis*, provided the effect of smoothing (using monthly anomalies) was taken into account (Figure 20, bottom). Since the actual atmospheric function was not known, it was assumed that the pressure is highly correlated in time with (21), which seems reasonable for the dominant EOF. Note here that the zero lag correlation in Figure 20 is quite large for the monthly anomalies, and it would be even larger for seasonal ones, although the SST is completely passive in the model. This is due to averaging and illustrates that large simultaneous correlations between atmospheric and SST anomalies as shown in Figure 2 are not sufficient to distinguish between cause and effect.

In general, only some of the atmospheric forcing terms in (19) can be estimated from data, and they also may contribute to the feedback. Since data separation between forcing and feedback cannot be done easily, the "known" atmospheric forcing must be allowed to contribute to feedback in the correlation analysis. To do so, we write (22) in the form

$$\partial T'/\partial t = H' + m' - \lambda_0 T' \quad (27)$$

where

$$H' = q' - \lambda_a T' \quad (28)$$

is the "known" part of the right-hand side terms in (9) which contribute a feedback term λ_a , q' , and m' are the stochastic forcing terms, and λ_0 is the oceanic feedback. Thus one has $\lambda = \lambda_0 + \lambda_a$, $F' = m' + q'$. For simplicity, we assume that q' and m' can both be represented as first-order Markov processes with the same decay time ν^{-1} , that the variance ratio between q' (or, to first order, H') and m' is n^2 , and that their

correlation is γ . Then, one has $R_{qq}(\tau) = n^2 R_{mm}(\tau)$, $R_{mq}(\tau) = \gamma n R_{mm}(\tau)$. If λ_a and λ_0 are $\lesssim O(\lambda)$ and $n \sim O(1)$, one finds

$$\begin{aligned} r_{TH}(\tau) &\approx \left(\frac{\lambda}{\nu}\right)^{1/2} \frac{(n+\gamma)}{(1+2n\gamma+n^2)^{1/2}} e^{\nu\tau} \\ &\quad - \frac{(1+2n\gamma+n^2)^{1/2} \lambda_a}{n(\nu\lambda)^{1/2}} e^{\lambda\tau} & \text{for } \tau \leq 0 \\ r_{TH}(\tau) &\approx \left(\frac{\lambda}{\nu}\right)^{1/2} \frac{(n+\gamma)}{(1+2n\gamma+n^2)^{1/2}} (2e^{-\lambda\tau} - e^{-\nu\tau}) \\ &\quad - \frac{(1+2n\gamma+n^2)^{1/2} \lambda_a}{n(\nu\lambda)^{1/2}} e^{-\lambda\tau} & \text{for } \tau \geq 0 \end{aligned} \quad (29)$$

Relation (29) is illustrated in Figure 21. Although the exact shape of the cross-correlation function depends on the parameters n^2 and γ , its general structure is solely determined by the relative value of λ_a . When the "known" atmospheric forcing function H' does not contribute to feedback ($\lambda_a = 0$), r_{TH} resembles (26) with a smaller amplitude. When H' contributes a negative feedback ($\lambda_a > 0$) as expected for the heat flux, the correlation function takes a more antisymmetric appearance with zero crossing near zero lag, negative values when SST leads, positive when it lags. Finally, if H' were contributing a positive feedback, r_{TH} would peak when SST lags but have the same positive sign throughout. As in (26), smoothing will increase the expected correlations and shift the maxima toward lags of 1.

Although (29) has not been compared rigorously with field data, it was used successfully by *Frankignoul and Reynolds* [1983] to interpret the correlations between the dominant EOF's in Figure 8. In particular, some of the correlations between SST and heat flux had the antisymmetric aspect expected from a negative feedback, suggesting that air-sea heat exchanges indeed contribute to damping existing SST anomalies.

An advantage of the stochastic viewpoint is that it links the dynamics directly to SST predictability studies. Indeed, (22) is the usual first-order autoregressive model already used by *Roden and Groves* [1960] to make statistical predictions of ocean temperature, and often considered as the first guess in a sequence of linear models of increasing order. The statistical prediction of SST anomalies and related atmospheric fields has been discussed by *Davis* [1976, 1978] and *Barnett and Hasselmann* [1979]. It is of interest to stress that because SST anomalies are well represented by a stochastic forcing model, the predictability of SST anomaly changes is limited. As discussed by *Hasselmann* [1976], the continuous and unpredictable forcing by the atmosphere induces a diffusion in the SST anomaly phase space that rapidly offsets the determinism of the trajectory induced by feedback and advection processes.

The stochastic forcing model may be refined by taking into account the seasonal variability of the feedback (Figure 11) and of the atmospheric forcing. This is discussed by *Ruiz de Elvira and Lemke* [1982], who showed in particular that the covariance function for the SST anomalies then depends on the phase of the annual cycle. The cyclostationary model represents significantly the autocovariances of SST anomalies in practically all the mid-latitude Pacific and explains in particular the secondary peaks observed at time lags of about 12 months [*Ortiz and Ruiz de Elvira*, 1985]. *Barnett* [1981a] has also shown how a seasonal dependence improved SST predictability studies.

Another formal refinement in the stochastic forcing model

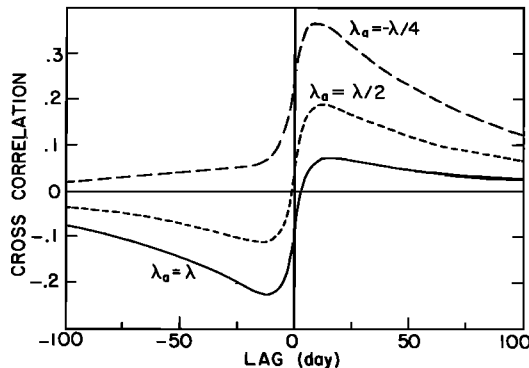


Fig. 21. Predicted correlation between the atmospheric forcing term H' in (28) and the SST anomalies for $\nu = (4 \text{ day})^{-1}$, $\lambda = (80 \text{ day})^{-1}$, $\gamma = 0$, and $n^2 = 2$. The solid line corresponds to the case where the known function H' includes all feedback, the short-dashed line to the case where H' contributes half the net negative feedback, and the long-dashed line to the case where H' contributes a positive feedback equal to (minus) one-fourth the net negative feedback.

has been proposed by *Blaauboer et al.* [1982], who considered the SST variability induced by stochastic changes in latent and sensible heat flux. Modeling explicitly T^a , q_s , q^a , and u^a in (11) and (12) as stochastic processes, they arrived at an equation similar to (22), except that the feedback was a stochastic coefficient. The solution involves elaborate algebra, but the results are of little interest, since the same SST response could be obtained by computing the fluxes directly from the bulk formulae.

4. ATMOSPHERIC RESPONSE TO SST ANOMALIES

Since the work of *Smagorinsky* [1953] the response of the atmosphere to large-scale, zonally asymmetric heating has been investigated in numerous studies. Most investigations were aimed at determining the origin of the large quasi-stationary planetary waves observed in the northern hemisphere atmospheric circulation, which can be forced by topography [*Charney and Eliassen*, 1949] and by the diabatic heating associated with land and sea thermal contrast. A broad variety of atmospheric models has been used, ranging from simple linear wave models to high-resolution GCM's. In linear wave models, a zonally symmetric basic state is generally prescribed, and the steady state perturbation response is calculated for given asymmetric forcing. In general, the diabatic heating is prescribed from observations. The earlier models are rather crude, often a β plane channel atmosphere in uniform zonal motion. However, the propagation of planetary waves is very sensitive to the vertical and meridional structure of the mean zonal wind [*Charney and Drazin*, 1961; *Dickinson*, 1968], and most recent work has been based on numerical models with a realistic basic zonal flow. Many simulations of the northern hemisphere winter show a rather good agreement with the observations, and it is generally agreed that the relative importance of topographic forcing increases with altitude [e.g., *Lin*, 1982], while thermal effects dominate near the sur-

face [*Held*, 1983]. In the northern hemisphere summer, diabatic heating seems to be the predominant forcing mechanism for the stationary waves [*Egger*, 1978].

A similar variety of atmospheric models has been used to investigate the extent to which the interannual variability of the stationary waves can be attributed to the influence of sea surface temperature anomalies. Since SST anomalies and the associated changes in the diabatic heating are small, linear wave models seem better adapted to this problem. However, there is much uncertainty in the link between SST and diabatic heating anomalies in the middle latitudes, and rather arbitrary relationships have to be assumed. The problem does not occur with GCM's, since heat exchanges, cloudiness, and precipitation are calculated. Unfortunately, the atmospheric response is small, and it is difficult to distinguish the signal forced by the SST anomaly from the model natural variability. Thus linear wave models and GCM each have serious drawbacks, and satisfactory results may not be achieved until the two approaches are combined.

The next section introduces the governing equations for the atmospheric response to diabatic heating. After examining how SST anomalies and heating may be related in linear wave models, we introduce the main features of the stationary wave response in the simple framework of a two-layer quasi-geostrophic channel atmosphere. Results with more realistic models are then reviewed briefly.

4.1. Stationary Wave Response to Diabatic Heating Anomalies

The basic equations for large-scale atmospheric motions are the primitive equations on the sphere which can be written in pressure coordinates as

$$\frac{du}{dt} - \left(f + \frac{u \tan \phi}{a} \right) v + \frac{1}{a \cos \phi} \frac{\partial \Phi}{\partial \lambda} = F_u \quad (30)$$

$$\frac{dv}{dt} + \left(f + \frac{u \tan \phi}{a} \right) u + \frac{1}{a} \frac{\partial \Phi}{\partial \phi} = F_v \quad (31)$$

$$\frac{\partial \Phi}{\partial p} + \frac{RT}{P} = 0 \quad (32)$$

$$\frac{1}{a \cos \phi} \frac{\partial u}{\partial \lambda} + \frac{1}{a \cos \phi} \frac{\partial}{\partial \phi} (v \cos \phi) + \frac{\partial \omega}{\partial p} = 0 \quad (33)$$

$$\frac{dT}{dt} - \frac{R}{C_p a_p} \omega T = \frac{q}{C_p a} + F_T \quad (34)$$

with

$$\frac{d}{dt} = \frac{\partial}{\partial t} + \frac{u}{a \cos \phi} \frac{\partial}{\partial \lambda} + \frac{v}{a} \frac{\partial}{\partial \phi} + \omega \frac{\partial}{\partial p} \quad (35)$$

and represent the horizontal momentum equations, the hydrostatic assumption, the continuity equation, and the thermodynamic equation, respectively. Here, $\Phi = gz$ is the geopotential; λ , ϕ , and p represent longitude, latitude and pressure, with $p = \rho^a RT$; a is the earth's radius; $\omega = dp/dt$ is the vertical velocity in the p system; R is the gas constant for air; q is the rate of diabatic heating per unit mass due to radiation, conduction, and phase changes. F_i represents friction and damping processes in the i equation.

In general circulation models, these equations are finite-differenced in space and time. In addition, there are elaborate parameterizations for heating and damping terms of the above and other variables (e.g., water content). In SST anomaly ex-

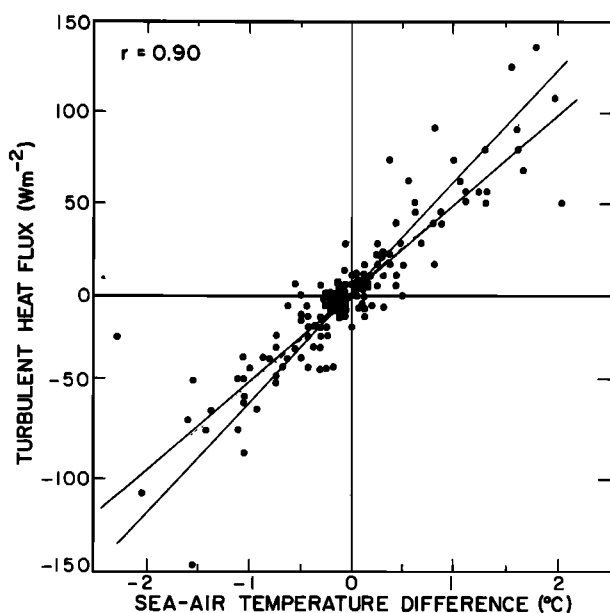


Fig. 22. Scatter plot of monthly anomalies in latent plus sensible heat flux versus sea-air temperature difference at weatherships P, N, and D for the period 1948-1972. The data are for January and July, as estimated by *Esbensen and Reynolds* [1981]. The regression line of each variable on the other is indicated, and r denotes the correlation coefficient.

periments, "anomaly runs" with a prescribed SST anomaly are compared to "control runs" where the sea surface temperature is fixed at its climatological value.

In linear wave models, the atmosphere is in a prescribed steady state, and the heating is treated as a small stationary perturbation. In most studies, the basic state is independent of longitude, and the effect of transient eddies is neglected. If the mean wind is zonal, $\bar{u} = \bar{u}(\phi, p)$, the equations then reduce to

$$\frac{\bar{u}}{a \cos \phi} \frac{\partial u'}{\partial \lambda} + \frac{v'}{a} \frac{\partial \bar{u}}{\partial \phi} + \omega' \frac{\partial \bar{u}}{\partial p} - \left(f + \bar{u} \frac{\tan \phi}{a} \right) v' + \frac{1}{a \cos \phi} \frac{\partial \Phi'}{\partial \lambda} = F_u' \quad (36)$$

$$\frac{\bar{u}}{a \cos \phi} \frac{\partial v'}{\partial \lambda} + \left(f + 2\bar{u} \frac{\tan \phi}{a} \right) u' + \frac{1}{a} \frac{\partial \Phi'}{\partial \phi} = F_v' \quad (37)$$

$$\frac{1}{a \cos \phi} \frac{\partial u'}{\partial \lambda} + \frac{1}{a \cos \phi} \frac{\partial}{\partial \phi} (v' \cos \phi) + \frac{\partial \omega'}{\partial p} = 0 \quad (38)$$

$$\frac{\bar{u}}{a \cos \phi} \frac{\partial T'}{\partial \lambda} + \frac{v'}{a} \frac{\partial \bar{T}}{\partial \phi} + \omega' \frac{\partial \bar{T}}{\partial p} - \frac{R}{C_p a p} \omega' \bar{T} = \frac{q'}{C_p a} + F_T' \quad (39)$$

At the top of the atmosphere the amplitude of the response vanishes. A radiation condition prevents artificial reflections, although a rigid lid condition ($w' = 0$) may suffice in models with very high vertical resolution [Kirwood and Derome, 1977]. In models with limited resolution the rigid lid condition that is generally imposed distorts the tropospheric wave patterns [Nakamura, 1976]. Nonetheless, coarse resolution models have often been used for simplicity, and there is some indication that even two-level models reproduce qualitatively the tropospheric response [Egger, 1977]. At the lower boundary, vertical motions are caused by convergence in the Ekman layer [Charney and Eliassen, 1949], and one has, in the absence of topography,

$$w' = w_E \quad \text{at } p = p_s \quad (40)$$

where w_E is the Ekman pumping.

Elimination of variables in (32), (36)–(40) would show how the anomalous diabatic heating forces the stationary waves. Of interest is that it is the vertical derivative of the heating rate within the atmosphere that plays the dominant role; surface heating also enters the problem (see, for example, Hendon and Hartmann [1982]). Sensitivity studies indicate correspondingly that the stationary wave response strongly depends on the vertical profile of the heating [Smagorinsky, 1953; Sankar Rao and Saltzman, 1969; Hoskins and Karoly, 1981].

Unfortunately, very little is known on the distribution of the heating associated with mid-latitude SST anomalies, and most studies have investigated the influence of an anomaly in the diabatic heating, rather than that of a SST anomaly [e.g., Roads, 1980; Opsteegh and Van den Dool, 1980; Hoskins and Karoly, 1981]. This is useful for studying planetary wave dynamics, but it is not satisfactory for investigating air-sea feedback and the climatic impact of SST anomalies. For this purpose it is crucial to model explicitly the link between SST and diabatic heating.

Observations in the middle latitudes show that the surface heat flux is highly correlated at low frequencies with the air-sea temperature difference. This is illustrated in Figure 22 for the turbulent heat flux at three weatherships; adding the radiation fluxes would only increase slightly the scatter. There was no significant geographical or seasonal dependence in the relation, and only little correlation between heat flux and SST.

Thus we may assume for simplicity that the surface heat flux is roughly given by

$$Q = K^*(T - T^a) \quad (41)$$

with $K^* = 40 \text{ W m}^{-2} \text{ }^\circ\text{K}^{-1}$. This is consistent with a linearization of the bulk formulae (11) and (12) and is in reasonable agreement with the mean heat flux data discussed by Haney [1971]. However, it is the heat released in the atmosphere that determines its response. The sensible heat is primarily inserted in the atmospheric boundary layer and is thus directly related to the sensible heat exchanged at the surface, but the latent heat is only released during rainfall, which may occur remotely from the evaporation.

Lacking observational evidence, some assumptions have to be made for the relation between evaporation and latent heat release. Here we shall assume for simplicity that, at least in winter conditions, the latent heat is mainly released locally. Indeed, it is the case for the climatological fluxes, where the sensible heat flux and the latent heat release estimated from

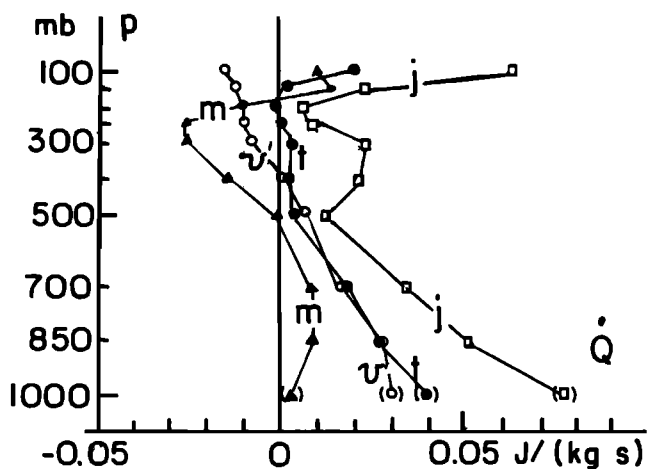
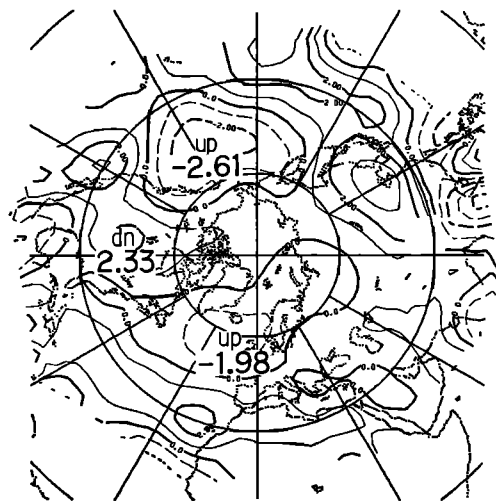


Fig. 23. (Top) Pressure velocity ω ($10^{-4} \text{ mbar s}^{-1}$) at 700 mbar, averaged for nine Januarys, 1971–1979. (Bottom) Vertical profile of the diabatic heating rate above the ocean estimated as the residual in the thermodynamic equation from data for the same nine Januarys (the value shown at 1000 mbar is a rough estimation using surface temperature for seven Januarys from 1973 to 1979). The curve labeled j corresponds to the region between 30°N and 45°N , 135°E and 150°E ; m to $30^\circ\text{--}45^\circ\text{N}$, $180^\circ\text{--}165^\circ\text{W}$; t to $30^\circ\text{--}45^\circ\text{N}$, $75^\circ\text{--}60^\circ\text{W}$; v' to $45^\circ\text{--}60^\circ\text{N}$, $45^\circ\text{--}30^\circ\text{W}$. (From Masuda [1983].)

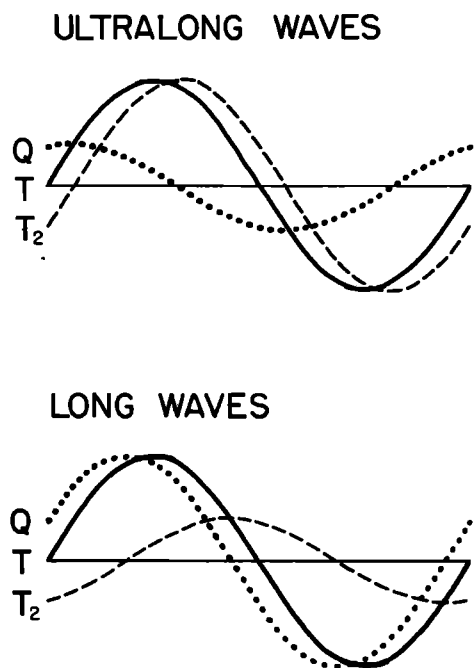


Fig. 24. Sketch of the relative phases and amplitudes of sea surface temperature T , air temperature T_2 , and surface heat flux into the atmosphere, Q , in the two-layer model, in the ultralongwave and longwave limits.

precipitation data are approximately in phase during winter in the middle latitudes but not in the subtropics [Egger, 1976b; Ashe, 1979]. Furthermore, the mean vertical motion is upward above the ocean and downward above continental areas (Figure 23). Thus, even if a SST anomaly was inducing a local subsidence, the net motion would still be ascending, and condensation could occur. Our assumption neglects the effects of water vapor advection but seems roughly consistent with data from the GISS general circulation model II.

Thus, in an admittedly crude approximation, we assume that the diabatic heating anomaly is given by

$$q' = K^*(T' - T^a)f(p) \quad (42)$$

where T^a is air temperature at the bottom of the atmosphere and $f(p)$ a prescribed normalized distribution for the heating. This seems better justified than the in-phase relationship between heating and SST anomalies that has been used by Egger [1977] and others. In (42) the heating depends not only on the SST but also on the dynamical response of the atmosphere, and it may be nonlocal. This interplay between the heating field and the stationary wave response is referred to as the "sensible heating feedback," and it was first considered by Döös [1962].

The vertical distribution of the diabatic heating anomalies can be assumed to be similar to that of the climatological heating. Although the latter is poorly known in the middle latitudes (see discussion in the work by Dickinson [1980]), the

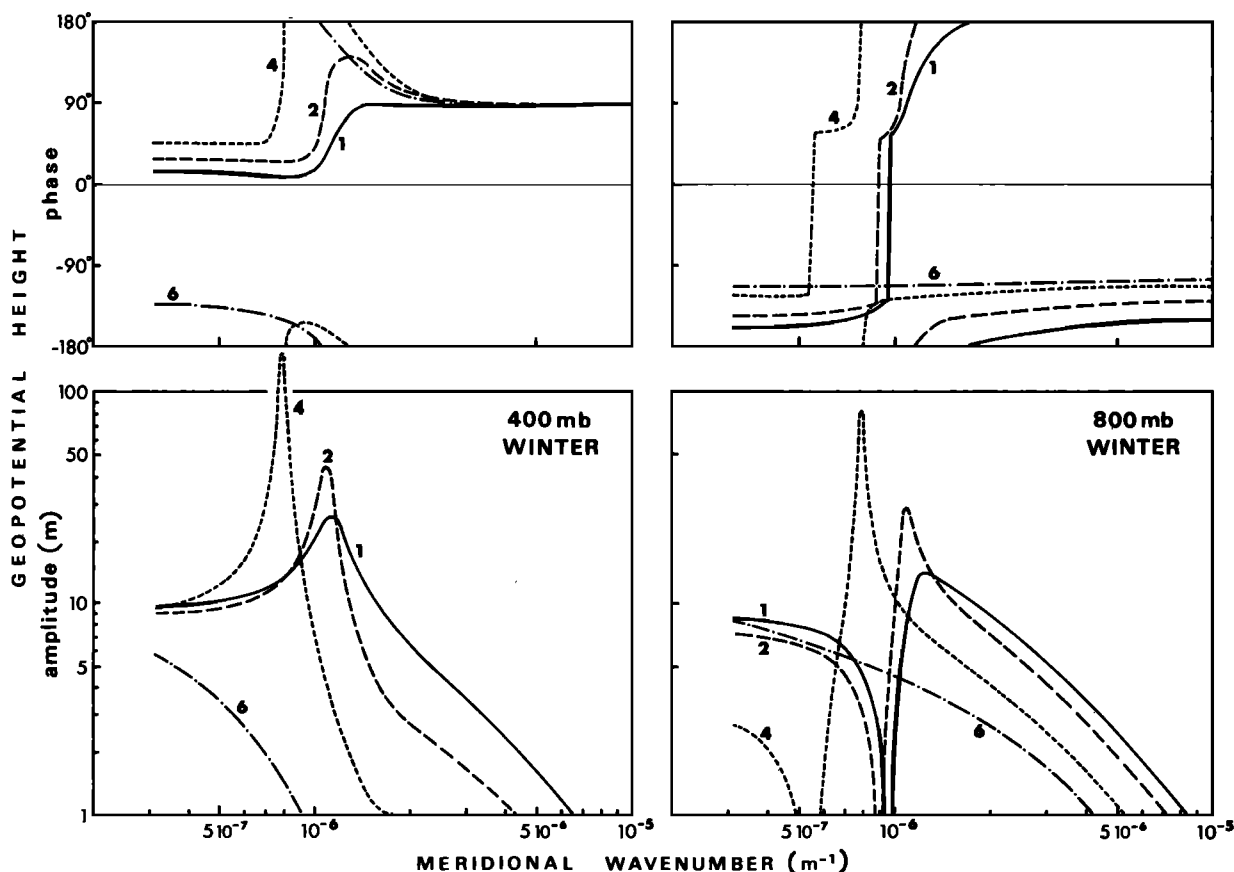


Fig. 25. Geopotential height response (meters) to an SST anomaly of 1°K amplitude for the two-layer β plane model in winter conditions for selected zonal wave numbers: $m = 1$ (solid line), $m = 2$ (long-dashed line), $m = 4$ (short-dashed line), and $m = 6$ (dashed-dotted line). The phase is with respect to the SST anomaly position.

heating mostly occurs below 500 mbar. Figure 23 (bottom) reproduces recent results from Masuda [1983], who remarked that the values above 500 mbar were unrealistic, due to the finite differencing of his data. Because of the above mentioned linear model sensitivity to the heating profile, it may be remarked incidentally that although models with high vertical resolution provide a more accurate representation of the atmospheric response to diabatic heating anomalies, they may not be more realistic than coarse resolution models.

A different type of thermal feedback has been explored by Webster [1981], who argued that latent heat would only be

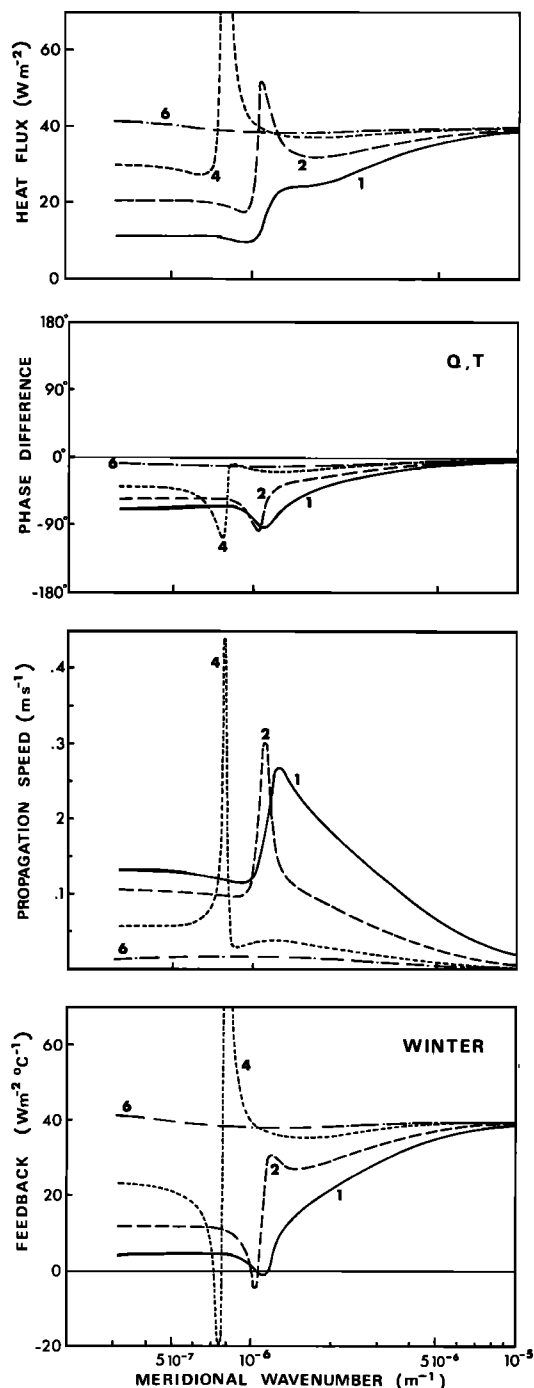


Fig. 26. (From top to bottom) Diabatic heating magnitude, phase difference between surface heat flux and SST, SST propagation speed (positive eastward), and feedback (positive for negative feedback) for the two-layer β plane model. Notations and conditions are as in Figure 25.

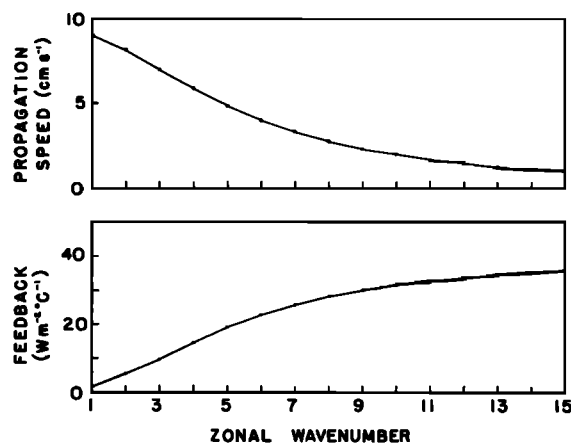


Fig. 27. Approximate value of the SST propagation speed (positive eastward) and feedback (positive for negative feedback) for the continuously stratified β plane model in uniform motion.

released where there is upward motion. To compute the diabatic heating, Webster considered an initial sensible heating anomaly (unfortunately in phase with the SST anomaly) and estimated the latent heating from the model response. The calculation was repeated iteratively with the total heating until a steady state was achieved. This feedback associated with moisture convergence leads to a strong enhancement of the initial heating at low latitudes but is negligible at high latitudes (see also Kang and Han [1984]). During summer it could be important in the lower mid-latitudes [Webster, 1982].

4.2. Air-Sea Feedback in β Plane Models

Several features of the stationary wave response to SST anomalies can be discussed simply by using a two-layer quasi-geostrophic model in the β plane approximation. This analytical model has severe limitations, but in off-resonance conditions it reproduces qualitatively many results of more realistic models [Egger, 1977]. First we describe the model response to diabatic heating, following Derome and Wiin-Nielsen [1971], Egger [1976a], and Roads [1980]. Then we present a new investigation of the model response to SST anomalies and of the resulting air-sea feedback. Since the two-layer model is inadequate when the heating profile changes rapidly with height, we also discuss briefly the feedback in a simple continuous model.

A two-layer model. The atmosphere is represented as a periodic β plane channel with a rigid lid, where the mean zonal wind $\bar{u}(p)$ does not depend on latitude. In the quasi-geostrophic approximation the governing equations for a small stationary disturbance are the linearized vorticity and thermodynamic equations, which are easily derived from (36)–(39):

$$\bar{u} \frac{\partial}{\partial x} \nabla^2 \psi' + \beta \frac{\partial}{\partial x} \psi' - f \frac{\partial}{\partial p} \omega' = 0 \quad (43)$$

$$\bar{u} \frac{\partial}{\partial x} \frac{\partial \psi'}{\partial p} - \frac{\partial \psi'}{\partial x} \frac{\partial \bar{u}}{\partial p} + \frac{\bar{\sigma}}{f} \omega' = \frac{-Rq'}{C_p^a f p} \quad (44)$$

where $\psi' = \Phi'/f$ is the geostrophic stream function and $\bar{\sigma}$ the mean static stability, defined by

$$\bar{\sigma} = \frac{R}{p} \left(\frac{R\bar{T}}{C_p^a p} - \frac{\partial \bar{T}}{\partial p} \right) \quad (45)$$

Internal dissipation is omitted for simplicity. The vorticity is calculated for each layer, and the thermodynamic equation is

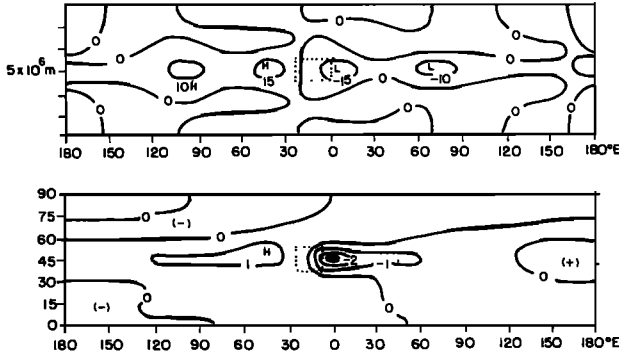


Fig. 28. (Top) Perturbation of the 800 mbar height (meters) due to a rectangular heat source $q/C_p^a \approx 10^{-5} \text{ K s}^{-1}$ (marked by dots) in a frictionless quasi-geostrophic β plane channel ($\bar{u}_1 = 21 \text{ m s}^{-1}$, $\bar{u}_2 = 7 \text{ m s}^{-1}$). (Bottom) Surface pressure perturbation (millibars) in the primitive equation hemispheric model with observed January zonal wind profile [from Egger, 1977].

estimated at the middle level. If the subscripts 1, 2, and 3 denote the upper, middle, and lower levels, respectively, and if $\bar{u}_2 = (\bar{u}_1 + \bar{u}_3)/2$, the system of equations is

$$\bar{u}_1 \frac{\partial}{\partial x} \nabla^2 \psi_1' + \beta \frac{\partial \psi_1'}{\partial x} - \frac{f}{\Delta p} \omega_2' = 0 \quad (46)$$

$$\bar{u}_3 \frac{\partial}{\partial x} \nabla^2 \psi_3' + \beta \frac{\partial \psi_3'}{\partial x} + \frac{f}{\Delta p} \omega_2' + \varepsilon \nabla^2 \psi_3' = 0 \quad (47)$$

$$\bar{u}_3 \frac{\partial}{\partial x} \psi_1' - \bar{u}_1 \frac{\partial}{\partial x} \psi_3' - \bar{\sigma} \frac{\Delta p}{f} \omega_2' = \frac{R \Delta p q'}{C_p^a f p_2} \quad (48)$$

where the surface wind is proportional to u_3 , $\Delta p = p_3 - p_1$, and ε is a surface friction coefficient.

In general, the meridional scale is constrained artificially by the presence of the lateral walls. We prefer to keep it as a continuous variable, and we consider heating anomalies of the form $q' = \bar{q} \cos kx \cos ly$, where $k = m/a \cos \phi$ with $m = 1, 2, \dots$ is the zonal wave number and l a meridional wave number ($K^2 = k^2 + l^2$). Then

$$\psi_i' = \text{Re}(\tilde{\psi}_i e^{ikx}) \cos ly \quad (49)$$

for $i = 1$ and 3 , where one has

$$\tilde{\psi}_1 = - \left[i(K^2 \bar{u}_3 - \beta) + \varepsilon \frac{K^2}{k} \right] \frac{Rf\bar{q}}{C_p^a \bar{\sigma} p_2 \Delta p k D} \quad (50)$$

$$\tilde{\psi}_3 = i(K^2 \bar{u}_1 - \beta) \frac{Rf\bar{q}}{C_p^a \bar{\sigma} p_2 \Delta p k D} \quad (51)$$

with

$$D = K^4 \bar{u}_1 \bar{u}_3 - K^2 \left[\beta(\bar{u}_1 + \bar{u}_3) - \frac{f^2}{\bar{\sigma} \Delta p^2} (\bar{u}_1^2 + \bar{u}_3^2) \right] + \beta \left[\beta - \frac{f^2}{\bar{\sigma} \Delta p^2} (\bar{u}_1 + \bar{u}_3) \right] + \frac{i\varepsilon K^2}{k} \left(K^2 \bar{u}_1 - \beta + \frac{f^2}{\bar{\sigma} \Delta p^2} \bar{u}_3 \right) \quad (52)$$

The atmospheric response to the heating anomaly is easily discussed by considering asymptotic forms of (49)–(52) in the frictionless case. For ultralong waves ($\beta \gg K^2 \bar{u}$) the main vorticity balance is between advection of planetary vorticity and divergence. In the middle latitudes one has $\beta < f^2(\bar{u}_1 + \bar{u}_3)/\bar{\sigma} \Delta p^2$ and $D < 0$; hence the upper stream function ψ_1 is 90° to the east or downstream of the heating, while ψ_3 has the same

amplitude but lies 90° to the west or upstream of the heating. This highly baroclinic response is maximum at the lowest wave numbers, since ψ behaves as k^{-1} . In the thermodynamic equation the mean zonal advection of heat balances the sum of diabatic and adiabatic heatings. The vertical velocity w is out of phase with the heating, while the air temperature T_2 , obtained from (32), is 90° downstream from the heat source.

For shorter waves in the longwave limit ($\beta \ll K^2 \bar{u}$), it is the zonal advection of relative vorticity which balances the divergence effects. Since one has $D > 0$, the phases of ψ_1 and ψ_3 are as above, but now the motion is larger in the lower layer ($\psi_1/\psi_3 \sim \bar{u}_3/\bar{u}_1$), and its amplitude decreases rapidly with decreasing scale. In the thermodynamic equation the main balance is between diabatic heating and adiabatic cooling; w is in phase with the heating, while T_2 is small but still 90° downstream from the heat source.

Resonance occurs between the two limits when $D = 0$. Then, the horizontal advection of heat exactly balances the adiabatic cooling, so that in the frictionless case the diabatic heating cannot be balanced. In mid-latitude conditions, resonance can occur at low zonal wave numbers; the meridional wave number is then slightly smaller than the resonant wave number of the corresponding barotropic flow, which is given by $K^2 = \beta/\bar{u}$ [Egger, 1976a]. The resonant mode is equivalent barotropic, and no resonance is possible for the internal modes. Note that the resonant modes in more realistic zonal flows are still equivalent barotropic [Held, 1983].

Surface friction ($\varepsilon = 0$) causes a shift in the position of the ridges and troughs, a tilt in the vertical axis of the standing waves, and it limits the wave amplitude at resonance. This is discussed by Egger [1976a].

To investigate the planetary wave response to a SST anomaly T' , we use the parameterizations (41)–(42), where the diabatic heating is proportional to the local air-sea temperature difference, in the form

$$q' = \frac{gK^*}{2\Delta p} (T' - T_2') \quad (53)$$

The use of the mid-tropospheric temperature to parameterize the air-sea heat exchange is unsatisfactory but follows from the simplicity of the two-layer quasi-geostrophic model. However, it is not unreasonable, since near-surface and mid-tropospheric temperature fluctuations are normally well correlated and of the same order.

Using the asymptotic results given above, we can link qualitatively the stationary wave response to diabatic heating to the prescribed SST anomaly. Both in the ultralong wave and in the longwave limits, T_2 is 90° downstream of the heating. Equation (53) then implies that this diabatic heating was caused by a SST anomaly also located downstream of the heating. In the ultralong wave limit (Figure 24, top), T_2 is relatively large, and the SST anomaly was located a little less than 90° to the east of the heating. In the long wave limit (Figure 24, bottom), T_2 is relatively small, and the SST anomaly was only slightly downstream of the heating.

To illustrate more quantitatively the model response to an SST anomaly in winter conditions, we have considered an anomaly of 1°K amplitude, $T' = \cos kx \cos ly$, using $\phi = 40^\circ$, $\Delta p = 400 \text{ mbar}$ (the rigid lid is at 200 mbar), $\varepsilon = 2 \times 10^{-6} \text{ s}^{-1}$ (6-day damping time), $\bar{u}_1 = 18 \text{ m s}^{-1}$, $\bar{u}_3 = 6 \text{ m s}^{-1}$, and $\bar{\sigma} = 3 \times 10^{-6} \text{ m}^4 \text{ s}^2 \text{ kg}^{-2}$. For this basic flow, resonance can occur for m between 1 and 5, and it is characterized by a large peak in the amplitude of the geopotential height at the corresponding meridional wave number (Figure 25). Note how easily the

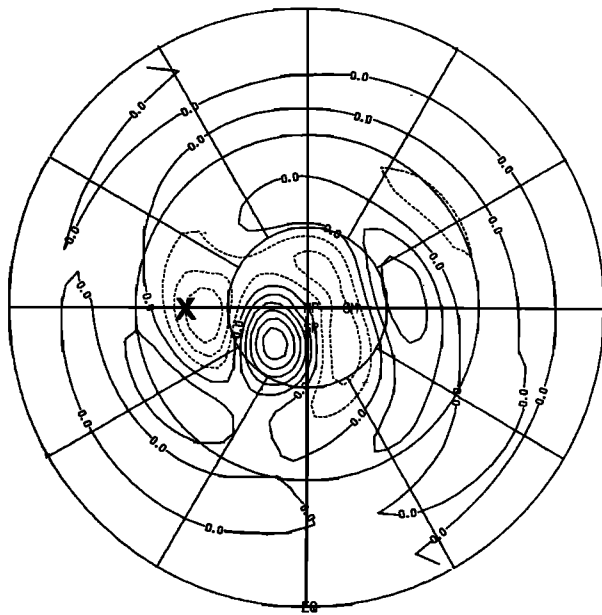


Fig. 29a

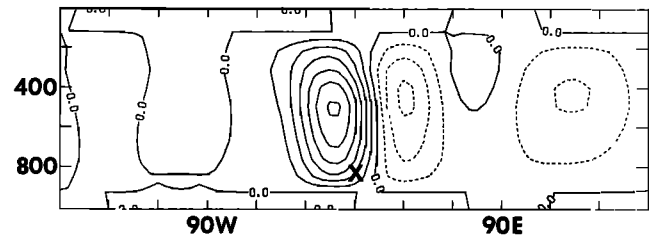


Fig. 29b

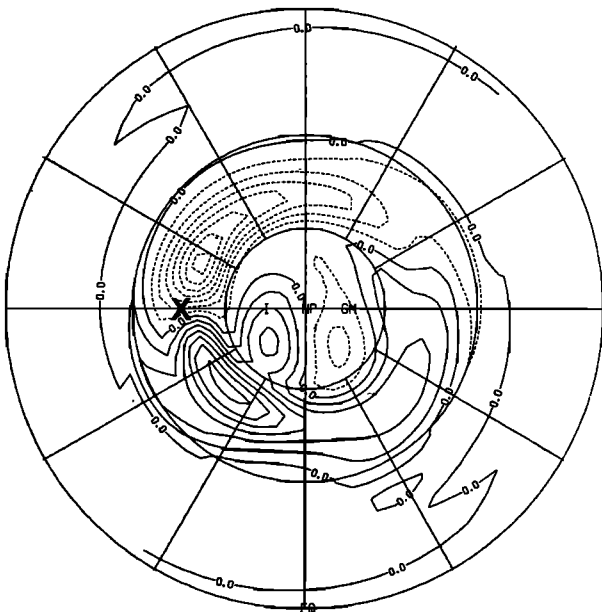


Fig. 29c

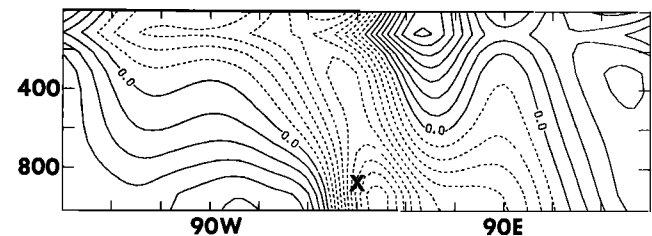


Fig. 29d

Fig. 29. Linear wave response to a large, shallow diabatic heating centered at 46°N on the heavy cross in a 12-level model. (a) The 310 mbar height perturbation (contour interval 40 m). (b) The longitude-pressure section at 46°N of the vertical velocity (contour interval 0.2 mbar h^{-1}). (c) The 928 mbar temperature perturbation (contour interval 1°K). (d) The longitude-pressure section of the height field at 46°N (contour interval 20 m). Negative values are dashed. (From *Hendon and Hartmann* [1982].)

choice of a channel width can be used to tune a β plane model. On the low wave number side of resonance the response has a moderate amplitude, with out-of-phase geopotential height perturbations of about 10 m at each level. On the high wave number side the response decays rapidly with increasing wave numbers, and it is trapped near the surface as predicted by the asymptotic analysis. Figure 25 represents the model response to the unit amplitude SST anomaly. Since the corresponding diabatic heating is wave number dependent and phase shifted with respect to the SST anomaly (Figure 26), the response differs from that to a prescribed heating. For instance, the relatively weak geopotential response found here

at low wave numbers is primarily due to the weakness of the diabatic heating, which in turn is caused by the large air temperature response (see Figure 24). Although our analysis depends on the heating parameterization (53), this suggests that for SST anomalies of reasonable magnitudes, the atmospheric response is relatively small, except near resonance. However, β plane channel models are known to produce an unrealistically large response in resonance conditions, and smaller values would be found if the mean zonal flow had a realistic meridional structure and if meridional propagation was allowed [*Egger, 1977; Held, 1983*].

We can also estimate the back interaction of the atmo-

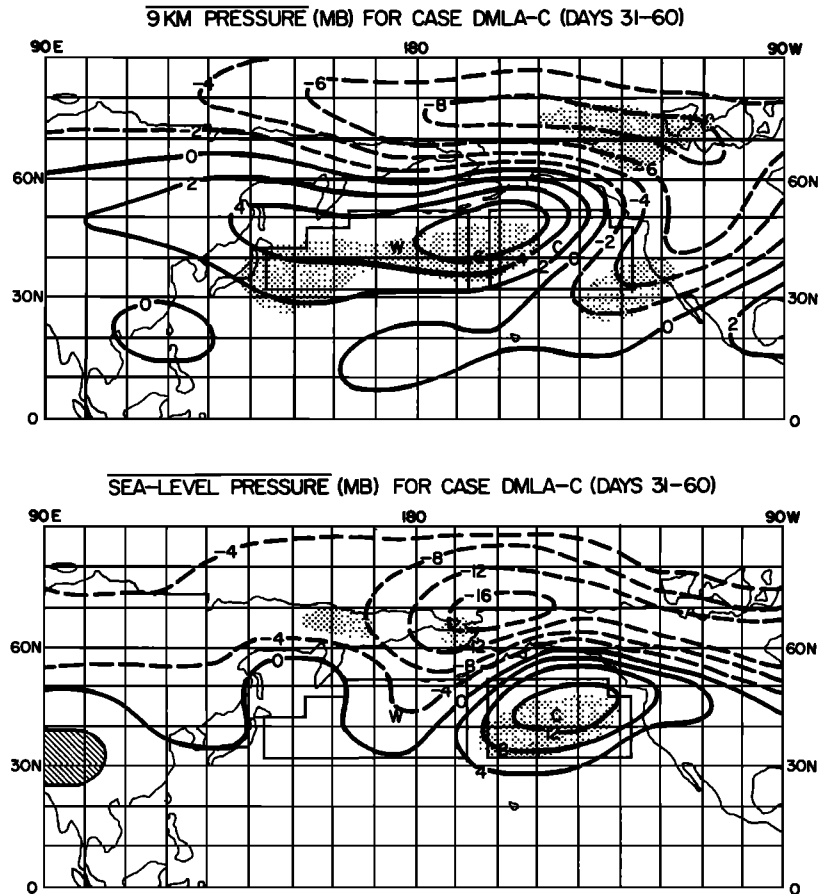


Fig. 30. Geographical distribution of the NCAR model response to a dipole mid-latitude superanomaly (DMLA), one 30-day anomaly run minus one 30-day control run (C) for 9 km pressure and sea level pressure. Stippled areas correspond to rejection of the null hypothesis at the 95% significance level, using a univariate test. The prescribed change region is boldly outlined and labeled with a w for warm anomaly (max 12°C) and c for cold anomaly (max -12°C) [from Chervin et al., 1980].

sphere on the SST anomaly, since heating of the atmosphere corresponds to cooling of the ocean. Its strength depends on the magnitude of the surface heat flux Q' per unit SST and on the phase shift between Q' and T' . The phase shift also tends to cause a zonal propagation of the SST anomaly, if it differs from 0° (negative feedback) or 180° (positive feedback). To evaluate these effects, we consider the simplest model for the SST anomaly, a copper plate mixed layer of constant depth \bar{h} , without advection or dissipation. Then, one has

$$\rho C_p \partial T' / \partial t = -Q' / \bar{h} \quad (54)$$

Now we assume that T' is given by $T' = T'(t) \cos k(x - ct) \cos ly$, and we use the model solutions above to express Q' as a function of T' . These results were obtained for fixed T' but would not be significantly altered if a weak time dependence had been allowed. The SST anomaly is found to decrease exponentially with time and to propagate eastward. Figure 26 illustrates this tendency, using 100 m as typical winter mixed-layer depth. For comparison with section 2.3 the back interaction has been represented as a surface heat flux per unit SST anomaly; damping times are obtained by dividing by $\rho C_p \bar{h}$, so that $40 \text{ W m}^{-2} \text{ } ^\circ\text{K}^{-1}$ corresponds to a 3.9-month decay time. At low wave numbers the heating per unit SST is weak and located west of the SST anomaly (Figure 24); hence there is a weak SST anomaly damping and a rapid eastward phase shift. As resonance is approached, there are large changes, but β

plane models are not reliable near resonance, as pointed out above. At smaller scales the amplitude of the atmospheric response decreases rapidly, which increases the negative feedback and decreases the eastward propagation speed. In the absence of air temperature adjustment the feedback tends to its limiting value K^* .

In summer conditions the mean zonal wind is weaker, and resonance can occur at smaller scales. Otherwise, the atmospheric response is similar to that in winter conditions, but the SST decay time should be shorter because the mixed layer is shallower.

A continuous model. To investigate the effect of near-surface heating, we have also considered an unbounded β plane model of constant Brunt-Väisälä frequency N and in uniform zonal motion \bar{u} , as used by Charney [1973] and Pedlosky [1979]. The heating profile decays exponentially with height and is given in z coordinates by

$$q(z) = \gamma Q e^{-\gamma z} \cos kx \sin ly \quad (55)$$

where Q is the vertically integrated heating. Pedlosky [1979, p. 365] has discussed the stationary response to such heating in much detail; hence no algebra will be given. With a radiation condition at large z , the response consists of a free and a forced part. If the wave number is small, the free part of the stationary wave response propagates vertically; if it is large, the waves are trapped in the vertical. The amplitudes are of

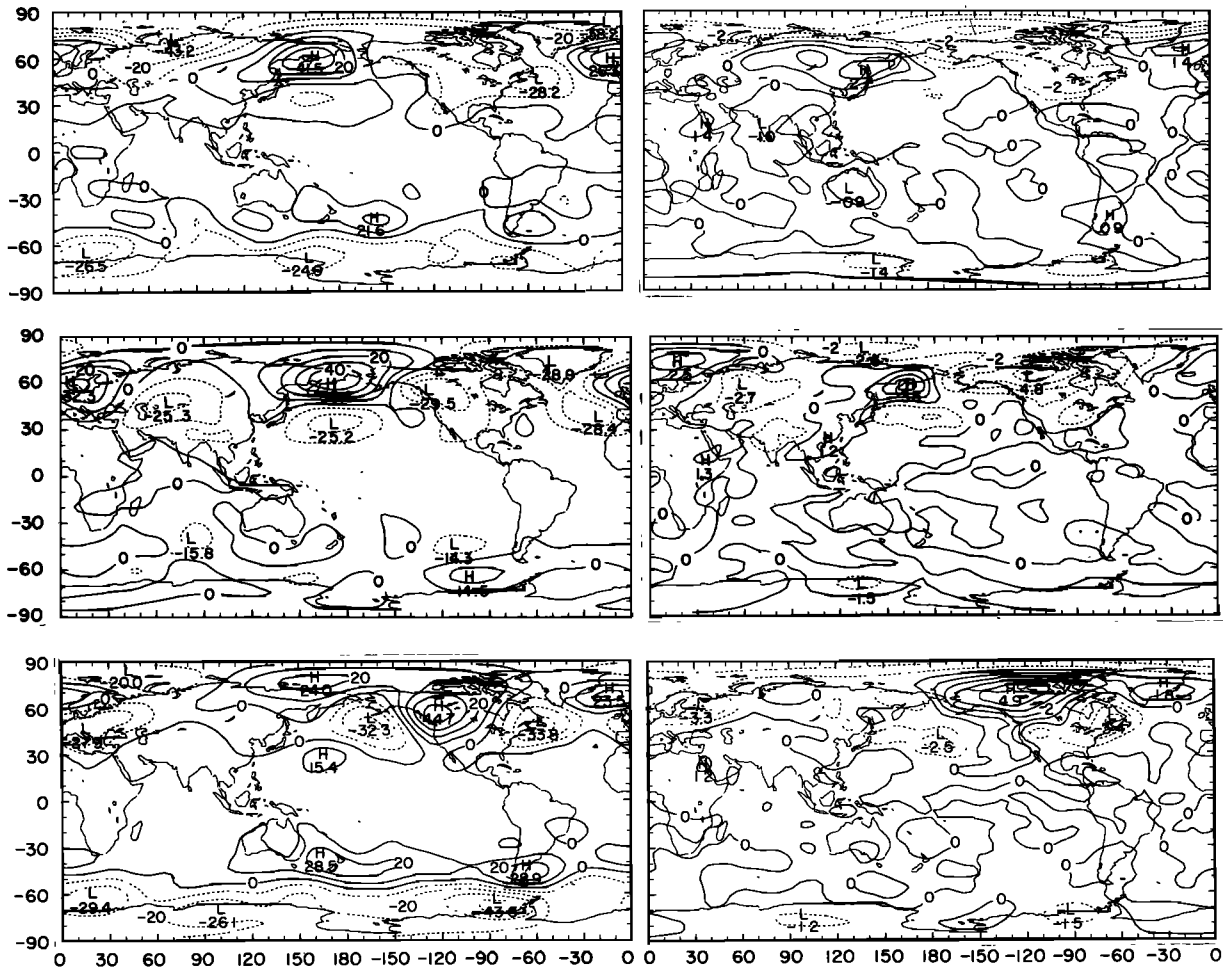


Fig. 31. Geographical distribution of the response of the NCAR Community Climate model to the winter 1976–1977 SST anomaly. Shown are the differences between ensemble means of the cool and control cases (upper panels), the cool-minus-warm (middle panels) cases, and the twice-as-cool-minus-control cases (lower panels) for (left) 700 mbar geopotential height (meters) and (right) surface air temperature (degrees Kelvin) (right). Significance levels are given in the original paper [from Pitcher *et al.*, 1985].

the same order as in the two-layer model, but note that there is no peak at resonance unless γ tends to zero, because the free and forced parts of the solution compensate.

For moderate friction it can be shown that the temperature response near the ground is given to a good approximation by the inviscid limit

$$T^a \approx \frac{\gamma Q}{k\bar{u}C_p^a} \sin kx \sin ly \quad (56)$$

and is approximately one-quarter wavelength east of the heating. If we assume that Q is equal to the surface heat flux and is parameterized by (41), the heating must again be upstream of the SST anomaly. The phase shift $\theta \approx \arctan(\gamma K^*/k\bar{u}C_p^a)$ increases with increasing zonal scale and vertical trapping and decreases with increasing mean zonal velocity, as noted by Döös [1962]. There is no meridional scale dependence. As in the two-layer model, the air-sea heat exchange should damp the SST anomaly and make it propagate eastward. This is illustrated in Figure 27 for $U = 15 \text{ m s}^{-1}$ and $\gamma = 4 \times 10^{-4} \text{ m}^{-1}$. The SST anomaly damping, very weak at large scales, increases with the zonal wave number until it reaches its limit-

ing value K^* . The propagation is always to the east, but the phase speed is low except at the largest scales.

Summary. In view of the simplicity of the β plane models and of assumptions (41) and (42), our results should be viewed with caution. Nonetheless, both models predict that SST anomalies induce only a small atmospheric response. The air-sea coupling causes an SST anomaly damping (weak at large scales, strong at small scales), and it acts as an eastward propagator for the anomalies (faster at large scales). The response to a local SST anomaly should of course depend on its wave number decomposition, and it might have been better depicted by a representation in terms of damped wavetrains. However, a Fourier component representation was preferred because it stresses the scale dependence of the air-sea feedback. As mentioned in section 3.3, the observed SST anomalies are more persistent at larger scales, which is consistent with the weaker atmospheric feedback predicted here at low wave numbers. It is more difficult to find observational evidence of the predicted eastward propagation, because the mean surface currents are also eastward in mid-latitudes.

Note that other air-sea feedback mechanisms have been

suggested. *Pedlosky* [1975] has investigated the interaction between a finite amplitude cyclone wave, the atmospheric zonal flow, the oceanic wind-driven circulation, and an SST anomaly and found that small "seed" SST anomalies could grow by a finite amplitude feedback instability, while they also propagate eastward. However, the model involves drastic assumptions (e.g., baroclinic adjustment of the gyre on the SST anomaly time scale) that are not realistic.

4.3. Linear Wave Response in a Spherical Atmosphere

The spherical geometry and the latitudinal changes in the mean zonal flow can have a strong effect on the meridional propagation of the quasi-stationary waves; hence hemispheric or global models and the observed basic flow must be used to get a more realistic picture of the linear wave response to SST anomalies. Here we shall only survey a few results from published numerical simulations in order to estimate the magnitude of the SST anomaly influence, and the expected air-sea feedback. A good review of quasi-stationary waves in the extratropical atmosphere has been given by *Held* [1983], and the interested reader is referred to it for an elegant discussion of wave propagation, zero-wind line effects, and other important theoretical issues.

As a link to the previous section we first show *Egger's* [1977] comparison between two-layer hemispheric and β plane model responses to a rectangular heat source (Figure 28). Although the response is affected by the spherical geometry and the wind profile, it has the same basic character in the two models. At low levels, a low with warm air is found downstream of the heating, and a high with cool air is seen upstream. However, the downstream low is deeper and the upstream high less intense in the hemispheric model (friction in the channel model would reduce the response by 30%). The differences at the upper level (not shown) were somewhat stronger, due to meridional propagation. As noted by *Roads* [1980], the response to very localized forcing is predominantly an ultralongwave one, as expected from the higher sensitivity of the atmosphere at low wave numbers.

This sensitivity is also demonstrated by *Opsteegh and Van den Dool* [1980], who have discussed the zonal wave number dependence of the linear wave response in another two-layer primitive equation model. Unfortunately, the heat source was latitude independent. Since tropical heating may also have a substantial influence on the middle and high latitudes, provided part of it is in the westerlies [e.g., *Opsteegh and Van den Dool*, 1980; *Webster*, 1981; *Hoskins and Karoly*, 1981], the relative contribution of tropical and extratropical heating is difficult to distinguish. Nonetheless, it appears that, except for a smaller peak near resonance, the hemispheric model behaves roughly in the middle latitudes like the β plane model. *Opsteegh and Van den Dool* [1980] also showed that the atmospheric response to a small-scale heat source was stronger in spring and summer than in winter and fall, because of the weaker mean zonal flow (see also *Webster* [1982]).

An insightful discussion of the linear wave response can be found in the work by *Hoskins and Karoly* [1981]. Using a five-layer primitive equation model, they investigated the effect of a localized thermal forcing at different latitudes and interpreted the results in terms of simple dynamical balances and wave propagation theory. In general, the low-level response was primarily confined to the neighborhood of the heat source, as in Figure 28, while in the upper troposphere the source generated wave trains similar to those given by

barotropic models, which propagate along "great circles." For mid-latitude forcing, the low-level response was shown to be crucially dependent on the vertical distribution of diabatic heating, because of the importance of horizontal advection in the thermal balance. We shall not reproduce *Hoskins and Karoly's* argument explaining why the air should be warm at low levels downstream from a shallow heat source, while it should be cold for a deep source (see also *Held* [1983]), since the shallow heating case is the most relevant to the extratropical regions. The linear wave response to shallow thermal forcing is illustrated in Figure 29 by a similar calculation from *Hendon and Hartmann* [1982], who used a 12-level model. The heat source peaks at 850 mbar and is distributed like a cosine square ellipse of axis 60° longitude and 30° latitude. It has a very large amplitude, corresponding to a 350 W m^{-2} surface flux. The high-level response is dominated by a nearly poleward propagating wave train which amplifies with latitude. There is also an equatorward wave path, better seen in vorticity maps [see *Hoskins and Karoly*, 1981]. This quasi-barotropic response is seen at low levels, but the dominant features near the surface are a low with warm air downstream of the heat source and a high with cold air upstream. The amplitudes are large, but for typical SST anomaly-induced heating they should be moderate, with a geopotential height response of at most 20–30 m, consistent with estimates based on β plane models or on the work by *Opsteegh and Van den Dool* [1980].

Further discussion of the planetary wave response to diabatic heating in a spherical atmosphere can be found in the climatological context. We should stress that several investigations [e.g., *Lindzen et al.*, 1982] have shown that the response was highly sensitive to the profile of the mean zonal wind, so that it is crucial that the latter be correctly specified.

There is some indication that the linear wave responses discussed above remain relevant in more realistic conditions. *Roads* [1980] has investigated the effects of transients and nonlinearities by comparing the response of a very low order two-layer GCM to that of the corresponding linear model. Except when the GCM moved into a linear resonant state, the linear prediction could be detected from the noise. In subsequent experiments with channel models [*Roads*, 1981; *Phillips*, 1982], the linear theory was found to be inadequate to predict the averaged nonlinear response to large forcing when the mean state was baroclinically unstable. However, in more realistic models, linear predictions compare quite favorably with the mean GCM state, as demonstrated for the climatology of the nine σ -level Geophysics Fluid Dynamics Laboratory spectral model by *Nigam* [1983]. Hence the above mentioned discrepancies should be attributed to deficiencies in the channel models and limited sampling. The influence of asymmetries in the basic mean flow has been investigated with a barotropic model by *Simmons* [1982] and *Simmons et al.* [1983] for tropical and subtropical forcing. The climatological standing waves were found to cause local barotropic instabilities in some circumstances, resulting in a low-frequency variability, but this differs from the forced wave response considered here.

The relevance of these studies to the mid-latitude SST anomaly problem is not obvious, since the heating was simply prescribed. If the parameterization (42) had been used, the phase relation between SST and heating would be essentially the same as on the β plane. Indeed, the temperature response in the work by *Opsteegh and Van den Dool* [1980] is about 90° downstream from the heating, and so is the low-level temperature in that by *Hoskins and Karoly* [1981] and *Hendon and*

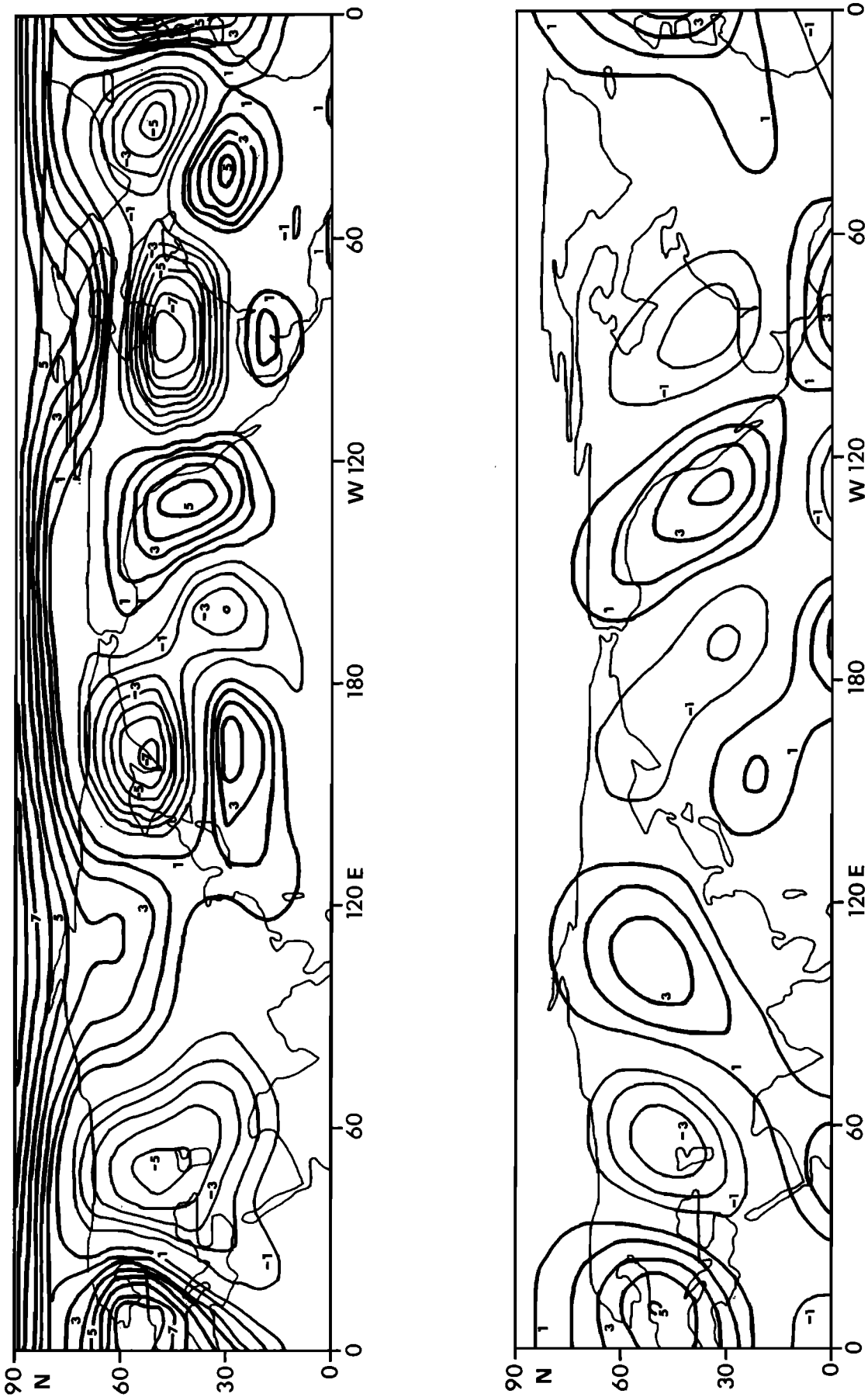


Fig. 32. (Top) Mean change in 200 mbar geopotential height (in tens of meters) for the GISS model II SST anomaly experiment. (Bottom) Significant part of the signal at the 95% level, when projected onto an a priori sequence of large-scale spherical harmonics [from Frankignoul, 1985].

Hartmann [1982] (Figure 29c). Thus the main characters of the air-sea feedback discussed in section 4.2 would remain valid. (Note that *Hendon and Hartmann* [1982] investigated the influence of sensible heating feedback on the response to a prescribed heating, but the link of the initial heating with changes in the boundary conditions was not discussed). It is more difficult to infer the amplitude of the response to SST anomaly forcing. However, a quantitative estimate is provided by a recent study with a two-layer model by *Kang and Han* [1984]. Using a refined version of (41) and (42) based on a linearization of the bulk formulae (11) and (12), they find that an elliptic SST anomaly centered at 40°N (peak at 3°K) creates a maximum 250-mbar height perturbation of less than 30 m (patterns are as in Figure 29a). The dissipation was strong and the truncation severe. Thus one can speculate that height anomalies of up to 20 or even 30 m could be associated with realistic SST anomalies in the middle latitudes. Interestingly, *Kang and Han* [1984] predict that the response would be much larger if the SST anomaly were at the equator, because of the strong cumulus heating feedback in the tropics (section 4.1). Yet, their model response has the same magnitude when the same heating is located in the tropics or in the mid-latitudes. This stresses again the need to represent explicitly the relation of heating to SST anomalies. Relation (41) is admittedly too simple, because it neglects humidity advection, but it stresses that the link is not local in the mid-latitudes.

4.4. GCM Experiments With Prescribed SST Anomalies

The GCM's, which are very similar to the models used for numerical weather prediction, are the most realistic models of the atmospheric circulation. The physical processes are represented in an increasingly complex fashion and include in particular the radiative transports, cloud physics, and boundary layer processes. GCM's have long been unsuccessful in establishing the effects of mid-latitude SST anomalies. However, with the increasing computational capabilities and the development of more powerful statistical analysis procedures, a clearer picture is starting to emerge.

The first experiments with mid-latitude SST anomalies [e.g., *Spar*, 1973; *Houghton et al.*, 1974] were designed to test the observed correlations between atmospheric and oceanic patterns reported by *Namias* [e.g., *Namias*, 1969] and others, but the results were inconclusive because there was no signal-to-noise analysis. Some progress followed the introduction by *Chervin and Schneider* [1976] of a univariate test of statistical significance to analyze GCM results, even though a correct assessment requires the use of multivariate tests [*Hasselmann*, 1979], as discussed below. At first, however, only experiments with highly exaggerated SST anomalies showed some clear-cut results.

Using "superanomalies" of magnitude $\pm 12^\circ\text{C}$ in the six-layer NCAR model, *Chervin et al.* [1976, 1980] and *Kutzbach et al.* [1977] were able to detect both local and hemispheric effects for an SST anomaly in the North Pacific. The mean changes caused by the superanomalies were then used as a reference to interpret the smaller response to somewhat more realistic SST anomalies. The response consisted mainly of a change in the planetary waves, primarily at wave numbers 3 and 4 (Figure 30), a direct thermal circulation with rising motions over warm SST anomalies and, to a lesser extent, sinking motions over cold ones, and an intensification (decrease) of the cyclonic activity above warm (cold) anomalies. The heating

anomalies were nearly in phase with the SST anomalies, implying a straightforward negative feedback for the latter [*Frankignoul*, 1979]. Such a direct behavior for the heating field is not found in more recent GCM's and may be due to the moist convection parameterization in this NCAR model. *Chervin et al.* [1980] showed that some of the features of the response and its amplitude could be predicted with a linear quasi-geostrophic β plane channel, but no signal-to-noise analysis was performed for this intercomparison.

Shukla and Bangaru [1979] have studied the response of the nine σ -level GLAS model to the large SST anomaly observed in the North Pacific during January 1977 (Figure 1). The emphasis was on testing whether the abnormally cold temperatures observed in eastern North America could be reproduced, and there seemed to be some degree of success. However, the relation to the prescribed SST anomaly was not clearly demonstrated. *Rowntree* [1979] has also evaluated the response of the British Meteorological Office's five-layer model to SST changes, but no evidence of a significant response was found for mid-latitude anomalies.

A much larger ensemble of simulations was available in more recent SST anomaly experiments. *Pitcher et al.* [1985] have used the nine σ -level NCAR Community Climate Model to investigate the effect of the large SST anomaly in Figure 1. In different runs the observed SST anomaly pattern was multiplied by 1.8, 3.6, -1.8 , and -3.6 , allowing useful comparisons of the model response (Figure 31). Although the analysis rested only upon univariate tests of significance, it could be established that in the vicinity of the anomaly there was a surface air temperature response of the same sign as the anomaly. Other features are of marginal significance at best: a weak temperature decrease over North America, downstream of the (mainly cold) SST anomaly; a weak high in the 700 mbar height to the north of the negative anomaly, and a weak low to the south. There is also some suggestion of a very weak global response (zonal wave number 2 and Pacific/North American pattern). Tropical SST anomalies were found to be more effective in forcing both a local and a remote response within the model.

Because different grid points and variables in GCM's do not provide independent information, univariate tests are not adequate to evaluate the global significance of sensitivity experiments. However, only a limited number of details (or parameters) can be considered with multivariate tests because the sample size is much smaller than the dimension of the GCM fields, and new analysis strategies had to be devised [*Hasselmann*, 1979; *Preisendorfer and Barnett*, 1983; *Hannoschöck and Frankignoul*, 1985].

A hypothesis-testing strategy where the anticipated GCM response to a prescribed change is represented by an a priori sequence of spherical harmonics was applied by *Hannoschöck and Frankignoul* [1985] to the response of a preliminary version of the GISS GCM (the seven σ -level model I) to the SST anomaly in Figure 1 (also multiplied by 1.8). In perpetual January conditions a significant response could be detected in the northern hemisphere, primarily of zonal wave number 1 character and quasi-barotropic. However, the natural variability in this model was also dominated by the lowest wave numbers, indicating that the model may be very sensitive at large scales.

The more realistic nine σ -level GISS model II was then used with the same SST anomaly [*Frankignoul*, 1985]. Although only a local change in the low-level air temperature could be detected with univariate tests, multivariate testing for an a

priori sequence of large-scale spherical harmonics permitted the detection of a significant tropospheric response. The signal extends throughout the northern hemisphere extratropics and is dominated by zonal wave numbers 3–5 at the 200-mbar level (Figure 32). Results were similar at lower levels, but the signal-to-noise ratio deteriorated rapidly toward the surface. Recent work (C. Frankignoul et al., unpublished manuscript, 1985) shows that the GCM signal can be explained in terms of forced linear waves in a baroclinic model with the GCM zonally averaged basic state, provided the heating anomaly is specified from the experiments. However, the relation between the heating anomaly and the SST anomaly, clearly not a local one, remains to be established.

It can be concluded that GCM's show both a local response to prescribed SST anomalies in the middle latitudes and a weak hemispheric one. The dominant scale of the latter is model dependent, and so are the amplitudes, but this should be explainable by the differences in parameterizations and in mean zonal states. For realistic SST anomalies the geopotential height response should not exceed 10–30 m, as suggested by Figures 30–32. Although it is not yet clear that these GCM results can be entirely predicted with linear wave models, the order of magnitude of the response is comparable. The weakness of the signal explains the difficulties in distinguishing it from the noise, and it is consistent with the limited success of statistical climate forecasts.

5. DISCUSSION

The dynamics of large-scale SST anomalies can be considered to be fairly well understood in the middle latitudes. The SST anomalies primarily reflect the response of the upper ocean to the daily changes in air-sea fluxes. Because of the large thermal inertia of the oceanic mixed layer and the weakness of the dissipation and damping processes, rather large and persistent SST anomalies are generated by the storms and the synoptic weather systems. On the long SST anomaly time scale the weather can be considered in a first approximation as a short time scale stochastic process; hence the SST anomalies have a random walk character.

The fluctuations in the surface heat exchange and the mechanical energy input by the wind are most important for the SST anomaly generation; advection by anomalous Ekman currents is generally less important. The relative strength of the different forcing mechanisms varies with the location and the season, and they should all be included in modeling studies. However, some degree of success has often been achieved with only part of the forcing because of the high correlation between the different atmospheric fields.

The processes responsible for the decay of the SST anomalies are less well understood. Entrainment effects associated with the deepening of the mixed layer and oceanic mixing certainly play an important role, and there is evidence that heat exchange with the atmosphere also contributes to the SST anomaly damping. In this paper we have found that the quasi-stationary wave response to SST anomalies could explain in part their increased persistence at large scales, because the air adjustment to an SST anomaly is largest at the largest scales. This air-sea coupling should also act as an eastward propagator for the large-scale anomalies. However, our analysis rests upon a crude parameterization of the relationship between SST anomalies and diabatic heating of the atmosphere, and further study is needed.

Three approaches used to model the evolution of SST anomalies have been reviewed. Case studies are based upon

monthly or seasonal maps of the large-scale SST and atmospheric anomalies. They can be rather satisfactory, but they suffer from the difficulty in estimating nonlinear relations (in the atmospheric forcing or the oceanic response) from low-passed atmospheric data. The problem does not arise when information on the daily weather changes is available. Thus simulations with one-dimensional mixed-layer models have been successful. However, for an accurate simulation of the long-term SST changes, advection must be taken into account. Because of the white noise character of the atmospheric forcing, the stochastic forcing models have also been quite successful, and they provide a useful link with the statistical predictability studies. For a detailed hindcasting or forecasting of the SST anomaly changes, the most suitable modeling tool is nonetheless a three-dimensional ocean model with an embedded mixed layer, provided that the forcing by synoptic weather events is taken into account explicitly.

To limit our topics, we have not discussed the connections between mid-latitude and tropical anomalies, although the global character of the El Niño-Southern Oscillation (ENSO) and the teleconnection patterns are becoming better documented [e.g., Horel and Wallace, 1981]. Observations suggest that ENSO events may initiate some of the SST variability in the middle latitudes [Barnett, 1981a; Reynolds and Rasmusson, 1983] via an atmospheric teleconnection. This should involve an increased persistence of some of the atmospheric patterns, which was not considered here.

The main difficulty in modeling the influence of mid-latitude SST anomalies on the atmospheric circulation lies in the uncertainty in the relationship between SST and diabatic heating. Most studies of the linear wave response to thermal forcing have considered the effect of a prescribed heat source, and attention should be devoted to the link with the SST anomalies. In this study we have assumed as a rough approximation that in winter conditions the diabatic heating anomaly will be proportional to the air-sea temperature difference. As a result, SST anomaly forcing is nonlocal and depends on the degree of adjustment of the air temperature. Using simple β plane channel models, we have shown that the latter is more important at low wave numbers, which should decrease the climatic impact of the large-scale SST anomalies. However, the atmosphere is more sensitive to low wave number thermal heating, and the large-scale SST anomalies are still dominant.

From our discussion of several studies of the stationary response to diabatic heating in linear wave models of various complexity, we have concluded that realistic mid-latitude SST anomalies have a weak influence on the atmospheric circulation, corresponding to changes in the geopotential height of 10–30 m at most. The linear wave response is sensitive to the mean zonal wind profile, and again it depends on the relationship between SST and diabatic heating anomalies, which was not considered explicitly in most calculations.

The link between linear wave studies and SST anomaly experiments with atmospheric GCM's is starting to emerge. The magnitudes of the SST anomaly-induced changes in GCM experiments are consistent with the linear wave model results, and even the response patterns seem predictable if the heating anomaly is specified from the GCM data. The GCM responses are model dependent, but this may be due to differences in parameterizations and mean flow conditions. However, such response studies must be viewed with caution until the differences are fully understood.

To conclude, we go back to the results of statistical predictability studies, which, as mentioned in the introduction, sug-

gest that mid-latitude SST anomalies have a very weak, but significant, impact on the short-term climate fluctuations. Figure 33 describes the observed low-frequency variability in wintertime conditions. The standard deviation of the 500 mbar geopotential height in middle and high latitudes ranges between 40 and 110 m for monthly means and between 20 and 80 m for seasonal means. If the mid-latitude SST anomaly effects are as suggested here, one would expect negligible impact on the monthly time scale but some influence on the seasonal time scale. *Blackmon et al.* [1984b] have shown that the long atmospheric time scales appeared to be of a different nature than the intermediate time scales (10–30 day period). The latter show signs of wave dispersion and energy propagation, while the longer fluctuations have fixed phases and are suggestive of a forced response. This is consistent with our

tentative conclusion: intermediate time scales in the atmosphere are dominated by blocking and other strong events, and they are not related to mid-latitude SST anomaly forcing. Longer time scales are affected by oceanic sources. The share of the mid-latitude SST anomalies in this forcing needs to be more firmly established, but it does not appear to be negligible.

NOTATION

- t time.
 (x, y, z) Cartesian coordinates.
 λ, ϕ longitude and latitude.
 $\nabla = (\partial/\partial x, \partial/\partial y)$ horizontal gradient operator.
 $\nabla^2 = (\partial^2/\partial x^2) + (\partial^2/\partial y^2)$ horizontal Laplacian.
 \mathbf{n} vertical unit vector.
 a earth radius.
 f Coriolis parameter, equal to $9.35 \times 10^{-5} \text{ s}^{-1}$ at 40°N .
 $\beta = df/dy$ β parameter, equal to $1.75 \times 10^{-11} \text{ m}^{-1} \text{ s}^{-1}$ at 40°N .
 p pressure.
 $\mathbf{v} = (u, v)$ horizontal velocity.
 w vertical velocity.
 w_e entrainment velocity.
 w_E Ekman pumping.
 $\omega = dp/dt$ pressure velocity.
 T temperature.
 Φ geopotential height.
 ψ stream function.
 g gravity, equal to 9.8 m s^{-2} .
 ρ water density, equal to 10^3 kg m^{-3} .
 ρ^a surface air density, equal to 1.2 kg m^{-3} .
 α coefficient of thermal expansion for water.
 q^a specific humidity.
 q_s saturation specific humidity.
 R gas constant, equal to $287 \text{ J kg}^{-1} \text{ }^\circ\text{C}^{-1}$.
 C_p water specific heat equal to $4 \times 10^3 \text{ J kg}^{-1} \text{ }^\circ\text{C}^{-1}$.
 C_p^a air specific heat at constant pressure, equal to $10^3 \text{ J kg}^{-1} \text{ }^\circ\text{C}^{-1}$.
 L latent heat of evaporation, equal to $2.5 \times 10^6 \text{ J kg}^{-1}$.
 τ surface wind stress.
 u_* friction velocity.
 Q surface heat flux (positive upward).
 q rate of diabatic heating per unit mass.
 h depth of the oceanic mixed layer.
 H density scale height of the atmosphere, equal to 7000 m.
 σ static stability.
 N Brunt-Väisälä frequency.
 κ horizontal mixing coefficient.

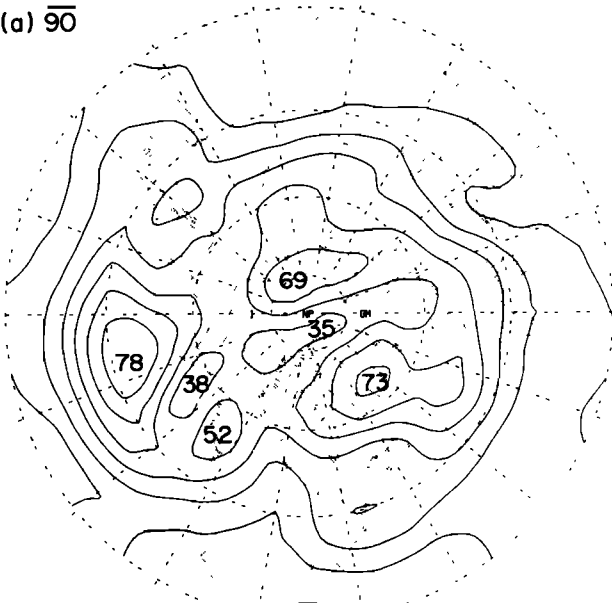
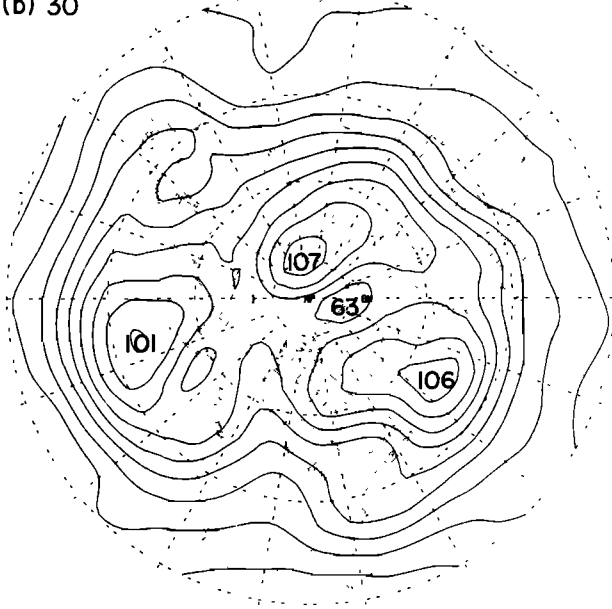
(a) $\overline{90}$ (b) $\overline{30}$ 

Fig. 33. Standard deviation of 500 mbar height for (a) 90-day averaged data and (b) 30-day averaged data for 18 winters. The annual signal has been removed, and the contour interval is 10 m [from *Blackmon et al.*, 1984a].

Acknowledgments. This research was mainly supported by the National Aeronautics and Space Administration, Climate Program Office, under grants NAG 5-137 and NGR-22009727 with the Massachusetts Institute of Technology, and by a research grant from IFREMER. The detailed comments of Bob Haney and an anonymous reviewer on an early version of the manuscript are gratefully acknowledged.

REFERENCES

- Adem, J., On the prediction of mean monthly ocean temperature, *Tellus*, 22, 410–430, 1970.

- Adem, J., Numerical-thermodynamical prediction of monthly ocean temperature, *Tellus*, 22, 541-551, 1975.
- Ashe, S., A nonlinear model for the time-average axially asymmetric flow induced by topography and diabatic heating, *J. Atmos. Sci.*, 36, 109-126, 1979.
- Barnett, T. P., Statistical prediction of North American air temperature from Pacific predictors, *Mon. Weather Rev.*, 109, 1021-1041, 1981a.
- Barnett, T. P., On the nature and causes of large-scale thermal variability in the central North Pacific Ocean, *J. Phys. Oceanogr.*, 11, 887-904, 1981b.
- Barnett, T. P., and K. Hasselmann, Techniques of linear prediction, with application to oceanic and atmospheric fields in the tropical Pacific, *Rev. Geophys.*, 17, 949-968, 1979.
- Barnett, T. P., and R. C. J. Somerville, Advances in short-term climate prediction, *Rev. Geophys.*, 21, 1096-1102, 1983.
- Barnett, T. P., D. H. Heinz, and K. Hasselmann, Statistical prediction of seasonal air temperature over Eurasia, *Tellus*, 36A, 132-146, 1984.
- Bjerknes, J., The recent warming of the North Atlantic, in *The Atmosphere and Sea in Motion*, edited by B. Bolin, pp. 65-73, Rockefeller Institute Press, New York, 1959.
- Bjerknes, J., A possible response of the atmospheric Hadley circulation to equatorial anomalies of ocean temperatures, *Tellus*, 18, 820-829, 1966.
- Bjerknes, J., Atmospheric teleconnections from the equatorial Pacific, *Mon. Weather Rev.*, 97, 163-172, 1969.
- Blaauboer, D., G. J. Komen, and J. Reif, The behavior of the sea surface temperature (SST) as a response to stochastic latent- and sensible heat forcing, *Tellus*, 34, 17-28, 1982.
- Blackmon, M. L., Y.-H. Lee, and J. M. Wallace, Horizontal structure of 500 mb height fluctuations with long, intermediate and short time scales, *J. Atmos. Sci.*, 41, 961-979, 1984a.
- Blackmon, M. L., Y.-H. Lee, J. M. Wallace, and H.-H. Hsu, Time variation of 500 mb height fluctuations with long, intermediate and short time scales as deduced from lag-correlation statistics, *J. Atmos. Sci.*, 41, 981-991, 1984b.
- Camp, N. T., and R. L. Elsberry, Oceanic thermal response to strong atmospheric forcing, II, The role of one-dimensional processes, *J. Phys. Oceanogr.*, 8, 215-224, 1978.
- Charney, J. G., Planetary fluid dynamics, in *Dynamic Meteorology*, edited by P. Morel, pp. 97-351, D. Reidel, Hingham, Mass., 1973.
- Charney, J. G., and P. G. Drazin, Propagation of planetary scale disturbances from the lower into the upper atmosphere, *J. Geophys. Res.*, 66, 83-110, 1961.
- Charney, J. G., and A. Eliassen, A numerical method for predicting the perturbations of the middle latitude westerlies, *Tellus*, 1, 38-54, 1949.
- Chervin, R. M., and S. H. Schneider, On determining the statistical significance of climate experiments with general circulation models, *J. Atmos. Sci.*, 33, 405-412, 1976.
- Chervin, R. M., W. M. Washington, and S. H. Schneider, Testing the statistical significance of the response of the NCAR general circulation model to North Pacific Ocean surface temperature anomalies, *J. Atmos. Sci.*, 33, 413-423, 1976.
- Chervin, R. M., J. E. Kutzbach, D. D. Houghton, and R. G. Gallimore, Response of the NCAR general circulation model to prescribed changes in ocean surface temperature, II, Midlatitude and subtropical changes, *J. Atmos. Sci.*, 37, 308-332, 1980.
- Clark, N. E., Specification of sea surface temperature anomaly patterns in the eastern North Pacific, *J. Phys. Oceanogr.*, 2, 391-404, 1972.
- Daly, W. T., The response of the North Atlantic sea surface temperature to atmospheric forcing processes, *Q. J. R. Meteorol. Soc.*, 194, 363-382, 1978.
- Davis, R. E., Predictability of sea surface temperature and sea level pressure anomalies over the North Pacific Ocean, *J. Phys. Oceanogr.*, 6, 249-266, 1976.
- Davis, R. E., Predictability of sea level pressure anomalies over the North Pacific Ocean, *J. Phys. Oceanogr.*, 8, 233-246, 1978.
- Davis, R. E., R. De Szoek, and P. Niiler, Variability in the upper ocean during MILE, II, Modeling the mixed layer response, *Deep Sea Res.*, 28A, 1453-1475, 1981.
- Denman, K. L., and M. Miyake, Upper layer modification at ocean station Papa: Observation and simulation, *J. Phys. Oceanogr.*, 3, 185-196, 1973.
- Derome, J., and A. Wiin-Nielsen, The response of a middle-latitude model atmosphere to forcing by topography and stationary heat sources, *Mon. Weather Rev.*, 99, 564-576, 1971.
- Dickinson, R. E., Planetary Rossby waves propagating vertically through weak westerly wind wave guides, *J. Atmos. Sci.*, 25, 984-1002, 1968.
- Dickinson, R. E., Orographic effects on planetary flows, *GARP Publ. Ser.*, no. 23, World Meteorological Association, Geneva, 1980.
- Döös, B. R., The influence of exchange of sensible heat with the earth surface on the planetary flow, *Tellus*, 14, 133-147, 1962.
- Egger, J., The linear response of a hemispheric two-level primitive equation model to forcing by topography, *Mon. Weather Rev.*, 104, 351-364, 1976a.
- Egger, J., On the theory of steady perturbations in the troposphere, *Tellus*, 28, 381-389, 1976b.
- Egger, J., On the linear theory of the atmospheric response to sea surface temperature anomalies, *J. Atmos. Sci.*, 34, 603-614, 1977.
- Egger, J., On the theory of planetary standing waves: July, *Contrib. Atmos. Phys.*, 51, 1-14, 1978.
- Elsberry, R. L., and N. T. Camp, Oceanic thermal response to strong atmospheric forcing, I, Characteristics of forcing events, *J. Phys. Oceanogr.*, 8, 206-214, 1978.
- Elsberry, R. L., and R. W. Garwood, Jr., Sea surface temperature anomaly generation in relation to atmospheric storms, *Bull. Am. Meteorol. Soc.*, 59, 786-789, 1978.
- Esbensen, S. K., and R. W. Reynolds, Estimating monthly averaged air-sea transfers of heat and momentum using the bulk aerodynamic method, *J. Phys. Oceanogr.*, 11, 457-465, 1981.
- Favorite, F., and D. R. McLain, Coherence in transpacific movements of positive and negative anomalies of sea surface temperature, 1953-60, *Nature*, 244, 139-143, 1973.
- Frankignoul, C., Large scale air-sea interactions and climate predictability, in *Marine Forecasting*, edited by J. C. J. Nihoul, pp. 35-55, Elsevier, New York, 1979.
- Frankignoul, C., Low-frequency temperature fluctuations off Bermuda, *J. Geophys. Res.*, 86, 6522-6528, 1981.
- Frankignoul, C., Multivariate analysis of sensitivity studies with atmospheric GCM's, in *Coupled Atmosphere-Ocean Models*, Elsevier *Oceanogr. Ser.*, vol. 40, edited by J. C. J. Nihoul, pp. 199-209, Elsevier, New York, 1985.
- Frankignoul, C., and K. Hasselmann, Stochastic climate models, II, Application to sea-surface temperature variability and thermocline variability, *Tellus*, 29, 284-305, 1977.
- Frankignoul, C., and R. W. Reynolds, Testing a dynamical model for mid-latitude sea surface temperature anomalies, *J. Phys. Oceanogr.*, 13, 1131-1145, 1983.
- Fung, I. Y., D. E. Harrison, and A. A. Lacis, On the variability of the net longwave radiation at the ocean surface, *Rev. Geophys.*, 22, 177-193, 1984.
- Garratt, J. R., Review of drag coefficients over oceans and continents, *Mon. Weather Rev.*, 105, 915-929, 1977.
- Garwood, R. W., Jr., Air-sea interaction and dynamics of the surface mixed layer, *Rev. Geophys.*, 17, 1507-1524, 1979.
- Gill, A. E., and P. P. Niiler, The theory of the seasonal variability in the ocean, *Deep Sea Res.*, 20, 141-177, 1973.
- Haney, R. L., Surface thermal boundary conditions for ocean circulation models, *J. Phys. Oceanogr.*, 1, 241-248, 1971.
- Haney, R. L., A numerical case study of the development of large-scale thermal anomalies in the central North Pacific Ocean, *J. Phys. Oceanogr.*, 10, 541-556, 1980.
- Haney, R. L., Midlatitude sea surface temperature anomalies: A numerical hindcast, *J. Phys. Oceanogr.*, 15, 787-799, 1985.
- Haney, R. L., W. S. Shiver, and K. H. Hunt, A dynamical-numerical study of the formation and evolution of large-scale ocean anomalies, *J. Phys. Oceanogr.*, 8, 952-969, 1978.
- Haney, R. L., B. H. Houtman, and W. H. Little, The relationship between wind and sea surface temperature anomalies in the mid-latitude North Pacific Ocean, *Atmos. Ocean*, 21, 168-186, 1983.
- Hannoschöck, G., and C. Frankignoul, Multivariate statistic analysis of a sea surface temperature anomaly experiment with the GISS general circulation model, *J. Atmos. Sci.*, 42, 1430-1450, 1985.
- Harnack, R. P., A further assessment of winter temperature predictions using objective methods, *Mon. Weather Rev.*, 107, 250-267, 1979.
- Harnack, R. P., Objective winter temperature forecasts: An update and extension to the western United States, *Mon. Weather Rev.*, 110, 287-295, 1982.
- Hasselmann, K., Stochastic climate models, I, Theory, *Tellus*, 28, 473-485, 1976.
- Hasselmann, K., On the signal-to-noise problem in atmospheric response studies, in *Meteorology of the Tropical Oceans*, edited by D. B. Shaw, pp. 251-259, Royal Meteorological Society, London, 1979.

- Haworth, C., Some relationships between sea surface temperature anomalies and surface pressure anomalies, *Q. J. R. Meteorol. Soc.*, **104**, 131–146, 1978.
- Held, I. M., Stationary and quasi-stationary eddies in the extratropical troposphere: Theory, in *Large Scale Dynamical Processes in the Atmosphere*, edited by R. P. Pearce and B. J. Hoskins, pp. 127–168, Academic, Orlando, Fla., 1983.
- Hendon, H. H., and D. L. Hartmann, Stationary waves on a sphere: Sensitivity to thermal feedback, *J. Atmos. Sci.*, **39**, 1906–1920, 1982.
- Horel, J. D., and J. M. Wallace, Planetary-scale atmospheric phenomena associated with the interannual variability of sea surface temperature in the equatorial Pacific, *Mon. Weather Rev.*, **109**, 813–829, 1981.
- Hoskins, B. J., and D. J. Karoly, The steady linear response of a spherical atmosphere to thermal and orographic forcing, *J. Atmos. Sci.*, **38**, 1179–1196, 1981.
- Houghton, D. D., J. E. Kutzbach, M. McClintock, and D. Suchman, Response of a general circulation model to a sea temperature perturbation, *J. Atmos. Sci.*, **31**, 857–869, 1974.
- Hsiung, J., and R. E. Newell, The principal nonseasonal modes of variations of global sea surface temperature, *J. Phys. Oceanogr.*, **13**, 1957–1967, 1983.
- Huang, J. C. K., Numerical case studies for oceanic thermal anomalies with a dynamical model, *J. Geophys. Res.*, **84**, 5717–5726, 1979.
- Jacob, W. J., Numerical semiprediction of monthly mean sea surface temperature, *J. Geophys. Res.*, **72**, 1681–1689, 1967.
- Julian, P. R., and R. M. Chervin, A study of the Southern Oscillation and Walker Circulation phenomenon, *Mon. Weather Rev.*, **106**, 1433–1451, 1978.
- Kang, I.-S., and Y.-J. Han, A study of atmospheric responses to large-scale forcing with linear spectral models, *Rep. 53*, Clim. Res. Inst., Oregon State Univ., Corvallis, 1984.
- Kirwood, E., and J. Derome, Some effects of the upper boundary condition and vertical resolution on modeling forced stationary planetary waves, *Mon. Weather Rev.*, **105**, 1239–1251, 1977.
- Kraus, E. B., and J. S. Turner, A one-dimensional model of the seasonal thermocline, II, *Tellus*, **19**, 98–106, 1967.
- Kutzbach, J. E., R. M. Chervin, and D. D. Houghton, Response of the NCAR general circulation model to prescribed changes in ocean surface temperature, I, *J. Atmos. Sci.*, **34**, 1200–1213, 1977.
- Lemke, P., E. W. Trinkl, and K. Hasselmann, Stochastic dynamic analysis of polar sea-ice variability, *J. Phys. Oceanogr.*, **10**, 2100–2120, 1980.
- Levitus, S., Climatological atlas of the world ocean, *NOAA Prof. Pap.* **13**, 173 pp., 1982.
- Lin, B.-D., The behavior of winter stationary planetary waves forced by topography and diabatic heating, *J. Atmos. Sci.*, **39**, 1206–1225, 1982.
- Lindzen, R. S., T. Aso, and D. Jacqmin, Linearized calculations of stationary waves in the atmosphere, *J. Meteorol. Soc. Jpn.*, **60**, 66–77, 1982.
- Liu, W. T., K. B. Katsaros, and A. J. Businger, Bulk parameterization of air-sea exchanges of heat and water vapor including the molecular constraints at the interface, *J. Atmos. Sci.*, **36**, 1722–1735, 1979.
- Madden, R. A., Estimates of the natural variability of time-averaged sea-level pressure, *Mon. Weather Rev.*, **104**, 942–952, 1976.
- Masuda, K., Dynamical estimation of atmospheric diabatic heating over the northern hemisphere in winter, *J. Meteorol. Soc. Jpn.*, **61**, 449–454, 1983.
- Maul, G. A., P. Webb de Witt, A. Yanaway, and S. R. Baig, Geostationary satellite observations of Gulf Stream meanders: Infrared measurements and time series analysis, *J. Geophys. Res.*, **83**, 6123–6135, 1978.
- Mellor, G. L., and P. A. Durbin, The structure and dynamics of the ocean surface mixed layer, *J. Phys. Oceanogr.*, **5**, 718–728, 1975.
- Michaelsen, J., A statistical study of large-scale, long-period variability in North Pacific sea surface temperature anomalies, *J. Phys. Oceanogr.*, **12**, 694–703, 1982.
- Miller, J. R., The salinity effect in a mixed layer ocean model, *J. Phys. Oceanogr.*, **6**, 29–35, 1976.
- Mitchell, J. M., Jr., Stochastic models of air-sea interaction and climatic fluctuation, *Mem. RM-5233-NSF*, Rand Corp., Santa Monica, Calif., 1966.
- Nakamura, H., Some problems in reproducing planetary waves by numerical models of the atmosphere, *J. Meteorol. Soc. Jpn.*, **54**, 129–146, 1976.
- Namias, J., Recent seasonal interactions between North Pacific waters and the overlying atmospheric circulation, *J. Geophys. Res.*, **64**, 631–646, 1959.
- Namias, J., Large-scale air-sea interactions over the North Pacific from summer 1962 through the subsequent winter, *J. Geophys. Res.*, **68**, 6171–6186, 1963.
- Namias, J., Macroscopic association between mean monthly sea surface temperature and the overlying winds, *J. Geophys. Res.*, **70**, 2307–2318, 1965.
- Namias, J., Seasonal interactions between the North Pacific ocean and the atmosphere during the 1960's, *Mon. Weather Rev.*, **97**, 173–192, 1969.
- Namias, J., Experiments in objectively predicting some atmospheric and oceanic variables for the winter of 1971–72, *J. Appl. Meteorol.*, **11**, 1164–1174, 1972.
- Namias, J., Thermal communication between the sea surface and the lower troposphere, *J. Phys. Oceanogr.*, **3**, 373–378, 1973.
- Namias, J., Negative ocean-air feedback systems over the North Pacific in the transition from warm to cold seasons, *Mon. Weather Rev.*, **104**, 1107–1121, 1976.
- Namias, J., Northern hemisphere seasonal 700 mb height and anomaly charts, 1947–1978, and associated North Pacific sea surface temperature anomalies, *CALCOFI Atlas 27*, 275 pp., Scripps Inst. of Oceanogr., La Jolla, Calif., 1979.
- Namias, J., and R. M. Born, Temporal coherence in North Pacific sea surface temperature patterns, *J. Geophys. Res.*, **75**, 5952–5955, 1970.
- Namias, J., and D. R. Cayan, Large-scale air-sea interactions and short-period climatic fluctuations, *Science*, **214**, 869–876, 1981.
- Nigam, S., On the structure and forcing of tropospheric stationary waves, Ph.D. thesis, Princeton Univ., Princeton, N. J., 1983.
- Niiler, P. P., Deepening of the wind-mixed layer, *J. Mar. Res.*, **33**, 405–422, 1975.
- Niiler, P. P., and E. B. Kraus, One-dimensional models of the upper ocean, in *Modeling and Prediction of the Upper Layers of the Ocean*, edited by E. B. Kraus, pp. 143–172, Pergamon, New York, 1977.
- Obuko, A., Oceanic diffusion diagrams, *Deep Sea Res.*, **18**, 789–802, 1971.
- Opsteegh, J. D., and H. M. Van den Dool, Seasonal differences in the stationary response of a linearized primitive equation model: Prospects for long-range weather forecasting?, *J. Atmos. Sci.*, **37**, 2169–2185, 1980.
- Ortiz, M. J., and A. Ruiz de Elvira, A cyclo-stationary model of sea surface temperature in the Pacific Ocean, *Tellus*, **37A**, 14–23, 1985.
- Pedlosky, J., The development of thermal anomalies in a coupled ocean-atmospheric model, *J. Atmos. Sci.*, **32**, 1501–1514, 1975.
- Pedlosky, J., *Geophysical Fluid Dynamics*, 624 pp., Springer-Verlag, New York, 1979.
- Phillips, T. J., On the interaction of surface heating anomalies with zonally symmetric and asymmetric atmospheric flows, *J. Atmos. Sci.*, **39**, 1953–1971, 1982.
- Pitcher, E. J., M. L. Blackmon, G. T. Bates, and S. Munoz, The effects of midlatitude Pacific sea-surface-temperature anomalies on the January climate of a general circulation model, *J. Atmos. Sci.*, in press, 1985.
- Pollard, R. T., P. B. Rhines, and R. O. R. Y. Thompson, The deepening of the wind-mixed layer, *Geophys. Fluid Dyn.*, **4**, 381–404, 1973.
- Preisendorfer, R. W., and T. P. Barnett, Numerical model-reality intercomparison tests using small-sample statistics, *J. Atmos. Sci.*, **40**, 1884–1896, 1983.
- Price, J. F., Upper ocean response to a hurricane, *J. Phys. Oceanogr.*, **11**, 153–175, 1981.
- Price, J. F., C. N. K. Mooers, and J. C. Van Leer, Observations and simulation of storm-induced mixed-layer deepening, *J. Phys. Oceanogr.*, **8**, 582–599, 1978.
- Reynolds, R. W., Sea surface temperature in the North Pacific Ocean, *Tellus*, **30**, 97–103, 1978.
- Reynolds, R. W., A stochastic forcing model of sea surface temperature anomalies in the North Pacific and North Atlantic, *Rep. 8*, Clim. Res. Inst., Oregon State Univ., Corvallis, 1979.
- Reynolds, R. W., and E. M. Rasmusson, The North Pacific sea surface temperature associated with El Niño events, in *Proceedings of the 7th Annual Climatic Diagnostics Workshop, NCAR, 1982*, National Oceanographic and Atmospheric Administration, Boulder, Colo., 1983.
- Rhines, P. B., The dynamics of unsteady currents, in *Marine Modelling, The Sea*, vol. 6, pp. 189–318, John Wiley, New York, 1977.
- Richman, J. G., C. Wunsch, and N. G. Hogg, Space and time scales of mesoscale motion in the western Atlantic, *Rev. Geophys.*, **15**, 385–420, 1977.
- Roads, J. O., Climatic-anomaly experiments in middle latitudes, *Tellus*, **32**, 410–427, 1980.

- Roads, J. O., Linear and nonlinear aspects of snow albedo feedbacks in atmospheric models, *J. Geophys. Res.*, **86**, 7411–7424, 1981.
- Roden, G. I., and G. W. Groves, On the statistical prediction of ocean temperatures, *J. Geophys. Res.*, **65**, 249–263, 1960.
- Rowntree, P. R., The influence of tropical east Pacific Ocean temperatures on the atmosphere, *Q. J. R. Meteorol. Soc.*, **98**, 290–321, 1972.
- Rowntree, P. R., The effects of changes in ocean temperature on the atmosphere, *Dyn. Atmos. Ocean*, **3**, 373–390, 1979.
- Ruiz de Elvira, A., and P. Lemke, A Langevin equation for stochastic climate models with periodic feedback and forcing variance, *Tellus*, **34**, 313–320, 1982.
- Salmon, R., and M. C. Hendershott, Large-scale air-sea interactions with a simple general circulation model, *Tellus*, **28**, 228–242, 1976.
- Sankar Rao, M., and B. Saltzman, On a steady-state theory of global monsoons, *Tellus*, **21**, 308–330, 1969.
- Saunders, P. M., Space and time variability of temperature in the upper ocean, *Deep Sea Res.*, **19**, 467–480, 1972.
- Schopf, P. S., and M. A. Cane, On equatorial dynamics, mixed layer physics and sea surface temperature, *J. Phys. Oceanogr.*, **13**, 917–935, 1983.
- Shukla, J., Effect of Arabian sea-surface temperature anomaly on Indian summer monsoon: A numerical experiment with the GFDL model, *J. Atmos. Sci.*, **32**, 503–511, 1975.
- Shukla, J., and B. Bangaru, Effect of a Pacific sea surface temperature anomaly on the circulation over North America, in *Fourth NASA Weather and Climate Program Science Review*, pp. 171–176, NASA Goddard Space Flight Center, Greenbelt, Md., 1979.
- Simmons, A. J., The forcing of stationary wave motions by tropical diabatic heating, *Q. J. R. Meteorol. Soc.*, **108**, 503–534, 1982.
- Simmons, A. J., J. M. Wallace, and G. W. Branstator, Barotropic wave propagation and instability, and atmospheric teleconnection patterns, *J. Atmos. Sci.*, **40**, 1363–1392, 1983.
- Simpson, J. J., and T. D. Dickey, Alternative parameterizations of downward irradiance and their dynamical significance, *J. Phys. Oceanogr.*, **11**, 876–882, 1981.
- Simpson, J. J., and C. A. Paulson, Mid-ocean observations of atmospheric radiation, *Q. J. R. Meteorol. Soc.*, **105**, 482–502, 1979.
- Smagorinsky, J., The dynamical influence of large-scale heat sources and sinks on the quasi-stationary mean motion of the atmosphere, *Q. J. R. Meteorol. Soc.*, **97**, 342–366, 1953.
- Spar, J., Some effects of surface anomalies in a global general circulation model, *Mon. Weather Rev.*, **101**, 91–100, 1973.
- Stevenson, J. W., The seasonal variation of the surface mixed-layer response to the vertical motions of linear Rossby waves, *J. Phys. Oceanogr.*, **13**, 1255–1268, 1983.
- Thompson, R., Climatological numerical models of the surface mixed layer of the ocean, *J. Phys. Oceanogr.*, **6**, 496–503, 1976.
- Thompson, R., Reply to Garwood and Camp, *J. Phys. Oceanogr.*, **7**, 470–471, 1977.
- Trenberth, K. E., A quasi-biennial standing wave in the southern hemisphere and interrelations with sea surface temperature, *Q. J. R. Meteorol. Soc.*, **101**, 55–74, 1975.
- Voorhis, A. D., E. H. Schroder, and A. Leetmaa, The influence of deep mesoscale eddies on the sea surface temperature in the North Atlantic subtropical convergence, *J. Phys. Oceanogr.*, **6**, 953–961, 1976.
- Walsh, J. E., and M. B. Richman, Seasonality in the associations between surface temperatures over the United States and North Pacific Ocean, *Mon. Weather Rev.*, **109**, 767–783, 1981.
- Weare, B. C., Empirical orthogonal analysis of Atlantic Ocean surface temperature, *Q. J. R. Meteorol. Soc.*, **103**, 467–478, 1977.
- Weare, B. C., A. R. Navato, and R. E. Newell, Empirical orthogonal analysis of Pacific sea surface temperature, *J. Phys. Oceanogr.*, **6**, 671–678, 1976.
- Webster, P. J., Mechanisms determining the atmospheric response to sea surface temperature anomalies, *J. Atmos. Sci.*, **38**, 554–571, 1981.
- Webster, P. J., Seasonality in the local and remote atmospheric response to sea surface temperature anomalies, *J. Atmos. Sci.*, **39**, 41–52, 1982.
- White, W. B., and R. L. Bernstein, Large-scale vertical eddy diffusion in the main pycnocline of the central North Pacific, *J. Phys. Oceanogr.*, **11**, 434–441, 1981.
- White, W. B., and A. E. Walker, Time and depth scales of anomalous subsurface temperature at ocean weather stations P, N, and V in the North Pacific, *J. Geophys. Res.*, **79**, 4517–4522, 1974.
- Willebrand, J., Temporal and spatial scales of the wind field over the North Pacific and North Atlantic, *J. Phys. Oceanogr.*, **8**, 1080–1094, 1978.
- Willson, M. A. G., A wavenumber-frequency analysis of large-scale tropospheric motions in the extratropical northern hemisphere, *J. Atmos. Sci.*, **32**, 478–488, 1975.
- World Meteorological Organization, *Orographic Effects on Planetary Flows*, GARP Publ. Ser., no. 23, Geneva, 1980.

C. Frankignoul, Laboratoire de Physique et Chimie Marines, Université Paris VI, 4 Place Jussieu, Paris 5^e, France.

(Received September 18, 1984;
accepted July 10, 1985.)